



**DERIVATION OF A SELF-CONSISTENT AURORAL OVAL MODEL USING THE  
AURORAL BOUNDARY INDEX**

THESIS

Keith A. Anderson, Captain, USAF  
AFIT/GAP/ENP/04-01

**DEPARTMENT OF THE AIR FORCE  
AIR UNIVERSITY  
AIR FORCE INSTITUTE OF TECHNOLOGY**

---

**Wright-Patterson Air Force Base, Ohio**

APPROVED FOR PUBLIC RELEASE; DISTRIBUTION UNLIMITED

The views expressed in this thesis are those of the author and do not reflect the official policy or position of the United States Air Force, Department of Defense, or the United States Government.

AFIT/GAP/ENP/04-01

DERIVATION OF A SELF-CONSISTENT AURORAL OVAL MODEL USING THE  
AURORAL BOUNDARY INDEX

THESIS

Presented to the Faculty  
Department of Engineering Physics  
Graduate School of Engineering and Management  
Air Force Institute of Technology  
Air University  
Air Education and Training Command  
In Partial Fulfillment of the Requirements for the  
Degree of Master of Science (Applied Physics)

Keith A. Anderson, BS  
Captain, USAF

June 2004

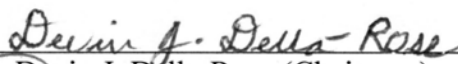
APPROVED FOR PUBLIC RELEASE; DISTRIBUTION UNLIMITED

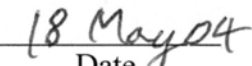
AFIT/GAP/ENP/04-01


DERIVATION OF A SELF-CONSISTENT AURORAL OVAL MODEL USING THE  
AURORAL BOUNDARY INDEX

Keith A. Anderson, BS  
Captain, USAF

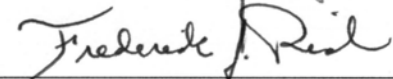
Approved:

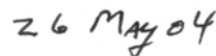
  
Devin J. Della-Rose (Chairman)

  
Date

  
Daniel E. Reynolds (Member)

  
Date

  
Frederick J. Rich (Member)

  
Date

## Abstract

The position and intensity of the auroral oval has many implications for the Air Force from determining the effects of incoming electron flux on DoD systems to modeling the ionosphere to exploit current HF communications capabilities. The auroral morphology is a good indicator of the level at which space weather and its near-Earth consequences are occurring, and thus it is important to develop an auroral prediction model. However, since no purely physics-based models exist to describe the temporal and spatial evolution of the auroral zone, space weather practitioners and researchers are forced to produce statistical representations, “organized” by some relevant geophysical parameter. Currently, the most widely used model is the Hardy *et al.* (1985) auroral oval model, which is binned according to the  $Kp$  index. The  $Kp$  index is a mid-latitude measure of planetary geomagnetic activity, and was presumed to be well-correlated to the size and shape of the auroral region. However, subsequent research has shown that  $Kp$  is probably not the best binning parameter.

This study used the Auroral Boundary Index (ABI) to parameterize the statistics of the auroral oval location since it is a measurement of the electron fluxes computed directly from sensors aboard the DMSP satellites. Thus, the current work represents a move toward a more self-consistent—and presumably more accurate—climatological representation of the auroral oval boundaries. This was accomplished by recreating the process performed by Hardy *et al.*, substituting the ABI for the  $Kp$  index and deriving an entirely new set of auroral ovals based on almost 11 years of DMSP data from the F8 and F9 satellites. To quantitatively assess the differences between the two models, electron flux values were compared to actual DMSP data of individual satellite passes. Preliminary findings suggest that the new ABI auroral oval model is, at worst, comparable to the results achieved by Hardy *et al.* Further refinement of this new model based on the ABI should increase its effectiveness and offer a more reliable alternative to previous auroral models.

## **Acknowledgments**

Events in my life over the past year and a half have made completing this thesis truly a monumental task. I would like to thank the entire ENP department for their generosity and flexibility in affording me every imaginable consideration to allow me to complete my degree requirements without further undo stress. Despite the sad times and setbacks, this has been my greatest assignment in the Air Force. I have made many lifelong friends including students and faculty and I will miss each and every one of them. I would particularly like to thank my faculty advisor, Maj Devin Della-Rose, for his unending guidance and support in both my academic and personal affairs. He played many roles in my life including father-figure, supervisor, advisor, teacher, mentor, and friend. I am eternally grateful to him. Others in the department who also affected me on a personal level are Maj Clark Groves and Dr. William Bailey. I am indebted to them for the influence they had on me both in and out of the classroom. Special thanks also go to my thesis committee members, Dr. Daniel Reynolds from the Air Force Institute of Technology, and Dr. Fred Rich from the Air Force Research Laboratory.

Probably most important were the love and support I received from my two children. They endured the long hours that I dedicated to my research and provided the greatest stress relief of all when I finally put my studies aside. I'm glad they were old enough to understand the importance of this phase of my life and that it would eventually be over.

Last, but surely not least, I would like to thank my fellow space weather classmates. We were a very tight-knit group that grew even tighter from the traumatic death of a classmate/friend. We learned together that graduate work is both stressful and rewarding but pales in comparison to the preciousness of life. These experiences have taught us to work hard but to enjoy life to its fullest.

Keith A. Anderson

## Table of Contents

	Page
Abstract .....	iv
Acknowledgments .....	v
List of Figures .....	viii
List of Tables .....	xii
1. Introduction .....	1-1
Background .....	1-1
Problem Statement .....	1-2
Proposed Solution .....	1-3
2. Literature Review .....	2-1
Aurora .....	2-1
Hardy Auroral Oval Model .....	2-6
Auroral Oval Boundary .....	2-9
<i>Kp</i> Index .....	2-10
Auroral Boundary Index .....	2-14
Defense Meteorological Satellite Program (DMSP) .....	2-18
Special Sensor Precipitating Electron and Ion Spectrometer (SSJ/4) .....	2-20
3. Methodology .....	3-1
Introduction .....	3-1
Auroral Boundary Index Data .....	3-1
DMSP SSJ/4 Data .....	3-3
Differential Flux Output .....	3-4
Integral Flux Output .....	3-6
Hardy Auroral Model Output .....	3-10
Tecplot .....	3-11
4. Results and Analysis .....	4-1
Introduction .....	4-1
ABI Auroral Model Ovals .....	4-1
Hardy Auroral Model Ovals .....	4-3
Smoothing and Removal of Non-Physical Integral Fluxes .....	4-3
Discussion of Features on ABI Auroral Model Plots .....	4-6

Integral Number Flux Plots.....	4-7
Integral Energy Flux Plots. ....	4-8
Average Energy Plots. ....	4-10
DMSP Passes.....	4-12
April 12, 1992 DMSP Pass. ....	4-15
July 12, 1988 DMSP Pass.....	4-18
April 6, 1994 DMSP Pass. ....	4-21
5. Conclusions and Further Study .....	5-1
Recommendations for Further Research .....	5-2
Appendix A. ABI Auroral Model Polar Projection Plots .....	A-1
Appendix B. Hardy Auroral Model Polar Projection Plots .....	B-1
Bibliography .....	BIB-1
Vita.....	V-1



## List of Figures

Figure	Page
2.1. Interaction of the Solar Wind with the Earth's Magnetosphere .....	2-2
2.2. Altitude profiles of the Neutral Densities (Schunk & Nagy, 2000).....	2-3
2.3. Shapes and Locations of the Discrete and Diffuse Aurora (Akasofu, 1981).....	2-4
2.4. Photometric measurements of the Diffuse and Discrete Aurora (Carlson and Egeland, 1995) .....	2-5
2.5. The Kp network in 1988 (adapted from Menvielle & Berthelier, 1991).....	2-12
2.6. Derivation of the Kp index from each station's K index (adapted from Menvielle & Berthelier, 1991).....	2-13
2.7. (a) ABI for 12 day period in 1989 using all boundaries for all MLT's .....	2-17
2.8. Schematic of the DMSP 5D-2 weather satellite .....	2-18
2.9. Combined orbital coverage of the DMSP F8 and F9 satellites.....	2-19
3.1. Frequency Distribution of ABI values from 1987 to 1994 .....	3-2
3.2. Grid structure used in binning the ABI auroral model. 48 divisions in magnetic local time and 30 divisions in corrected geomagnetic latitude .....	3-6
3.3. Percentage of fluxes discarded for each channel .....	3-8
4.1. Total number of fluxes that were averaged in each ABI zone.....	4-2
4.2. ABI auroral model, zone 58-58.9, before discarding unphysical fluxes for (a) number flux and (b) energy flux.....	4-4
4.3. ABI auroral model, zone 58-58.9, after discarding unphysical fluxes for (a) number flux and (b) energy flux.....	4-5
4.4. ABI auroral model, zone 58-58.9, prior to bin smoothing for (a) number flux and (b) energy flux .....	4-6
4.5. ABI auroral model, zone 58-58.9, after bin smoothing for (a) number flux and (b) energy flux.....	4-6

	Page
4.6. Number flux for (a) ABI auroral model, zone 65-65.9 and (b) Hardy auroral model, Kp = 1 .....	4-8
4.7. Number flux for (a) ABI auroral model, zone 58-58.9 and (b) Hardy auroral model, Kp = 6 .....	4-8
4.8. Energy flux for (a) ABI auroral model, zone 65-65.9 and (b) Hardy auroral model, Kp = 1 .....	4-9
4.9. Energy flux for (a) ABI auroral model, zone 58-58.9 and (b) Hardy auroral model, Kp = 6 .....	4-10
4.10. Average energy, cool electrons for (a) ABI auroral model, zone 63-63.9 and (b) Hardy auroral model, Kp = 3.....	4-11
4.11. Average energy, hot electrons for (a) ABI auroral model, zone 59-59.9 and (b) Hardy auroral model, Kp = 5 .....	4-11
4.12. April 12, 1992 DMSP F8 pass overlaid on (a) Hardy auroral model, Kp = 1, number flux (b) Hardy auroral model, Kp = 1, energy flux (c) ABI auroral model, zone 65-65.9, number flux (d) ABI auroral model, zone 65-65.9, energy flux .....	4-13
4.13. July 12, 1988 DMSP F9 pass overlaid on (a) Hardy auroral model, Kp = 3, number flux (b) Hardy auroral model, Kp = 3, energy flux (c) ABI auroral model, zone 62-62.9, number flux (d) ABI auroral model, zone 62-62.9, energy flux .....	4-14
4.14. April 6, 1994 DMSP F8 pass overlaid on (a) Hardy auroral model, Kp = 5, number flux (b) Hardy auroral model, Kp = 5, energy flux (c) ABI auroral model, zone 60-60.9, number flux (d) ABI auroral model, zone 60-60.9, energy flux .....	4-15
4.15. April 12, 1992 actual DMSP F8 data compared to ABI auroral model and Hardy auroral model, magnetic latitude vs. number flux .....	4-17
4.16. April 12, 1992 actual DMSP F8 data compared to ABI auroral model and Hardy auroral model, magnetic latitude vs. energy flux.....	4-17
4.17. April 12, 1992 smoothed DMSP F8 data compared to ABI auroral model and Hardy auroral model, magnetic latitude vs. number flux.....	4-18

	Page
4.18. April 12, 1992 smoothed DMSP F8 data compared to ABI auroral model and Hardy auroral model, magnetic latitude vs. energy flux .....	4-18
4.19. July 12, 1988 actual DMSP F9 data compared to ABI auroral model and Hardy auroral model, magnetic latitude vs. number flux .....	4-20
4.20. July 12, 1988 actual DMSP F9 data compared to ABI auroral model and Hardy auroral model, magnetic latitude vs. energy flux.....	4-20
4.21. July 12, 1988 smoothed DMSP F9 data compared to ABI auroral model and Hardy auroral model, magnetic latitude vs. number flux.....	4-21
4.22. July 12, 1988 smoothed DMSP F9 data compared to ABI auroral model and Hardy auroral model, magnetic latitude vs. energy flux.....	4-21
4.23. April 6, 1994 actual DMSP F8 data compared to ABI auroral model and Hardy auroral model, magnetic latitude vs. number flux .....	4-22
4.24. April 6, 1994 actual DMSP F8 data compared to ABI auroral model and Hardy auroral model, magnetic latitude vs. energy flux.....	4-23
4.25. April 6, 1994 smoothed DMSP F8 data compared to ABI auroral model and Hardy auroral model, magnetic latitude vs. number flux.....	4-23
4.26. April 6, 1994 smoothed DMSP F8 data compared to ABI auroral model and Hardy auroral model, magnetic latitude vs. energy flux.....	4-24
A.1. ABI auroral model zone 49-49.9 for (a) number flux and (b) energy flux .....	A-1
A.2. ABI auroral model zone 50-50.9 for (a) number flux and (b) energy flux .....	A-2
A.3. ABI auroral model zone 51-51.9 for (a) number flux and (b) energy flux .....	A-3
A.4. ABI auroral model zone 52-52.9 for (a) number flux and (b) energy flux .....	A-4
A.5. ABI auroral model zone 53-53.9 for (a) number flux and (b) energy flux .....	A-5
A.6. ABI auroral model zone 54-54.9 for (a) number flux and (b) energy flux .....	A-6
A.7. ABI auroral model zone 55-55.9 for (a) number flux and (b) energy flux .....	A-7
A.8. ABI auroral model zone 56-56.9 for (a) number flux and (b) energy flux .....	A-8

A.9.	ABI auroral model zone 57-57.9 for (a) number flux and (b) energy flux .....	A-9
A.10.	ABI auroral model zone 58-58.9 for (a) number flux and (b) energy flux .....	A-10
A.11.	ABI auroral model zone 59-59.9 for (a) number flux and (b) energy flux .....	A-11
A.12.	ABI auroral model zone 60-60.9 for (a) number flux and (b) energy flux .....	A-12
A.13.	ABI auroral model zone 61-61.9 for (a) number flux and (b) energy flux .....	A-13
A.14.	ABI auroral model zone 62-62.9 for (a) number flux and (b) energy flux .....	A-14
A.15.	ABI auroral model zone 63-63.9 for (a) number flux and (b) energy flux .....	A-15
A.16.	ABI auroral model zone 64-64.9 for (a) number flux and (b) energy flux .....	A-16
A.17.	ABI auroral model zone 65-65.9 for (a) number flux and (b) energy flux .....	A-17
A.18.	ABI auroral model zone 66-66.9 for (a) number flux and (b) energy flux .....	A-18
A.19.	ABI auroral model zone 67-67.9 for (a) number flux and (b) energy flux .....	A-19
A.20.	ABI auroral model zone 68-68.9 for (a) number flux and (b) energy flux .....	A-20
B.1.	Hardy auroral model Kp zone 0 for (a) number flux and (b) energy flux .....	B-1
B.2.	Hardy auroral model Kp zone 1 for (a) number flux and (b) energy flux .....	B-2
B.3.	Hardy auroral model Kp zone 2 for (a) number flux and (b) energy flux .....	B-3
B.4.	Hardy auroral model Kp zone 3 for (a) number flux and (b) energy flux .....	B-4
B.5.	Hardy auroral model Kp zone 4 for (a) number flux and (b) energy flux .....	B-5
B.6.	Hardy auroral model Kp zone 5 for (a) number flux and (b) energy flux .....	B-6
B.7.	Hardy auroral model Kp zone 6 for (a) number flux and (b) energy flux .....	B-7

## List of Tables

Table	Page
2.1. Description of the Kp categories used in the Hardy auroral model (adapted from Hardy et al., 1985).....	2-7
2.2. Stations in the Kp network (adapted from Linthe, 2004) .....	2-12
2.3. Regression coefficients of auroral equatorward boundaries vs. Kp for all boundaries, 1983-1990 (Madden & Gussenhoven, 1990) .....	2-15
2.4. Relation between Kp* and the ABI using Equation (2.6) .....	2-16
3.1. Division of ABI values into 20 zones .....	3-3
3.2. Categories of differential flux (in units of $\text{el}/\text{cm}^2 \text{ s sr eV}$ ) used to isolate abnormally high fluxes .....	3-8
4.1. Kp values for April 12, 1992 .....	4-16
4.2. Kp values for July 12, 1988 .....	4-19
4.3. Kp values for April 6, 1994 .....	4-22

# DERIVATION OF A SELF-CONSISTENT AURORAL OVAL MODEL USING THE AURORAL BOUNDARY INDEX

## 1. Introduction

### Background

The Department of Defense (DoD) relies heavily on space and ground based systems to support and defend the United States. Space weather impacts are a major concern in order to keep these systems fully operational. Space weather refers to any disturbance on the Sun and in the solar wind, magnetosphere, ionosphere, and thermosphere that can degrade the performance and reliability of space and ground based systems or cause a threat to human life or health. Some examples of affected systems include (but is not limited to) satellite communications (SATCOM), HF radio communications, Global Positioning System (GPS), weather satellites, high-flying aircraft, and any ground based radar systems.

The auroral oval is a good indicator to determine the level at which space weather and its near-Earth consequences are occurring. The auroral oval is a region several degrees wide that encircles both magnetic poles and is caused by energetic particles flowing into both polar regions from the tail of the magnetosphere. An increase of electron particle flux into the magnetosphere due to elevated activity from the Sun causes the diffuse auroral oval boundary to expand equatorward. The diffuse aurora is the equatorward portion of the auroral oval and is created by electrons entering the upper

atmosphere from the central plasma sheet. In other words, the diffuse auroral boundary expands and contracts in response to geomagnetic and solar wind forcing. By understanding the details of the auroral oval boundary locations, we can learn more about the way the solar wind interacts with the geomagnetic field. A derived auroral oval can be used by ionospheric models to help predict how to best exploit HF communications and over-the-horizon radar capabilities. Also, a derived auroral oval can be used as a “first look” product to determine whether an energetic particle event will affect a given DoD system.

### **Problem Statement**

Currently, the most widely used model is the Hardy auroral oval model. It is used to determine the average characteristics of auroral electron precipitation as a function of magnetic local time, magnetic latitude, and geomagnetic activity as measured by the  $Kp$  index [Hardy *et al.*, 1985]. According to Dr. Frederick Rich, Air Force Research Laboratory (AFRL) at Hanscom AFB MA, this model does have some deficiencies. One deficiency is that the equatorward edge of the auroral boundary is much wider in the model than actual measurements taken from the Defense Meteorological Satellite Program (DMSP) satellites. One factor contributing to this discrepancy is that the Hardy auroral oval model is binned according to the  $Kp$  index, which is a measure of planetary geomagnetic activity and not directly correlated to the auroral oval boundary.

Information about the location and size of the aurora is critically important for determining the rate of energy deposition into the upper atmosphere by electron precipitation into the atmosphere and is a key input to global circulation models which

are needed to improve the prediction of ionospheric storm effects which can severely disrupt satellite orbits, electricity grids, and radio communication. Since the science of space physics is still in its early stages, one of the best ways to predict auroral boundaries is to statistically relate measured DMSP flux values with another parameter that is dependent upon geomagnetic activity. For the Hardy auroral model, the parameter of  $Kp$  was chosen since it is related to auroral currents, strengthens during high-latitude magnetic storms, and is computed in a timely manner. Studies have shown that as a geomagnetic storm becomes more intense, the  $Kp$  index increases and the edge of the auroral boundary typically moves to lower latitudes. Unfortunately, the  $Kp$  index is not completely correlated with the auroral boundary, and therefore binning the Hardy auroral model according to  $Kp$  has the effect of ‘blurring’ the oval boundary.

### **Proposed Solution**

Dr. Rich has proposed that the Hardy auroral model be recomputed using the Auroral Boundary Index [Madden & Gussenhoven, 1990]. The Auroral Boundary Index (ABI) should provide a more accurate assessment of the auroral oval boundary since it is computed directly from the SSJ/4 sensors aboard the DMSP satellites. A computer algorithm returns the position of the equatorward boundary in corrected geomagnetic latitude (MLAT), the hourly magnetic local time (MLT) sector in which the boundary is located, and the universal time (UT) that the boundary was observed. The ABI is then computed using these input parameters to predict the low-latitude edge of auroral electron precipitation projected to local midnight. This new parameter for electron precipitation is therefore more self-consistent with the actual DMSP satellite data since it is derived directly from the source.



The procedure to recompute a new model with the ABI will follow the same basic development of the current Hardy auroral model. The main goal is to produce the integral number flux, integral energy flux, and average energy for each level of geomagnetic activity as measured by the ABI. Two sets of databases will be utilized to accomplish this task, one being the set of ABI data and the other the raw set of SSJ/4 sensor data.

The set of ABI data must be statistically evaluated and divided into relatively equal parts. The raw SSJ/4 data for each DMSP satellite must be converted into differential flux values. Finally, an algorithm must be written to correlate the SSJ/4 data with the ABI and compute the three quantities above for each level of activity.

Once the program is set up properly, computing the integral fluxes for different sets of satellite data is a relatively simple procedure. It wouldn't matter if the program were run on one year of data or twenty years of data. To compare this model against the original Hardy auroral model, the oval for a particular ABI will be matched up with an oval for the corresponding  $Kp$  index. This will allow direct comparison of the auroral boundary output from each model. Also, actual measurements of the auroral boundary obtained from a DMSP pass will be compared with the predictions of both models. The results should show that the new model based on the ABI gives a more accurate representation of the diffuse auroral boundary than the Hardy auroral model based on the  $Kp$  index.

## **2. Literature Review**

### **Aurora**

The aurora borealis and aurora australis (often referred to as the northern and southern lights, respectively) occur at mostly high latitudes from 100 to 300 km above the Earth. The main source of the aurora is an electrical discharge in the upper atmosphere [Akasofu, 1981]. It is powered by a solar wind and magnetospheric interaction (Akasofu, 1981) and is best described by the following:

...an aurora is the optical manifestation of auroral-particle precipitation and its interaction with atmospheric constituents. Auroral emissions are produced by particles, origination from the sun and the earth's atmosphere, that collide with the earth's atmosphere along streamlines modulated by electric and magnetic fields in the magnetosphere and ionosphere. The size and form of the aurora thereby reflect the forces acting on these auroral particles as they journey from their source to the earth's upper atmosphere. [Carlson & Egeland, 1995]

The solar wind is a stream of magnetized electrons and protons that is continually emitted by the Sun. This particle stream is ejected in all directions and travels at 400 kilometers per second on average. When the solar wind reaches the Earth, it compresses the lines of the Earth's magnetic field on the sunward side and stretches them into a long tail on the opposite side. This creates a cavity around the Earth called the magnetosphere. In addition, the magnetic field of the Earth is typically described as being dipolar, meaning field lines begin in one hemisphere and terminate in the other hemisphere and are considered 'closed'. However, at high latitudes the field lines are 'open', meaning they originate from Earth, but are tied to the plasma of the magnetotail, and eventually merge with the magnetic field of the solar wind. The aurora is formed around the magnetic north and south poles and along these boundaries where the closed geomagnetic field

lines become open. See Figure 2.1 for a diagram of the interaction of the solar wind with the magnetosphere. The open/closed boundary usually occurs at approximately  $77^\circ$  magnetic latitude at noon and at  $67^\circ$  magnetic latitude at midnight for periods of quiet to moderate activity. With this boundary connected to the solar wind, the intensity of the aurora is closely related to solar activity. Energetic eruptions from solar flares can send huge amounts of charged particles into space, and if directed Earthward, can increase nominal incoming energy levels by three orders of magnitude. The result is an expanded auroral oval into lower latitudes.

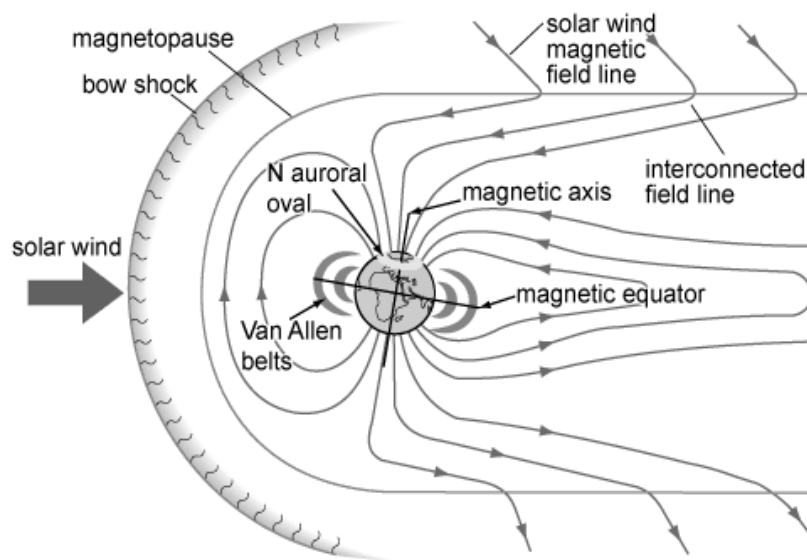


*Figure 2.1. Interaction of the Solar Wind with the Earth's Magnetosphere*

The optical spectrum of an aurora is very similar to that produced by the discharge of gas under extremely high voltage. Energetic electrons from the solar wind trapped in the Earth's magnetotail flow down along magnetic field lines and collide with neutral and ionized atoms in the upper atmosphere. The collisions force some of the

electrons in those atoms to become excited as they absorb the energy and are pushed to a higher energy state. As the excited electrons return to their initial, lower energy state, they will release the extra energy as photons in the ultraviolet (UV), visible, and infrared (IR) wavelengths [Carlson & Egeland, 1995]. Ultraviolet radiation coming from the Sun dissociates oxygen molecules into atomic oxygen, which becomes one of the main components of the upper atmosphere (ionosphere) (Figure 2.2). When these atoms are excited by precipitating electrons, they emit the typical greenish-white light of the aurora. Higher energy electrons can penetrate deeper into the lower part of the atmosphere and excite the neutral nitrogen molecules there to produce a pink or violet-red color. Ionized nitrogen molecules emit violet-blue light [Akasofu, 1991].

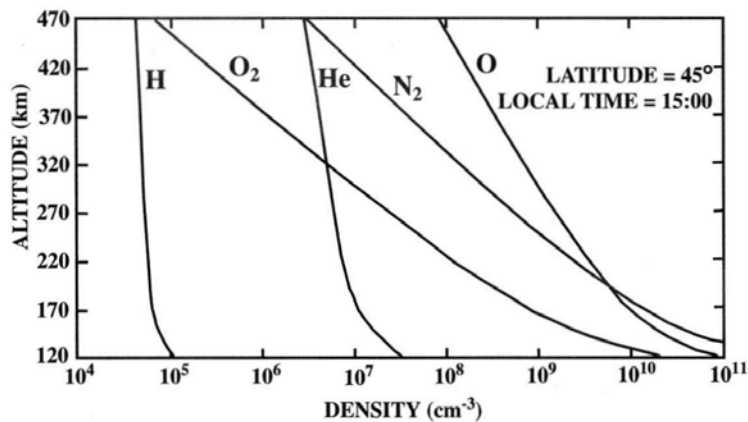
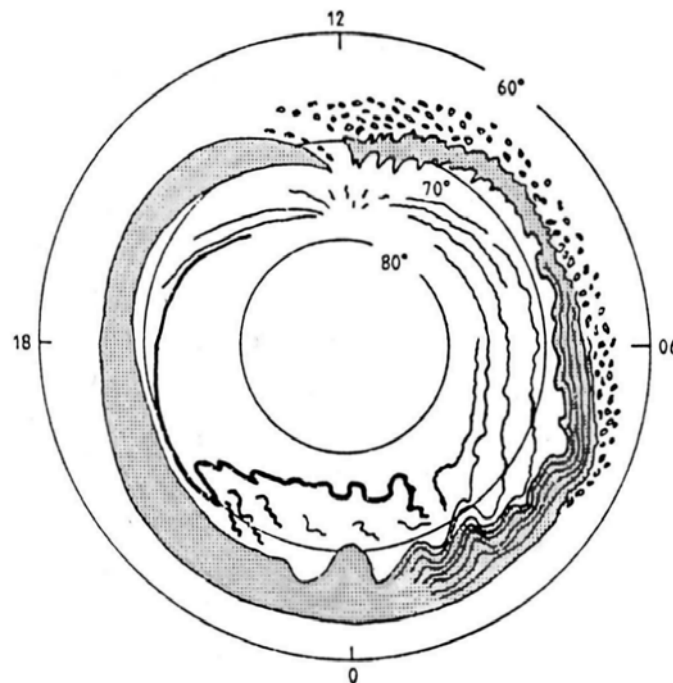


Figure 2.2. Altitude profiles of the Neutral Densities (Schunk & Nagy, 2000)

The aurora comes in various forms and sizes but most tend to be grouped into two very distinct classifications called diffuse and discrete aurora. The discrete aurora is what we tend to see when we look up into the sky. They are the ever-changing ribbons and arcs. The particles that power the discrete aurora have a different origin than those that

power the diffuse aurora. The discrete aurora particles are due to the parallel acceleration of electrons down along the Earth's magnetic field lines into the upper atmosphere and consist mainly of energies greater than 1 keV. The individual parts of the discrete aurora have a relatively short life-span and can intensify, drift, and fade very quickly. It often forms a multi-banded structure and occurs statistically in the premidnight regions. Auroral substorms are comprised mostly of the discrete aurora and are arcs that move poleward and westward called the westward traveling surge [Akasofu, 1981]. With an increase in geomagnetic activity, the discrete aurora will increase in intensity, number, and strength [Tascione, 1994].

The diffuse aurora, unlike the discrete aurora, is more difficult to see from the Earth because it is relatively dim and lacks sharp outlines. However, it is much more expansive and spread out than the discrete aurora. See Figure 2.3 for the some of the



*Figure 2.3. Shapes and Locations of the Discrete and Diffuse Aurora (Akasofu, 1981)*

characteristics of the shapes and locations of the discrete and diffuse aurora. The diffuse aurora (Figure 2.4) still contains some discrete-like structures but they are weak and difficult to observe. The diffuse aurora is found mainly on the equatorward side of the auroral zone. Here, the precipitating particles are drifting around the Earth with electrons traveling eastward and protons traveling westward [Carlson & Egeland, 1995]. The source of the diffuse aurora comes from particles slowly drifting in from the central plasma sheet due to wave-particle interactions that scatter electrons and give them velocities that are more parallel to the magnetic field lines. This change in velocity puts the electrons in the loss cone in phase space where they precipitate down into the upper atmosphere and create the diffuse aurora. The particles responsible for the diffuse aurora cover a fairly broad range of energies, from a few hundred eV to a few tens of keV. As geomagnetic activity

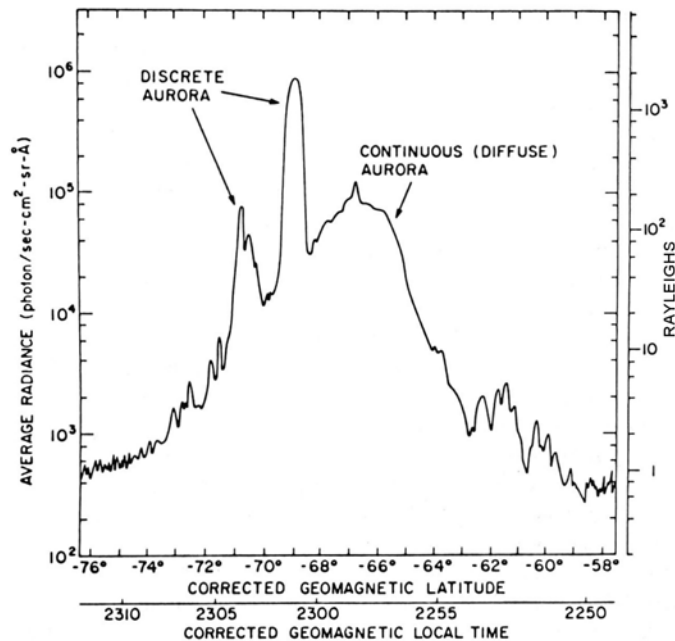


*Figure 2.4. Photometric measurements of the Diffuse and Discrete Aurora (Carlson and Egeland, 1995)*

increases, the diffuse auroral oval will expand equatorward along with a brightening of the diffuse and discrete aurora [Tascione, 1994].

By creating a statistical model of the auroral oval, both the discrete and diffuse auroral forms will be captured. Now, even though the discrete auroral intensity can be significantly larger than the diffuse aurora (see Figure 2.4), this is somewhat compensated by the transient nature of the discrete aurora. Thus, one would expect both discrete and diffuse auroral forms to contribute significantly to the statistics of any long-term climatological model [Della-Rose, pers. comm., 2004].

### **Hardy Auroral Oval Model**

Currently, the most widely used auroral oval model is the Statistical Model of Auroral Electron Precipitation developed by D.A. Hardy and M.S. Gussenhoven at the Air Force Geophysics Laboratory, Hanscom Air Force Base Massachusetts and E. Holeman at the Physics Research Division, Emmanuel College, Boston Massachusetts. It measures the global pattern of auroral electron precipitation as a function of MLT, MLAT, and geomagnetic activity using the *Kp* index as its input parameter [Hardy *et al.*, 1985]. See the section entitled *Kp* Index later in this chapter for a description of this index.

Hardy *et al.* (1985) constructed the model using the Defense Meteorological Satellite Program (DMSP) F2 and F4 satellites and the Satellite Test Program (STP) P78-1 satellite for the years 1977-1980. Data were collected from the SSJ/3 cylindrical curved plate electrostatic analyzers in 16 energy channels covering energy ranges from 50 eV to 20 keV resulting in a complete spectrum recorded once per second. Bins were created by dividing MLT into 48 30-minute sections and by dividing MLAT from 50° to

90° into 30 sections. To do this, latitudes between 50° to 60° and 80° to 90° were incremented every 2° and latitudes between 60° to 80° were incremented every 1°. This resulted in 1440 bins [Hardy *et al.*, 1985]. Table 2.1 describes how the *Kp* index was categorized.

*Table 2.1. Description of the Kp categories used in the Hardy auroral model (adapted from Hardy et al., 1985)*

<b>Zone</b>	<b><i>Kp</i> Index</b>
1	0, 0+
2	1-, 1, 1+
3	2-, 2, 2+
4	3-, 3, 3+
5	4-, 4, 4+
6	5-, 5, 5+
7	6-, 6, 6+, 7-, 7, 7+, 8-, 8, 8+, 9-, 9

Twenty-seven total months of data were used from all three satellites. Fifteen months from the F2 and F4 satellites and one year from the P78-1 satellite. The combined temporal coverage of all three satellites was from September 1977 through August 1980. All the data collected were grouped according to the seven zones of *Kp* as listed above. For each zone, the average and standard deviation of the differential number flux for all 16 energy channels in each bin was calculated. The final product is the average differential number flux in each bin for each level of activity. The averages for each energy channel were then input into the following equations to obtain three integral quantities for each bin in each *Kp* zone. The quantities calculated were the integral number flux in units of  $\text{el}/\text{cm}^2 \cdot \text{s} \cdot \text{sr}$  defined as:



$$J_{tot} = j(E_1)(E_2 - E_1) + \sum_{i=2}^{15} \left[ j(E_i) \cdot \frac{(E_{i+1} - E_{i-1})}{2} \right] + j(16)(E_{16} - E_{15}) \quad (2.1)$$

the integral energy flux in units of keV/cm<sup>2</sup>·s·sr defined as:

$$JE_{tot} = E_1 \cdot j(E_1)(E_2 - E_1) + \sum_{i=2}^{15} \left[ (E_i) \cdot j(E_i) \cdot \frac{(E_{i+1} - E_{i-1})}{2} \right] + E_{16} \cdot j(E_{16})(E_{16} - E_{15}) \quad (2.2)$$

and the average energy in units of keV defined as:

$$E_{ave} = \frac{JE_{tot}}{J_{tot}} \quad (2.3)$$

In these equations,  $j(E_i)$  is the average differential number flux in the  $i$ th energy channel and  $E_i$  is the central energy of the  $i$ th energy channel [Hardy *et al.*, 1985].

Additional smoothing was applied to the integral quantities to help reduce residual noise in the data collected by the SSJ/3 sensors. The following equation was applied to each integral quantity in each bin.

$$\alpha_{ij} = \frac{3 \cdot \alpha_{ij} + \alpha_{i-1,j} + \alpha_{i+1,j} + \alpha_{i,j+1} + \alpha_{i,j-1}}{7} \quad (2.4)$$

The value ' $\alpha_{ij}$ ' corresponds to an individual bin where ' $i$ ' is the MLT position and ' $j$ ' is the latitude position. For the bins at the pole (88° to 90°), the average was computed for all 48 MLT bins. Also, for the bins from 50° to 52°, the  $\alpha_{i,j-1}$  term was omitted and the sum was divided by 6 rather than 7. This smoothing equation was applied to the integral quantities three times [Hardy *et al.*, 1985].

The result is a model based on past statistics that can be used to specify the current auroral location. In addition, given a prediction of a future  $Kp$  value, a 'forecast' of the future location of the auroral oval boundary is obtained. With the input of a

geomagnetic activity level or  $Kp$  index, the model will produce an output file containing a list of the integral number flux, integral energy flux, and average energy for each MLT/MLAT bin. This can then be plotted to give a graphical representation of what the auroral oval would look like.

### **Auroral Oval Boundary**

The reason for computing an auroral model is because not enough is known about the fundamental physics to create a model that fully describes the auroral structure as a function of space and time. Therefore, a statistical relationship must be developed between the average auroral oval location and a parameter that is also highly connected to auroral physics.

For the Hardy auroral model, the  $Kp$  index was chosen since it is a measure of ionospheric currents which intensify during high-latitude magnetic storms. However, a deficiency of the Hardy auroral model is that the equatorward edge of the auroral boundary it predicts can be wider than actual measurements taken from the DMSP satellites. One argument for this inconsistency is due to the model's use of the  $Kp$  index as its input parameter which, as will be discussed in later in this chapter, is a measure of planetary geomagnetic activity in the magnetosphere and not directly correlated to the auroral oval boundary. Therefore, binning the Hardy auroral model according to the  $Kp$  index has the effect of 'blurring' the auroral oval boundary. A typical crossing of a DMSP satellite at the equatorward boundary of the auroral zone takes 2 to 4 seconds (0.1 to 0.3 deg). In this small latitudinal range, the flux increases by a factor of 100 or more. In the Hardy auroral model, the same increase occurs over a 3 to 5 degree latitudinal range. The reason is that even when geophysical conditions as determined by some

proxy such as  $Kp$  seem to be the same, the real auroral zone has a range of sizes. The Hardy auroral model captures the average of the range of sizes instead of the size at any instant in time [Rich, pers. comm., 2003]. By using a self-consistent binning parameter instead, a more definitive auroral boundary will hopefully be derived.

Under the direction of Dr. Fred Rich, a new statistical auroral oval model was derived using the Auroral Boundary Index (based on the equivalent midnight boundary) [Madden & Gussenhoven, 1990]. The Auroral Boundary Index (ABI) should provide a more accurate assessment of the auroral oval boundary since it is computed directly from the SSJ/4 sensors aboard the DMSP satellites. A computer algorithm automatically selects the equatorward auroral boundary as the DMSP satellite orbits the Earth. This information is then used as input to compute the ABI [Madden & Gussenhoven, 1990]. This new parameter for electron precipitation is therefore more self-consistent with the actual DMSP satellite data since it is derived directly from the source.

The advantage of using a more self-consistent binning parameter has been proven with the boundary-oriented electron precipitation model of Sotirelis & Newell (2000). Their model uses the b2i boundary (the peak precipitating energy flux of 3 – 30 keV ions, which can be derived from DMSP SSJ data) as a proxy for the degree of magnetotail stretching. At magnetic latitudes below the b2i boundary, magnetic field lines are no longer curved enough to allow pitch angle scattering of ions into the loss cone. As a result, the ion energy flux decreases below this latitude. The latitude of the b2i boundary, projected to magnetic midnight, serves as the “binning” parameter to organize their model.

## ***Kp* Index**

For this section on the *Kp* index, I draw heavily on the work by Menvielle & Berthelier (1991). The transient variations of the geomagnetic field at the Earth's surface are the signature of the currents throughout the entire magnetosphere, under the influence of the solar wind. These transient variations can be monitored by ground-based magnetic observations by measuring the two horizontal field components, H and D.

In 1938, J. Bartels proposed a network of observatories to measure these localized variations and categorize them as the *K* index. It was a code deduced from observed amplitude ranges using observatory-based classes. The *K* index is computed at approximately 200 geomagnetic observatories since its introduction by Bartels.

Soon after, Bartels also proposed a planetary index utilizing a certain number of strategically located observatories from the newly computed *K* index. After several years of trial and error, Bartels introduced the current *Kp* index (planetarische Kennziffer) (Linthe, 2004) in 1949. Its computation has remained unchanged since then.

The global *Kp* index is obtained as the mean value of the disturbance levels in the two horizontal field components, observed at 13 selected, subauroral stations. Figure 2.5 shows the locations of the 13 current stations and Table 2.2 lists their names, locations, and latitudes. The original *Kp* network contained 11 observatories, with most of them located in North America and Western Europe, and only one in the southern hemisphere. With the addition of two stations, one in 1954 and another in 1970, there are now 13 total observatories comprising the *Kp* network. Due to their sparseness and clustered nature, it is not difficult to understand why the 13 observatories do not provide a true picture of the Earth's geomagnetic activity.

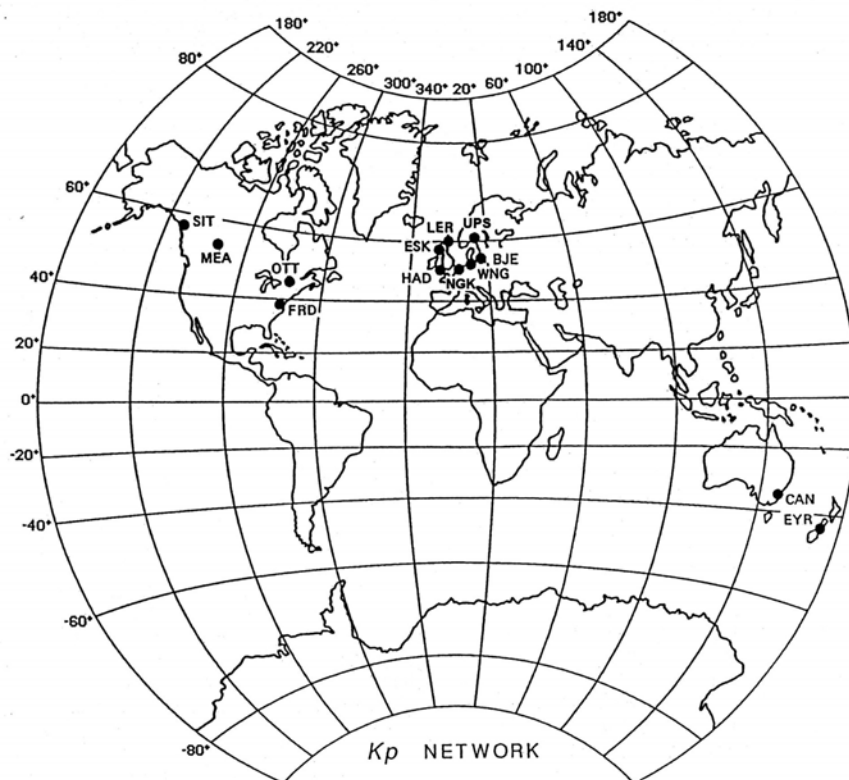


Figure 2.5. The Kp network in 1988 (adapted from Menvielle & Berthelier, 1991)

Table 2.2. Stations in the Kp network (adapted from Linthe, 2004)

Observatory	Code	Location	Geomagnetic Latitude
<i>Northern Hemisphere</i>			
Meanook	MEA	Canada	61.7°
Sitka	SIT	Alaska	60.4°
Lerwick	LER	Scotland	62.0°
Ottawa	OTT	Canada	55.8°
Uppsala	UPS	Sweden	58.5°
Eskdalemuir	ESK	Scotland	57.9°
Brorfelde	BFE	Denmark	55.4°
Fredericksburg	FRD	Virginia	48.6°
Wingst	WNG	Germany	54.1°
Niemegk	WIT	Germany	51.9°
Hartland	HAD	England	54.0°
<i>Southern Hemisphere</i>			
Eyrewell	EYR	New Zealand	47.2°
Canberra†	CNB	Australia	42.9°

To compute the  $Kp$  index, each of the 13 observatory's  $K$  index is converted into a  $Ks$  standardized value using conversion tables developed by Bartels. This conversion to a standardized value is meant to overcome any local time influences, which can vary from season to season. However, it has been proven that these standardized conversion tables are only valid for the time period used in their formulation. To compute the  $Kp$  index, the average of  $Ks$  is taken using the formula shown in Figure 2.6. The  $Ks$  data for the two stations Brorfelde and Uppsala, as well as for Eyrewell and Canberra, are combined so that their average enters into the final calculation with the divisor remaining 11.

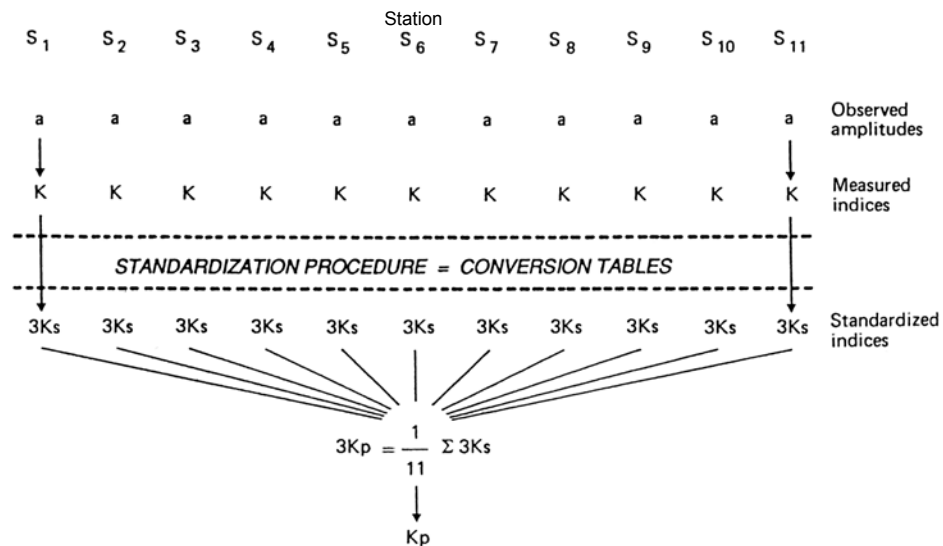


Figure 2.6. Derivation of the  $Kp$  index from each station's  $K$  index (adapted from Menvielle & Berthelier, 1991)

The  $Kp$  index was undoubtedly a pioneering effort to condense massive amounts of data into a usable index when proposed by Bartels in 1949, and it has been unquestionably essential in the measurements of geomagnetism, but the fact remains clear that it is not perfect. As shown by Menvielle & Berthelier (1991), the am or  $Km$

indices prove to indicate the planetary geomagnetic activity level much better than  $Kp$ , whose continued use is really only out of tradition.

The  $Kp$  index is published yearly in the International Service of Geomagnetic Indices (ISGI) Bulletin 32. However, the U.S. Air Force has compiled its own network of observatories and computes a “non-official”  $Kp$  index in real-time.

### **Auroral Boundary Index**

The information for this entire section on the Auroral Boundary Index is cited from the work by Madden & Gussenhoven (1990). The official name of the index is "The Air Force Research Laboratory Auroral Boundary Index", or ABI, and was developed at the USAF Research Laboratory, Hanscom AFB MA. It is the latitude of the equatorward edge of the diffuse aurora, projected to magnetic midnight, and is routinely calculated with about 30 min resolution from DMSP precipitating electron data.

The auroral ovals encircle the magnetic poles rather than the geographic poles. In addition, as geomagnetic activity increases, the oval will be offset toward the postmidnight local time sector. It is therefore increasingly difficult to correlate the auroral oval boundaries measured at different local times with the same geomagnetic activity. To aid in these measurements, a scaling process needed to be incorporated. This was accomplished by statistically determining the auroral oval boundaries for every local time sector as a function of a magnetic activity index.

The establishment of regression coefficients for a linear fit of equatorward auroral boundaries to  $Kp$  values was conducted by a statistical survey. This was completed for all magnetic local time sectors. Table 2.3 lists these regression coefficients by magnetic local time sector. The climatological relation of the regression coefficients, A and B,

MLAT ( $L$ ), and geomagnetic activity,  $Kp$ , at one MLT sector,  $T$ , is shown by Equation 2.5.

$$L_T = A_T + B_T \cdot Kp \quad (2.5)$$

*Table 2.3. Regression coefficients of auroral equatorward boundaries vs.  $Kp$  for all boundaries, 1983-1990 (Madden & Gussenhoven, 1990)*

<b>Magnetic Local Time</b>	<b>Number of Boundaries</b>	<b>Intercept <math>A_T</math></b>	<b>Slope <math>B_T</math></b>	<b>Correlation Coefficient</b>
00-01	2349	67.57	-1.62	-0.73
01-02	43	68.31	-1.39	-0.66
02-03	41	68.92	+0.03	+0.03
03-04	2741	67.07	-1.50	-0.56
04-05	12900	66.56	-1.82	-0.76
05-06	20682	67.28	-1.79	-0.78
06-07	16186	68.10	-1.83	-0.74
07-08	13369	68.17	-1.65	-0.68
08-09	17422	68.98	-1.58	-0.67
09-10	17873	69.13	-1.24	-0.56
10-11	6565	68.99	-1.00	-0.46
11-12	2218	68.54	-0.62	-0.30
12-13	1056	68.90	-0.34	-0.16
13-14	1296	70.76	-0.37	-0.18
14-15	1564	71.48	-0.63	-0.29
15-16	1785	72.73	-1.12	-0.50
16-17	3332	73.22	-1.46	-0.71
17-18	8193	72.20	-1.48	-0.74
18-19	19946	71.64	-1.64	-0.80
19-20	17347	71.09	-1.85	-0.82
20-21	17539	69.71	-1.66	-0.78
21-22	14175	69.25	-2.07	-0.84
22-23	16234	67.89	-1.88	-0.83
23-24	11205	67.18	-1.75	-0.81

For each 100-minute orbit, the DMSP satellite crosses the northern auroral oval twice and the southern auroral oval twice. For each boundary crossing, the following data are collected: MLAT (same as  $L_T$  in Equation (2.5)), MLT, and UT. Using the regression coefficients (Table 2.3) derived from the linear regression relation (equation



2.5) between the equatorward auroral boundary and the actual  $Kp$  index, the DMSP measured latitude,  $L_T(t)$ , can now be correlated to a statistical  $Kp^*$  using the following equation:

$$Kp^*(t) = [L_T(t) - A_T] / B_T \quad (2.6)$$

An equivalent midnight boundary is then computed using  $Kp^*(t)$  to predict the low-latitude edge of auroral electron precipitation projected to local midnight. In other words, the actual boundary, at magnetic local time  $T$ , is projected to the midnight sector at magnetic local time  $T = 00$  by applying  $Kp^*(t)$  to the following equation:

$$L_{00}(t) = A_{00} + B_{00} \cdot Kp^*(t) = A_{00} + (B_{00}/B_T) \cdot (L_T(t) - A_T) \quad (2.7)$$

where  $A_{00}$  and  $B_{00}$  are the regression coefficients at midnight and  $L_{00}(t)$  is the equivalent midnight boundary. The continuing time series of these computed equivalent midnight boundaries is what comprises the the Auroral Boundary Index.

The relation between the statistical  $Kp^*$  and its equivalent midnight boundary is shown in Table 2.4.

*Table 2.4. Relation between  $Kp^*$  and the ABI using Equation (2.6)*

$Kp^*$	ABI	$Kp^*$	ABI	$Kp^*$	ABI	$Kp^*$	ABI
0	67.67	2+	63.79	5-	60.01	7	56.23
0+	67.03	3-	63.25	5	59.47	7+	55.69
1-	66.49	3	62.71	5+	58.93	8-	55.15
1	65.95	3+	62.17	6-	58.39	8	54.61
1+	65.41	4-	61.63	6	57.85	8+	54.07
2-	64.87	4	61.09	6+	57.31	9-	53.53
2	64.33	4+	60.55	7-	56.77	9	52.99

The only boundaries used to create the ABI were those that were evening boundaries and those where the negative of the boundary correlation with  $Kp$  was greater

than 0.75. Therefore, the selection criteria consisted of only the evening boundaries between 18 and 24 MLT (see Table 2.3). Figure 2.7(a) shows a 12 day period in 1989 using all boundaries for all MLTs (before selection criteria was applied). This figure indicates many data points that are extremely high or low which occur fairly randomly. Notice also the large variability from data point to data point. This was a result of mapping both the morning and the evening boundaries to midnight. Figure 2.7(b) shows the same time period after applying the selection criteria. By using only the evening boundaries, the obviously extreme data points are eliminated.

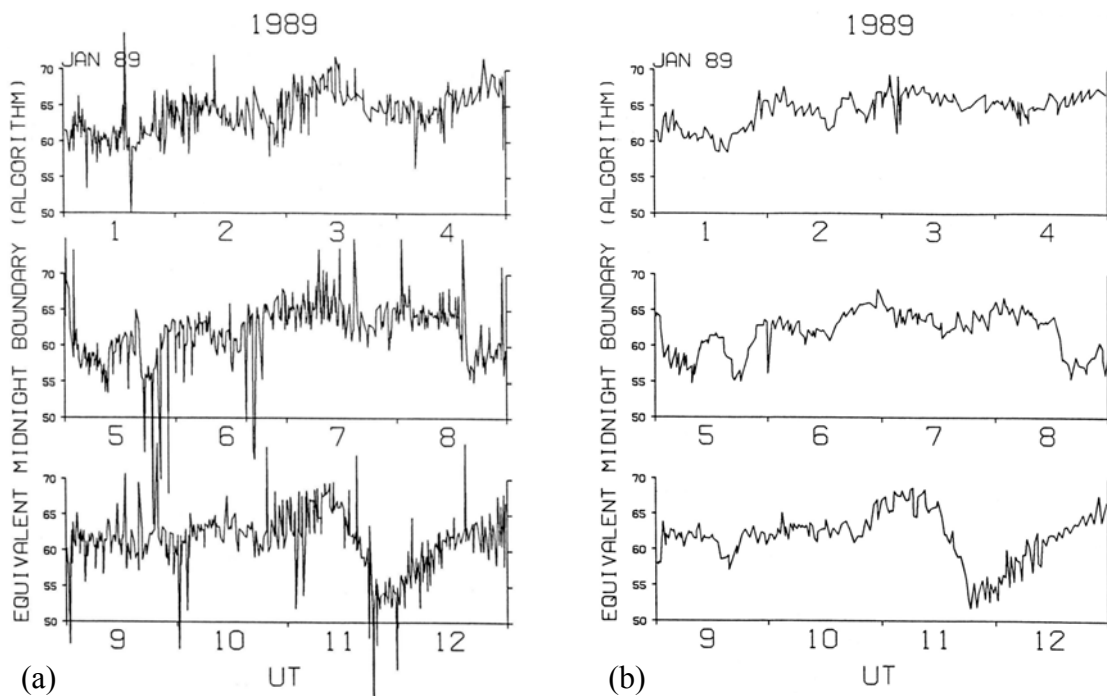
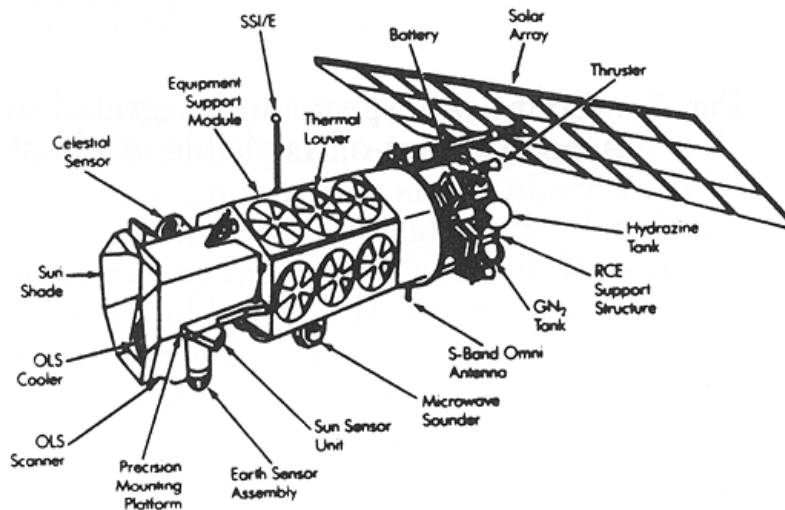


Figure 2.7. (a) ABI for 12 day period in 1989 using all boundaries for all MLT's  
 (b) Same period after applying selection criteria (Madden & Gussenhoven, 1990)

## Defense Meteorological Satellite Program (DMSP)

All of the technical information for this section was obtained from an internet website hosted by the Global Hydrology Resource Center, Marshall Space Flight Center and maintained by Greg Deuel with a revision date of June 11, 1997.

The Defense Meteorological Satellite Program (DMSP) 5D-2 is the military's sixth generation of weather satellites (Figure 2.8). The DMSP satellites operate in two satellite constellations to provide worldwide near real-time meteorological, oceanographic and solar-terrestrial physics measurements in support of DoD operations. The two DMSP satellites used for this study were the F8 and F9 with operational lifetimes from June 1987 to August 1991 and February 1988 to March 1992, respectively. Both satellites are near-circular, polar orbiting, and sun-synchronous



*Figure 2.8. Schematic of the DMSP 5D-2 weather satellite*

The visible and infrared sensors aboard the satellite collect images of global cloud distribution across a 3,000 km swath during both daytime and nighttime conditions. The

coverage of the microwave imager and temperature sounder is approximately one-half the visible and infrared sensor's coverage, covering the polar regions above 60 deg on a twice-daily basis and the equatorial region on a daily basis. The F8 satellite flies in the local time meridian of 0600/1800 MLT and the F9 satellite in the local time meridian of 0932/2132. Figure 2.9 shows the orbital coverage of both the F8 and F9 satellites which provide coverage of most of the auroral region except for two sections postmidnight and postnoon.

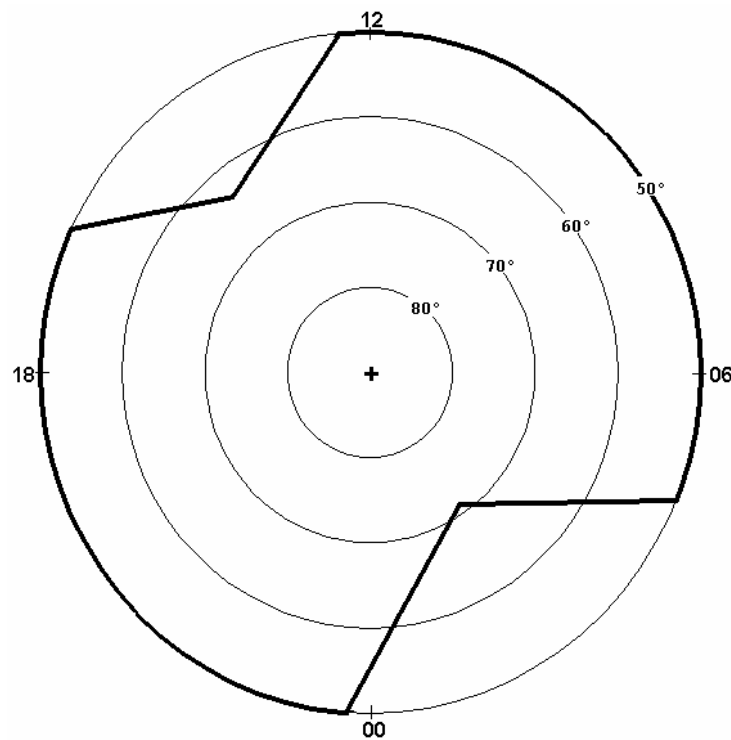


*Figure 2.9. Combined orbital coverage of the DMSP F8 and F9 satellites*

The F8 and F9 satellites were built by General Electric's Astro-Space Division and are the military version of NOAA's TIROS weather satellites. They measure 3.5 meters long and 1.2 meters wide with a 725 kilogram mass.

Command and control was provided by the 6th Satellite Operations Group at Offutt AFB, Nebraska with data transmitted to tactical terminals worldwide and processed by the Air Force Weather Agency (AFWA) also at Offutt AFB and by the Fleet Numerical Meteorological and Oceanography Center (FNMOC) at Monterey, California.

The space environmental sensors record along-track plasma densities, velocities, composition, and drifts and include: Operational Linescan System (OLS) - visible/infrared imager, Special Sensor Microwave Temperature Sounder (SSM/T) - atmospheric sounder producing cloud temperature profiles, Special Sensor Ionospheric and Electron Scintillation Meter (SSI/ES) – measuring ambient electron and ion density and temperatures and plasma drift and scintillation, Special Sensor Microwave Imager (SSM/I) - microwave imager measuring ice coverage, precipitation areas and intensities, cloud water content, and ocean surface wind speeds, Special Sensor Gamma/X-Ray Detector (SSB/X-M) - gamma and x-ray spectrometer, Special Sensor Precipitating Electron and Ion Spectrometer (SSJ/4) - measures ion and electron densities.

***Special Sensor Precipitating Electron and Ion Spectrometer (SSJ/4).***

The SSJ/4 sensor provides a complete energy spectrum of the particles that cause the aurora and other phenomena. The data consists of electron and ion particle fluxes in 20 energy channels between 30 eV and 30 keV recorded every second [Hardy *et al.*, 1984].

The SSJ/4 instrument was designed to measure the flux of charged particles as they enter the Earth's upper atmosphere from the near-Earth space environment. It consists of four cylindrical curved plate electrostatic analyzers with a look direction

oriented radially outward from the Earth. Each analyzer consists of three components; an aperturing system, a set of two concentric cylindrical curved plates, and a pair of channeltrons. The aperture system aligns the incoming particles for access to the cylindrical plates. Electrons and ions of the selected energy are deflected toward the inner plate by an imposed electric field (100 volts for electrons) applied across the two plates. For a particle to be counted, its centrifugal force produced from the electric field must equal the electric field force itself. When this occurs, the particle is channeled between the plates and contacts the channeltron. Lower energy particles between 30 eV and 1000 eV are measured logarithmically by one set of cylindrical plates with a radius of curvature of  $127^\circ$ . Higher energy particles between 1 keV and 30 keV are measured logarithmically by another set of cylindrical plates with a radius of curvature of  $60^\circ$  [Hardy *et al.*, 1984].

### **3. Methodology**

#### **Introduction**

The Hardy Auroral Oval Model is the most widely used auroral model in use today by the Air Force. There exist many other versions of auroral models, each with their own limitations. With this in mind, the initial focus of this thesis was to only improve upon the already proven model. This was accomplished by recreating the process performed by Hardy *et al.* (1985), substituting the Auroral Boundary Index for the  $Kp$  index and thereby allowing for a more self-consistent result. With the increase in computing power since 1985, a larger sample size was chosen to help ensure statistical significance of the results. In addition, much of the code had to be reproduced, which absorbed a large portion of the allotted research time. The remainder of this chapter focuses on the data, methods, techniques, and criteria used to produce a statistical auroral oval model based on the Auroral Boundary Index.

#### **Auroral Boundary Index Data**

The data for the Auroral Boundary Index was obtained from Dr. Rich for the years from 1987 through 1994. The only days with missing values were November 6, 1987 and October 27, 1992 through November 2, 1992. This didn't affect the final result, though, as those days were also missing from the DMSP data. The number of ABI values averaged out to approximately 39 per day. The data was ordered by year, day, second, and ABI value.

First, a statistical evaluation was performed on the raw ABI data. A FORTRAN program was written to read in the eight separate raw data files, sort the ABI values, and

total the number of occurrences for each value. See Figure 3.1 for the distribution of these values. Note that the occurrences are small for the lower ABI values (very high geomagnetic activity) and for the higher ABI values (very low geomagnetic activity). The peak of the distribution occurs between ABI values of 63 and 64 which is an average geomagnetic activity level. This program also attempted to evaluate this distribution of ABI values at five percent, 10 percent, and 20 percent intervals. Eventually, it was decided to not group any values into ranges, but to proceed with one degree ABI intervals. Table 3.1 lists the final zones.

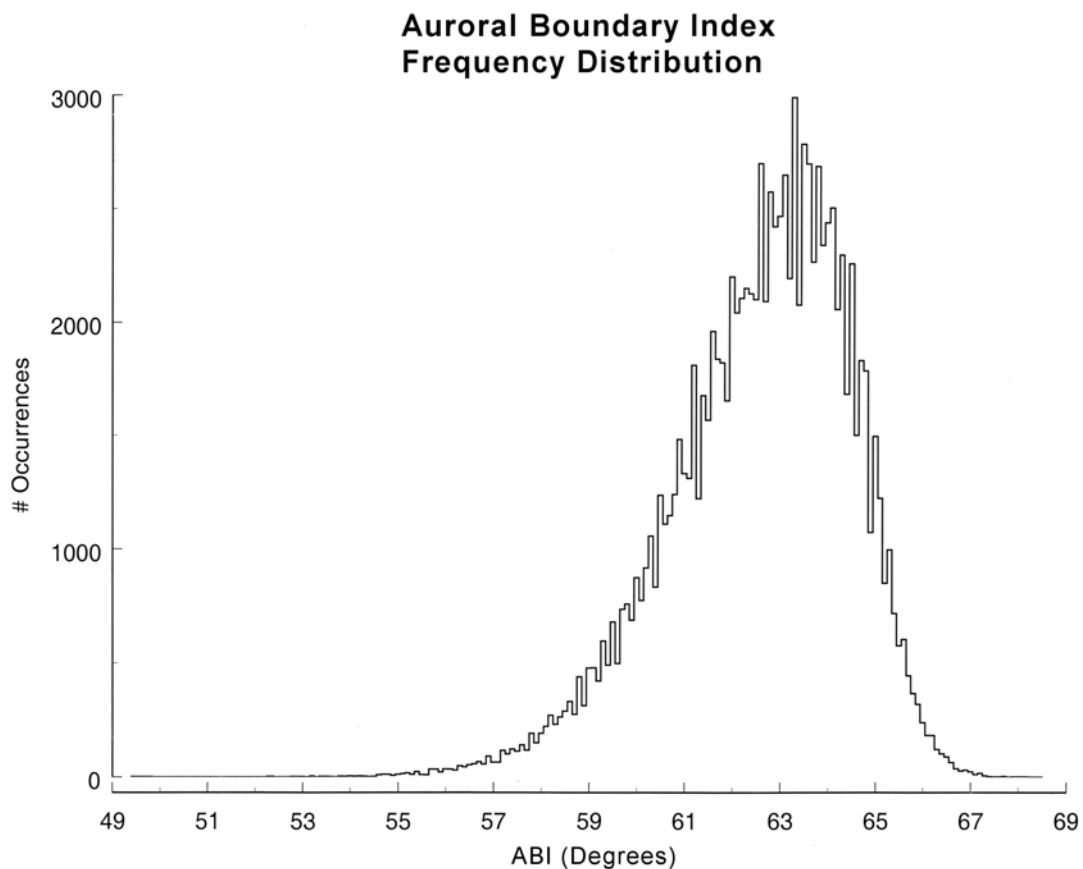


*Figure 3.1. Frequency Distribution of ABI values from 1987 to 1994*



Table 3.1. Division of ABI values into 20 zones

<b>Zone</b>	<b>ABI Range</b>	<b>Zone</b>	<b>ABI Range</b>	<b>Zone</b>	<b>ABI Range</b>
1	49 to 49.9	8	56 to 56.9	15	63 to 63.9
2	50 to 50.9	9	57 to 57.9	16	64 to 64.9
3	51 to 51.9	10	58 to 58.9	17	65 to 65.9
4	52 to 52.9	11	59 to 59.9	18	66 to 66.9
5	53 to 53.9	12	60 to 60.9	19	67 to 67.9
6	54 to 54.9	13	61 to 61.9	20	68 to 68.9
7	55 to 55.9	14	62 to 62.9		

Another FORTRAN program was written to also read in the eight separate raw data files, convert all time values from seconds to minutes of the day, and interpolate between these minute values to convert the database into one record per minute to cover an entire day. This resulted in one output file containing 4,196,160 records (1440 minutes per day times 2914 total days). This file was then used as input to associate ABI values with the differential flux data recorded by the DMSP satellites.

#### **DMSP SSJ/4 Data**

Almost 11 years of DMSP data was statistically averaged in deriving this new auroral oval model. For the DMSP F8 satellite, data was included from June 25, 1987 through August 1, 1994, which accounted for a little over seven years of the total. A total of 31 days from this time period were not used either because they were unavailable or corrupt. The following is a list of those days:

July 17-21, 1987  
November 6, 1987  
April 11, 1992  
October 27, 1992 – November 2, 1992  
June 28, 1993 – July 13, 1993  
July 29, 1994

For the DMSP F9 satellite, data was included from February 8, 1988 through December 31, 1991, which accounted for almost four years of the total. Only one day (February 18, 1988) was excluded from this time period because it was either unavailable or corrupt.

These data, also obtained from Dr. Rich, consisted of 12.6 gigabytes of raw, binary DMSP SSJ/4 data. Each record contained one minute of flight data including electron and ion spectra, along with the year, day, UT, MLT, and position in geographic and magnetic coordinates both at altitude and mapped down to 110 km. For this study, like the original Hardy model, only the electron spectra were used to create the auroral model, and data from both poles were used and averaged together.

### **Differential Flux Output**

Dr. Rich also provided an Interactive Data Language (IDL) program to read the binary DMSP SSJ/4 data files and convert the data first to counts, then to electron differential number fluxes. This program gave me a platform to create my own version of differential flux output. The code was greatly modified both in its input and its output. The basic portion of the program that manipulated the data to produce the differential flux values remained unaltered.

The original program created a color spectrogram of the differential number fluxes. The first step was to turn off this feature as only the raw differential flux numbers were needed. Next, the code was changed to allow the input of more than one file. Each day of DMSP SSJ/4 data is contained within its own file. Since there were 3986 of these files that had to be read into the program, automating the process was crucial. The program also required the input of the satellite number for each file. This was needed in

order to access the correct geometric factors data. Since each file's name included the satellite number, a portion of code was added to extract it.

One of the most important steps was associating each record of the SSJ/4 data with the ABI data. The entire file of 4,196,160 records of ABI data was read into an array and accessed by year, day, and minute to extract the ABI value for the current SSJ/4 record. This step was checked many times to ensure the correct values were being extracted.

The program allowed for the output resolution to be changed to suit the user's needs. For instance, it could be adjusted via an input parameter to produce a record for every minute of data or a record for every second of data. Since a DMSP satellite flies at approximately 7.4 km/s, one minute resolution would have skipped entire bins or at least drastically reduced the amount of differential flux values available to average in each bin. Therefore, the output of the program was set to one second resolution. However, the SSJ/4 data contained only one latitude value per minute. So another very important modification to the program was to interpolate the latitude between each minute so that each second had its own latitude.

Finally, rather than write one huge output file of differential fluxes, they were written just like the input files with one day's data per file. The final result was 3986 binary files totaling 14.7 gigabytes. Each record of data in the output files was for one second as noted above and contained all pertinent information for that second including the year, day, universal time, magnetic local time, magnetic latitude, ABI, and the differential flux values for all 20 channels.

## Integral Flux Output

To create a statistical auroral oval model, the result must be a grid containing three averaged quantities: integral number flux, integral energy flux, and average energy. The same gridding procedure that Hardy *et al.* (1985) used was followed. The goal was to try and deviate as little as possible from the original Hardy auroral model. To accomplish this, a polar projection plot was created with the center at the geomagnetic pole. Magnetic local time was divided into one-half-hour sections for a total of 48 divisions in the circumference. Geomagnetic latitude was separated into 30 divisions in the radial with  $2^\circ$  increments between  $50^\circ$  and  $60^\circ$  and between  $80^\circ$  and  $90^\circ$ . The range from  $60^\circ$  to  $80^\circ$  was incremented every  $1^\circ$ . This basic grid structure is shown in Figure 3.2.

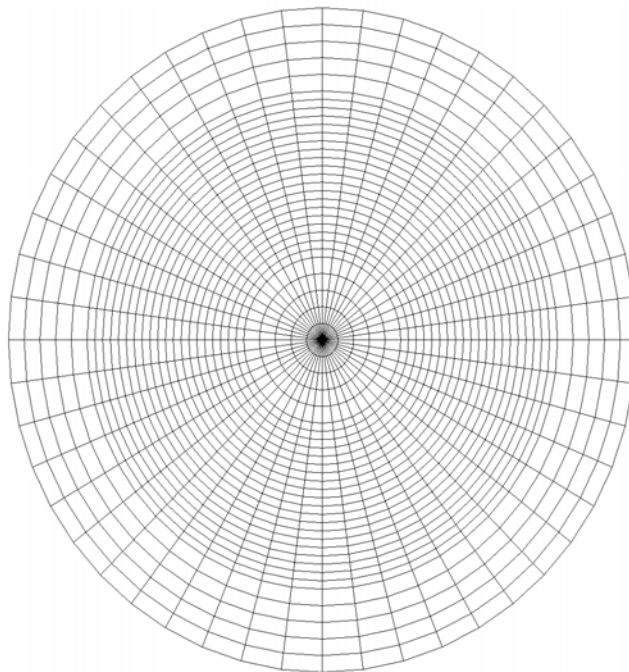


*Figure 3.2. Grid structure used in binning the ABI auroral model. 48 divisions in magnetic local time and 30 divisions in corrected geomagnetic latitude*

The reason for separating the ABI into 20 zones (or geomagnetic activity levels) is because one of these grids must be created for each of these activity levels. An IDL program was written to read in the 3986 differential flux binary files and order each flux by ABI zone, MLT, MLAT, and energy channel. Recall that each differential flux output record contains a flux for each of the 20 energy channels. Thus, for a given ABI zone, each one of the 1440 MLT/MLAT “bins” had to record 20 electron differential flux values (corresponding to the 20 channels of data). As the differential fluxes were read in, they were sorted by these criteria, and a running average was computed for each channel for all of the bins. To do this, another element of the array had to keep track of exactly how many flux values went into each channel’s average. By now, the array to handle all of this data was over 1.1 million elements. This was only possible with the massive computational and memory capacity of today’s computers.

On the preliminary run of this model, spikes in the final averages caused major problems with the smoothness of the auroral oval plots. Due to the random positioning and extreme magnitude of these spikes (two orders of magnitude larger than the next highest integral energy flux values), we deemed them as unphysical fluxes, and set out to eliminate them from the statistics. To do this, an IDL program was written to evaluate, for each channel, the occurrences of differential flux values in predefined categories. Table 3.2 lists these categories.

Table 3.2. Categories of differential flux (in units of  $\text{el}/\text{cm}^2 \text{ s sr eV}$ ) used to isolate abnormally high fluxes

Lower Limit		Upper Limit	
$>$	0	$<$	5
$\geq$	5	$<$	10
$\geq$	10	$<$	50
$\geq$	50	$<$	100
$\geq$	100	$<$	500
$\geq$	500	$<$	1000
$\geq$	1000	$<$	5000
$\geq$	5000	$<$	10000
$\geq$	10000	$<$	50000

Lower Limit		Upper Limit	
$\geq$	50000	$<$	100000
$\geq$	100000	$<$	500000
$\geq$	500000	$<$	1000000
$\geq$	1000000	$<$	5000000
$\geq$	5000000	$<$	10000000
$\geq$	10000000	$<$	50000000
$\geq$	50000000	$<$	100000000
$\geq$	100000000	$<$	500000000
$\geq$	500000000	$<$	1000000000

Only the very highest flux values for each channel were then discarded. Figure 3.3 represents the percentages where the cutoffs were made for each channel. No more than 0.00134% of the values were removed for any of the channels. This method completely eliminated the unphysical spikes and allowed the final plots to take on a more “oval-like” appearance.

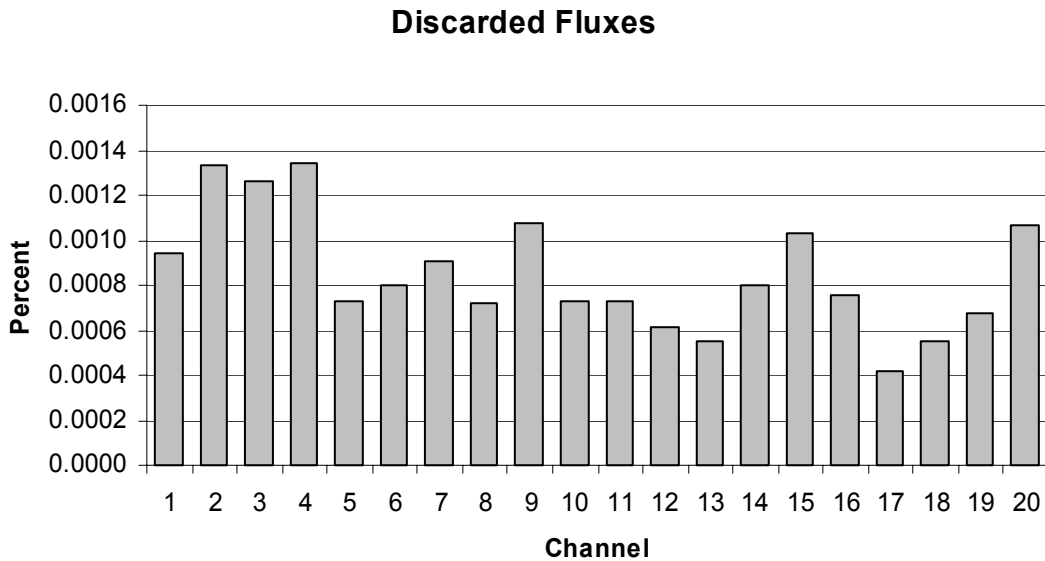


Figure 3.3. Percentage of fluxes discarded for each channel

Additionally, for unknown reasons, a small fraction of the differential fluxes were negative. Dr. Rich [pers. comm., 2004] informed us that differential fluxes of -1 can occur when the SSJ/4 instrument is turned off. However, many of the negative fluxes had absolute values greater than one. We do not yet know the source of such negative fluxes; however, since they have no physical meaning, they were also removed from our computations.

Both of these sets of discarded data accounted for only 570,185 of the over 3.1 billion fluxes evaluated. The number of negative values discarded totaled 543,645, while the high flux values discarded totaled only 26,540 or 0.000853% of the total.

Once all of the averaged channels were calculated, the integral equations were then applied to each bin for each of the 20 geomagnetic activity levels. The quantities calculated were the integral number flux in units of  $\text{el}/\text{cm}^2 \cdot \text{s} \cdot \text{sr}$  defined as:

$$J_{tot} = j(E_1)(E_2 - E_1) + \sum_{i=2}^{19} \left[ j(E_i) \cdot \frac{(E_{i+1} - E_{i-1})}{2} \right] + j(20)(E_{20} - E_{19}) \quad (3.1)$$

the integral energy flux in units of  $\text{keV}/\text{cm}^2 \cdot \text{s} \cdot \text{sr}$  defined as:

$$JE_{tot} = E_1 \cdot j(E_1)(E_2 - E_1) + \sum_{i=2}^{19} \left[ (E_i) \cdot j(E_i) \frac{(E_{i+1} - E_{i-1})}{2} \right] + E_{20} \cdot j(E_{20})(E_{20} - E_{19}) \quad (3.2)$$

and the average energy in units of keV defined as:

$$E_{ave} = \frac{JE_{tot}}{J_{tot}} \quad (3.3)$$

In these equations,  $j(E_i)$  is the average differential number flux in the  $i$ th energy channel and  $E_i$  is the central energy of the  $i$ th energy channel [Hardy *et al.*, 1985].

After the integral quantities were computed, additional smoothing was applied to the integral quantities to help reduce residual noise in the data collected by the SSJ/4 sensors. Again, this was exact procedure performed by Hardy *et al.* (1985). The following equation was applied to both the integral number flux and the integral energy flux in each bin.

$$\alpha_{ij} = \frac{3 \cdot \alpha_{ij} + \alpha_{i-1,j} + \alpha_{i+1,j} + \alpha_{i,j+1} + \alpha_{i,j-1}}{7} \quad (3.4)$$

The value ‘ $\alpha_{ij}$ ’ corresponds to an individual bin where ‘i’ is its MLT position and ‘j’ is its latitude position. For the bins at the pole (88° to 90°), the average was computed for all 48 MLT bins. Also, for the bins from 50° to 52°, the  $\alpha_{i,j-1}$  term was omitted and the sum was divided by 6 rather than 7. This smoothing equation was applied to the integral quantities three times [Hardy *et al.*, 1985].

The final step in this integral flux IDL program was to write the results to a file. It contained all pertinent information for each bin in each activity level including the ABI, MLT and latitude positions, integral flux values, average energy, and the number of fluxes that went into that bin’s average. For maximum flexibility, the file was written in both ASCII and binary. Not only were the files written containing the smoothed quantities, but also before the smoothing was applied. This will allow comparison of both if needed.

### **Hardy Auroral Model Output**

The Hardy auroral model code was also obtained through Dr. Rich. It was written in FORTRAN and with the input of the geomagnetic activity as a *Kp* index from 0 to 6, and the input of a MLT, it would write to the screen the integral quantities from 55° to



85° in increments of 5°. Slight modification to the code had to be made to allow its output to be for all MLTs so a complete auroral oval could be generated. Also, only the portions of the code that produced the integral number flux, integral energy flux, and the average energy were used. All other parts were deleted. Finally, code was added to allow for output files to be written containing the integral quantities, MLT, and MLAT for each  $Kp$ .

### **Tecplot**

Once the data files containing the integral quantities were generated, they needed to be converted into visual representations of the auroral oval. Tecplot was chosen as the plotting software to do this since it was capable of creating high-quality plots from simple XY plots to sophisticated 3-D plots from data sets of up to millions of data points. The actual auroral ovals generated by Tecplot for this thesis are 3-D contours (2-D when view from the top) and can be rotated to view at virtually any angle. For the purpose of this study, though, only the top-view is shown to make direct comparisons of different ovals easier.

To be able to generate these ovals in Tecplot, two IDL programs had to be written to convert the integral flux output files into Tecplot input files. One was written for the new ABI auroral oval model data files and one was written for the Hardy auroral model data files. Both programs were different in the files that were opened and written, but the data contained within the written files were the same.

One of the main steps when creating these Tecplot input files was to convert each bin from an MLT and MLAT coordinate system to an XY coordinate system in units of kilometers with the geomagnetic pole at the origin. This resulted in an XY plot that was

4444.444 km by 4444.444 km since each degree of latitude is 111.111 km and the radial distance was the latitude which ranged from 50° to 90°. Equations (3.5) and (3.6) accomplished these conversions for the new ABI auroral oval model. For the Hardy auroral model, the equations were the same except the MLT had to be divided by 100 (to arrive at MLT in hours and tenths of hours).

$$X = [(90 - \text{latitude}) \cdot 111.111] \cdot \cos \left[ [(\text{MLT} \cdot 15) - 90] \cdot \frac{\pi}{180} \right] \quad (3.5)$$

$$Y = [(90 - \text{latitude}) \cdot 111.111] \cdot \sin \left[ [(\text{MLT} \cdot 15) - 90] \cdot \frac{\pi}{180} \right] \quad (3.6)$$

The equations also oriented the noon MLT pointing up and the midnight MLT pointing down. As an example, a bin located at 0.50 MLT (30 minutes past midnight) and 51° geomagnetic latitude converts to an XY position of X = 565.6 km and Y = -4296.3 km.

Each Tecplot input file required a header with a title, variable names, and how the data was ordered. The values included with each file were the XY coordinates, integral number/energy flux, average energy, and the log of both the integral number and energy flux.

## **4. Results and Analysis**

### **Introduction**

With the auroral ovals generated for both models, it was possible to begin evaluating the results of reparameterizing the auroral model with the Auroral Boundary Index. This chapter focuses on analyses of the ABI auroral model ovals along with a comparison with the Hardy auroral model using actual DMSP satellite measurements.

A polar projection plot is the most practical way of displaying an auroral oval and allows for quick visual identification of patterns. They offer a complete image of the auroral oval at high latitudes. For this reason, these plots are used extensively throughout this chapter. They were generated by creating 2-D contour plots in a quasi polar coordinate system (see the section about Tecplot in Chapter 3) of the integral quantities centered on the geomagnetic pole. Note that the results represent both north and south poles as all data from both poles were used and averaged together. The edge of the plots represents  $50^\circ$  corrected geomagnetic latitude with rings spaced  $10^\circ$  apart. Local noon points upward and local midnight points downward, with dawn to the right and dusk to the left. The Earth rotates counterclockwise underneath this high latitude pattern.

### **ABI Auroral Model Ovals**

In Appendix A, the polar projection plots of the integral number flux and the integral energy flux are presented for each of the twenty levels of the ABI. The fluxes are plotted ranging from  $10^{7.5}$  to  $10^{9.5}$  in units of  $\text{el}/\text{cm}^2\cdot\text{s}\cdot\text{sr}$  for the integral number flux and units of  $\text{keV}/\text{cm}^2\cdot\text{s}\cdot\text{sr}$  for the integral energy flux. This range was chosen because it offered a very distinctive oval and helped to reduce the amount of noise and background

flux not associated with the auroral oval. It was also consistent with the magnitude of the fluxes obtained by Hardy *et al.* (1985). This range was used for all of the plots generated for continuity.

Initially, these plots were analyzed for their statistical completeness.

Unfortunately, several ovals were not complete mainly due to the infrequent nature of extremely high—or extremely low—geomagnetic activity. The bottom line is there is just not enough data for these extremes to render a statistically valid oval. Figure 4.1 shows the total number of fluxes that formed each ABI zone’s averages. For low

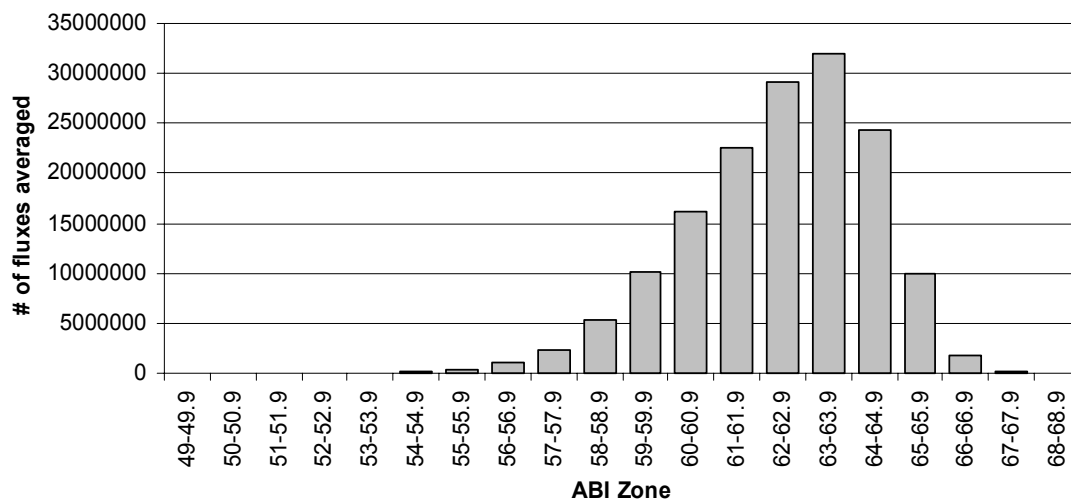


Figure 4.1. Total number of fluxes that were averaged in each ABI zone

activity, the ovals for ABI zones 67-67.9 and 68-68.9 contain too little data to be very useful. Note that these plots represent a geomagnetic activity with a “statistical”  $Kp^*$  index (see the Auroral Boundary Index section of the methodology chapter) of 0 to 0+. On the high geomagnetic activity end of the spectrum, the ABI zones from 49-49.9

through 54-54.9 ( $Kp^*$  greater than 8-) also contained too little data. The two ABI zones, 55-55.9 and 56-56.9, were transition zones from incomplete ovals to complete ovals.

Figure 4.1 shows which zones were the most statistically “complete.” These were ABI zones 57-57.9 through 66-66.9 with the number of fluxes averaged ranging from 2 to 32 million per ABI zone. The following discussion focuses mainly on these ovals.

In the polar projection plots in Appendix A, note the two triangular areas that occur between magnetic midnight and 0430 MLT ( $50^\circ$ - $70^\circ$  MLAT) and from just past magnetic noon to 1600 MLT ( $50^\circ$ - $63^\circ$  MLAT). These are due to the areas that the F8 and F9 satellite orbits cannot cover. See Figure 2.9 for the combined orbital coverage of both satellites. No data were added, or interpolation done, to try to fill in these gaps. The data are presented as acquired directly from the satellites and mapped to the nearest half hour in MLT and the nearest geomagnetic latitude as discussed in the section titled Integral Flux Output in chapter 3.

### **Hardy Auroral Model Ovals**

A complete set of integral number flux and integral energy flux ovals for the seven levels of  $Kp$  produced from the Hardy *et al.* (1985) study are presented in Appendix B. The plots are set up exactly the same as those in Appendix A so that regions of interest can be compared one to one with the same color spectrum and spatial positions. The fluxes are plotted ranging from  $10^{7.5}$  to  $10^{9.5}$  in units of  $\text{el}/\text{cm}^2\cdot\text{s}\cdot\text{sr}$  for the integral number flux and units of  $\text{keV}/\text{cm}^2\cdot\text{s}\cdot\text{sr}$  for the integral energy flux.

### **Smoothing and Removal of Non-Physical Integral Fluxes**

This section covers the results of the ABI auroral oval plots for two different methods of smoothing. The first method was discussed in the Integral Flux Output

section in Chapter 3. It was a process to rid the initial auroral oval plots of random spikes that plagued the data. Most of the time, the spikes were not apparent in the integral number flux plots, but when the integral energy flux equation was applied to the averaged differential fluxes, the errors in the data were very obvious. By eliminating only the most extreme high values and all negative values in the differential flux data, the spikes vanished and the auroral oval became visible. Figures 4.2 and 4.3 represent one ABI auroral oval before and after this first method of smoothing was applied.

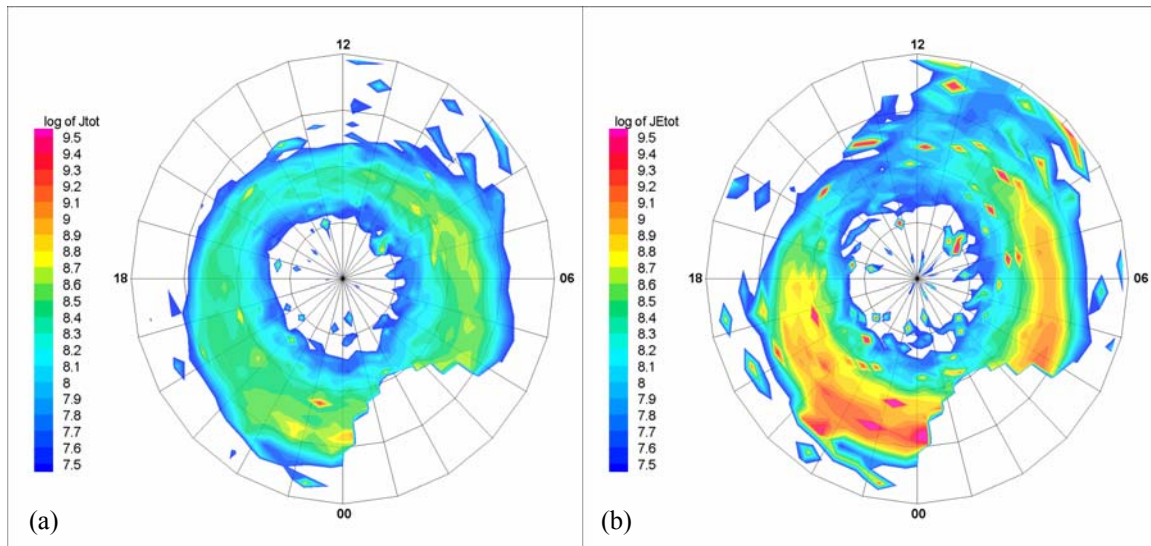


*Figure 4.2. ABI auroral model, zone 58-58.9, before discarding unphysical fluxes for (a) number flux and (b) energy flux*

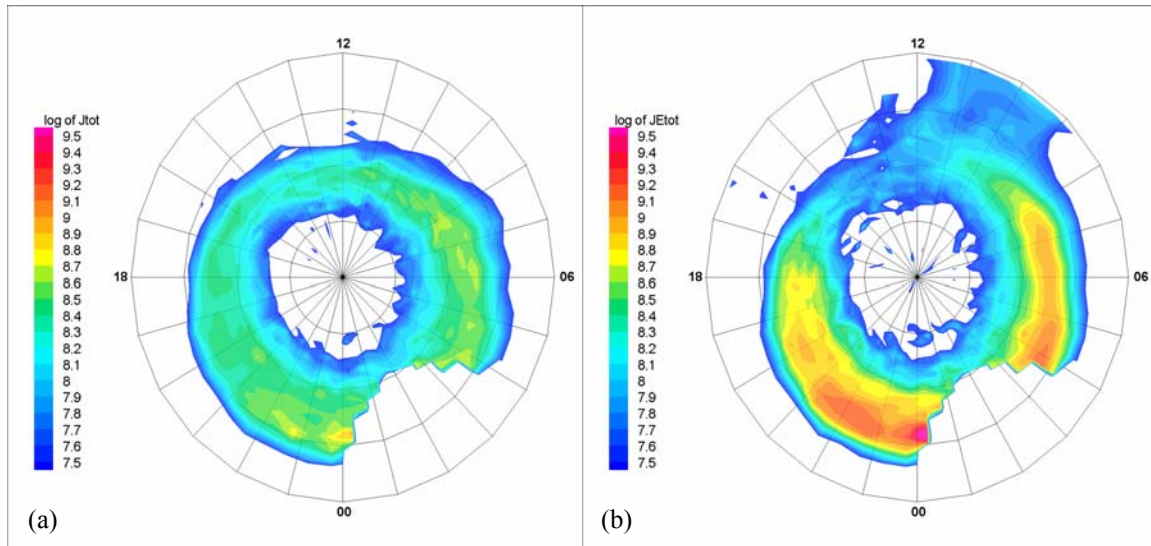


Figure 4.3. ABI auroral model, zone 58-58.9, after discarding unphysical fluxes for (a) number flux and (b) energy flux

The Integral Flux Output section in Chapter 3 also introduced the second method of smoothing. This was a procedure to smooth the integral quantities as applied in the original study by Hardy *et al.* (1985). To remain true to this original study, each bin of integral number and energy flux was smoothed according to equation 3.4. Figures 4.4 and 4.5 represent one ABI auroral oval before and after this second method of smoothing was applied and also after the first method of smoothing was applied. Appendix A contains the ABI auroral ovals for all activity levels with both methods of smoothing applied. For the remainder of this chapter, only those ovals with both methods of smoothing will be displayed, except for Figures 4.15 through 4.26 which show the line plots for both the smoothed and unsmoothed grids.

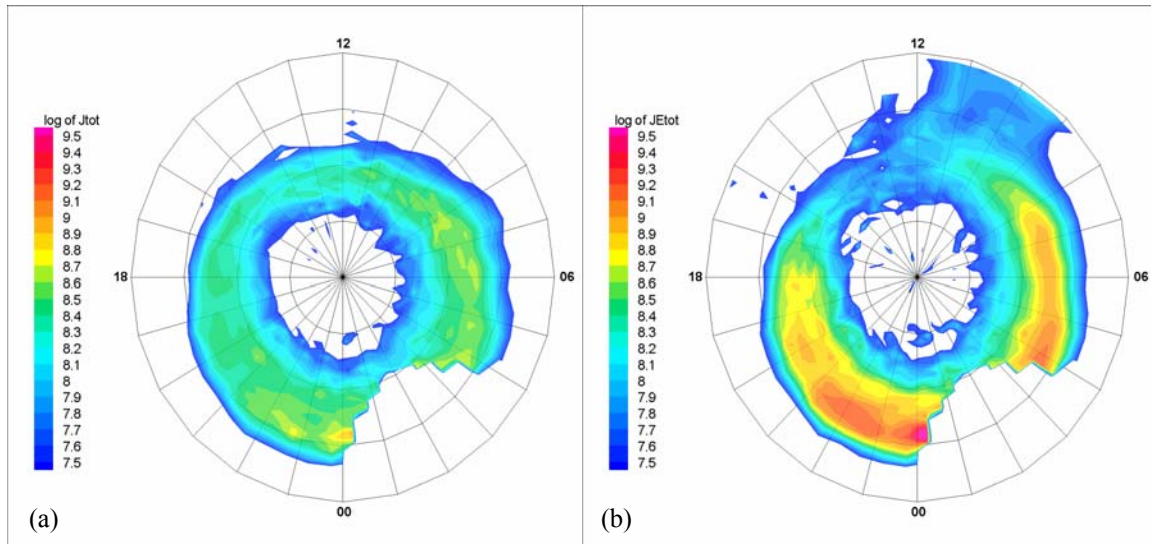


Figure 4.4. ABI auroral model, zone 58-58.9, prior to bin smoothing for (a) number flux and (b) energy flux

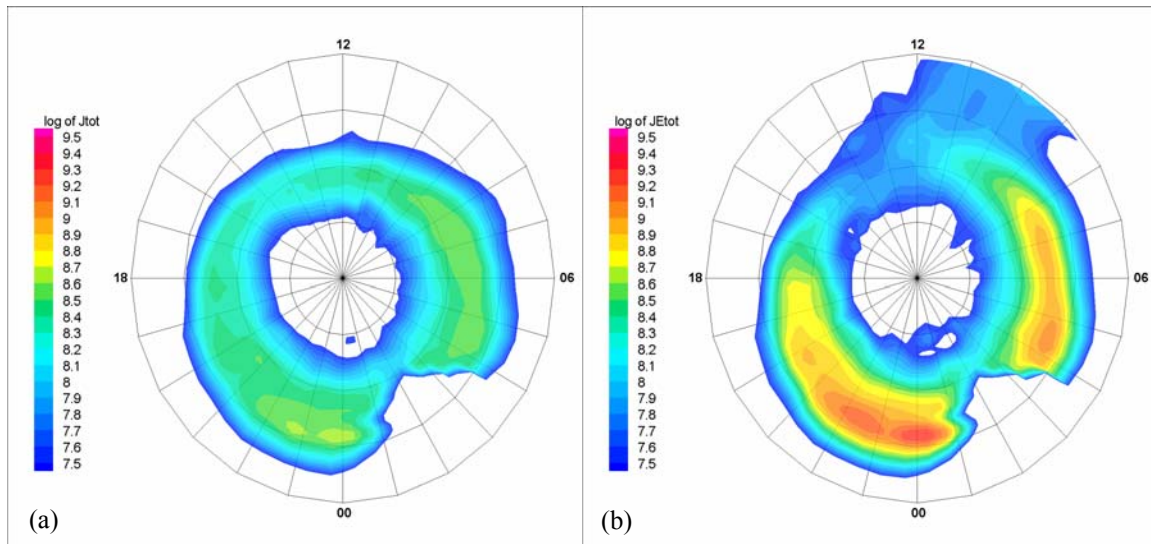


Figure 4.5. ABI auroral model, zone 58-58.9, after bin smoothing for (a) number flux and (b) energy flux

### Discussion of Features on ABI Auroral Model Plots

The next three sections discuss the general features found on the ABI auroral model plots located in Appendix A. Where applicable, the Hardy auroral model plots are



shown at comparable activity levels. To determine the appropriate Hardy oval to compare against the ABI model output, Table 2.4 was used to choose the statistical  $Kp^*$  value corresponding to the ABI range (zone) of interest.

***Integral Number Flux Plots.***

Figures 4.6 and 4.7 compare the ABI and Hardy model integral number flux for two different ABI ranges (zones). Figure 4.6(a) is for an ABI range of 65 to 65.9 degrees; this equates to a  $Kp^*$  of 1, and so the Hardy model for the  $Kp = 1$  case is shown in Figure 4.6(b). Likewise, Figure 4.7(a) is for the ABI range of 58 to 58.9 degrees, which equates to a  $Kp^*$  of about 6. The statistically “complete” ABI ovals fall between these two extremes of ABI values. Both figures show excellent overall agreement between the two models with respect to the shape and magnitudes of auroral features. Also, both models seem to respond in very similar fashion as the level of magnetic activity rises. However, as discussed previously, one can also see the post-midnight absence of F-8 and F-9 data in the ABI auroral ovals, especially visible in Figure 4.7(a). To achieve a complete comparison between the two models, one would have to devise a reasonable method to “fill in” this data-starved region.

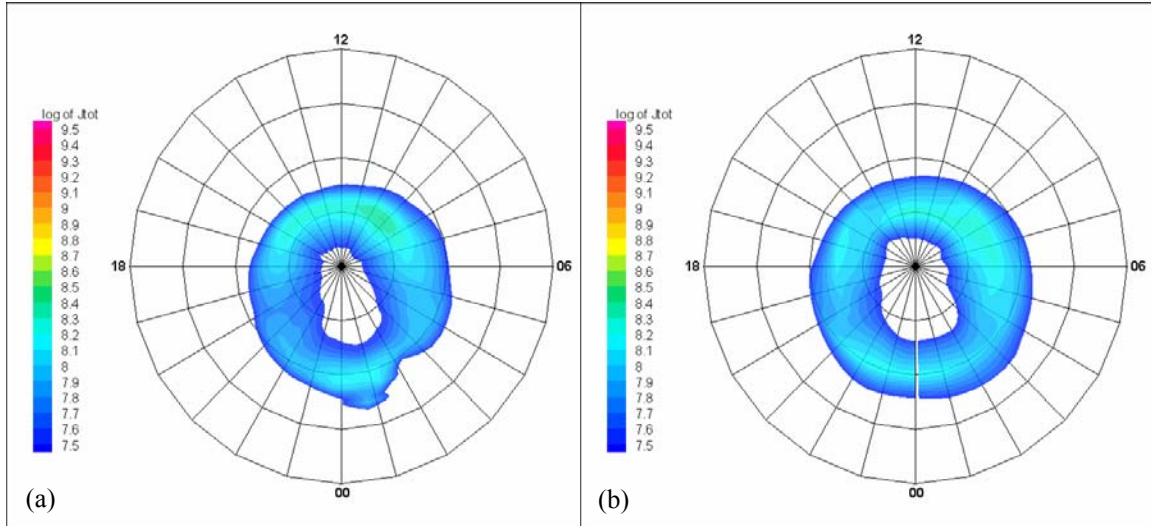


Figure 4.6. Number flux for (a) ABI auroral model, zone 65-65.9 and (b) Hardy auroral model,  $Kp = 1$

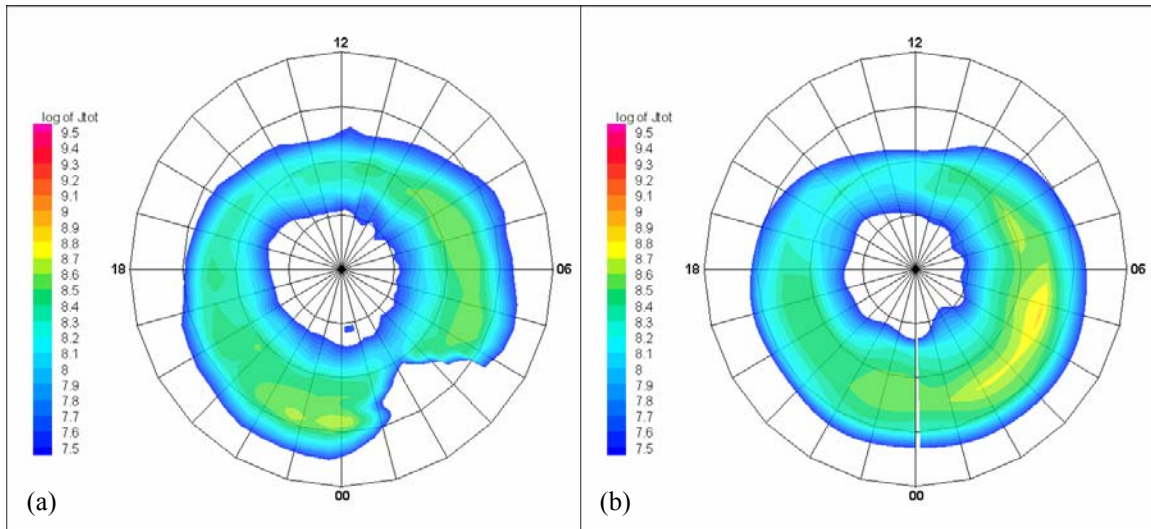


Figure 4.7. Number flux for (a) ABI auroral model, zone 58-58.9 and (b) Hardy auroral model,  $Kp = 6$

### ***Integral Energy Flux Plots.***

Figures 4.8 and 4.9 compare the ABI model versus Hardy integral energy flux pattern for the same ABI (and  $Kp^*$ ) ranges as shown in Figures 4.6 and 4.7, respectively. The overall agreement between the Hardy and ABI results is still very good, but not as

close as in the integral number fluxes. Higher energy fluxes occur on the night side of the both ovals between  $60^\circ$  and  $70^\circ$  latitude. Similar to the results obtained by Hardy *et al.* (1985), the high energy flux region forms a horseshoe shape with the base centered at approximately 0200 MLT. Unlike the results by Hardy *et al.*, though, the peak in ABI energy flux appears to occur premidnight, however, this may be due only to the cutout in data postmidnight and cannot be resolved at this time. As the magnetic activity level increases, the energy flux into the night side oval also increases and the entire oval expands equatorward towards lower latitudes. This is apparent in Figures 4.9(a) and 4.9(b) with a comparison of the ABI auroral model to the Hardy auroral model at high activity. Note how the ABI auroral oval expands slightly more equatorward on the night side than the Hardy oval. On the dayside in both figures, however, the ABI model has a much more extended region of low-energy background fluxes. It is possible that such low flux values were also present in the original Hardy model, but were simply excluded when the model was computerized.

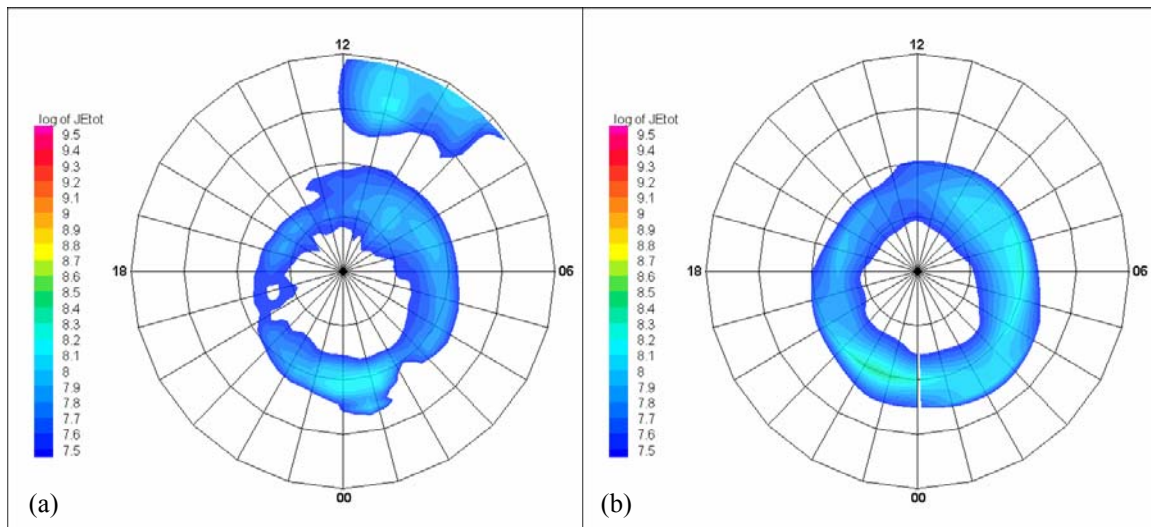


Figure 4.8. Energy flux for (a) ABI auroral model, zone 65-65.9 and (b) Hardy auroral model,  $K_p = 1$

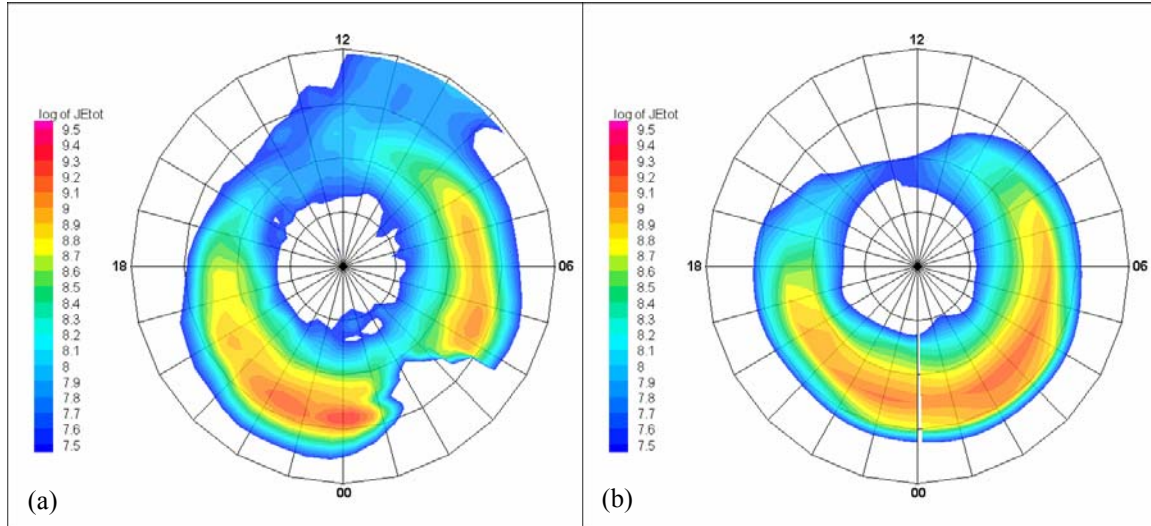


Figure 4.9. Energy flux for (a) ABI auroral model, zone 58-58.9 and (b) Hardy auroral model,  $K_p = 6$

### Average Energy Plots.

There are a few characteristics to point out on the average energy plots. Only a few of the plots are included in this section. They are divided into cool electrons ( $E_{\text{ave}} \leq 600$  eV) and hot electrons ( $E_{\text{ave}} \geq 600$  eV) [Hardy *et al.*, 1985]. Each ABI zone is compared to its equivalent  $K_p^*$  from Table 2.4.

The plots of the cool electrons (Figures 4.10(a) and 4.10(b)) show a minimum as a crescent shaped region poleward of the auroral oval, centered around noon, and positioned between  $75^\circ$  and  $85^\circ$ . The ABI auroral model and the Hardy auroral model compare very well both in location and magnitude of this minimum.

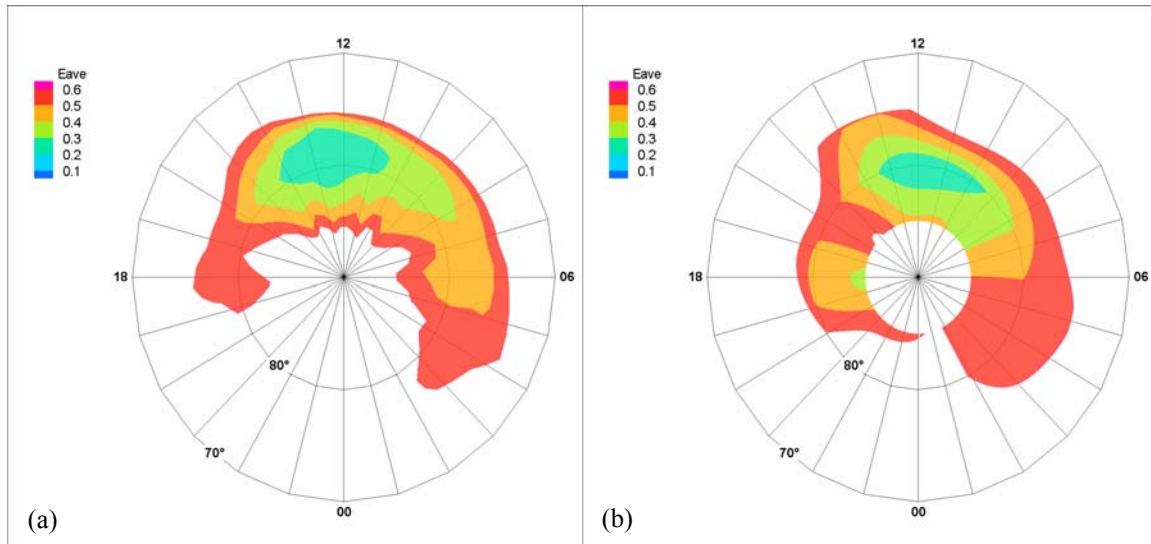


Figure 4.10. Average energy, cool electrons for (a) ABI auroral model, zone 63-63.9 and (b) Hardy auroral model,  $K_p = 3$

In the plots of the hot electrons (Figures 4.11(a) and 4.11(b)) there exists a maximum close to prenoon and positioned between  $60^\circ$  and  $70^\circ$  latitude. Another maximum also lies premidnight and is located between  $60^\circ$  and  $70^\circ$  latitude. The band of maximum average energy corresponds well with the position of the actual auroral oval for both the ABI auroral model and the Hardy auroral model.

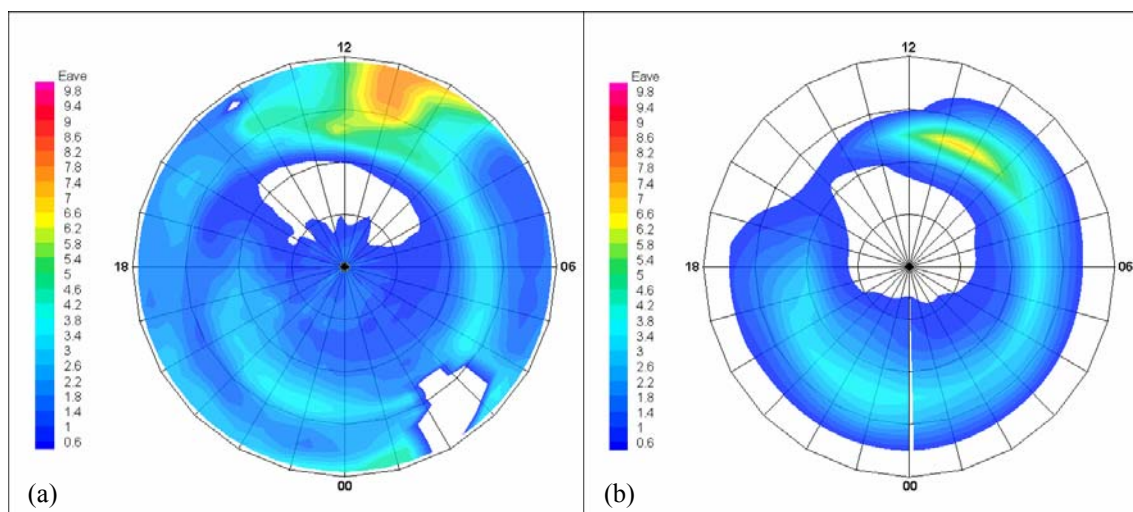


Figure 4.11. Average energy, hot electrons for (a) ABI auroral model, zone 59-59.9 and (b) Hardy auroral model,  $K_p = 5$

## DMSP Passes

Having established the general agreement between the ABI and Hardy models through visual comparisons, we now quantitatively assess the differences between the two models via comparisons with actual DMSP data from individual satellite passes.

The raw differential flux data from selected DMSP F8 and F9 passes were used to compute the integral fluxes in the same manner as for the derived ABI auroral model. Initially, the integral fluxes from the individual passes were not smoothed. Therefore, many spikes and valleys exist in the raw DMSP data which must be taken into account when comparing them to the statistical data of the two models. Next, Tecplot was used to smooth the DMSP passes to try and reduce noise and lessen discontinuities in the DMSP data. The DMSP fluxes were smoothed three times with each pass shifting the flux at each data point towards an average of the flux at its neighboring data points.

Line plots of integral flux value versus magnetic latitude were generated for each separate DMSP polar pass. Each line of data is separated by color for each model or DMSP pass; red corresponds to the actual data obtained from the DMSP pass, green corresponds to the Hardy auroral model based on the *actual*  $Kp$  index (*not* the statistical  $Kp^*$ ), and blue corresponds to the ABI oval extracted from the actual ABI value for the DMSP pass. In all of the line plots, evening/night is on the left side and morning/day is on the right.

The satellite passes were chosen where the ABI values were in the 57-67 degree range to ensure comparison with a statistically complete ABI oval. Passes were selected from the DMSP data by searching for days that had fairly consistent  $Kp$  and ABI values. Then an individual pass was used from that day. A total of three passes were chosen with



varying  $Kp$  and ABI values. They are listed by date from lowest to highest activity level and are: April 12, 1992 (F8), July 12, 1988 (F9), and April 6, 1994(F8). Figures 4.12, 4.13, and 4.14 illustrate the exact locations of the DMSP paths and their correspondence with the integral number flux and integral energy flux of both the ABI auroral ovals and the Hardy auroral ovals.

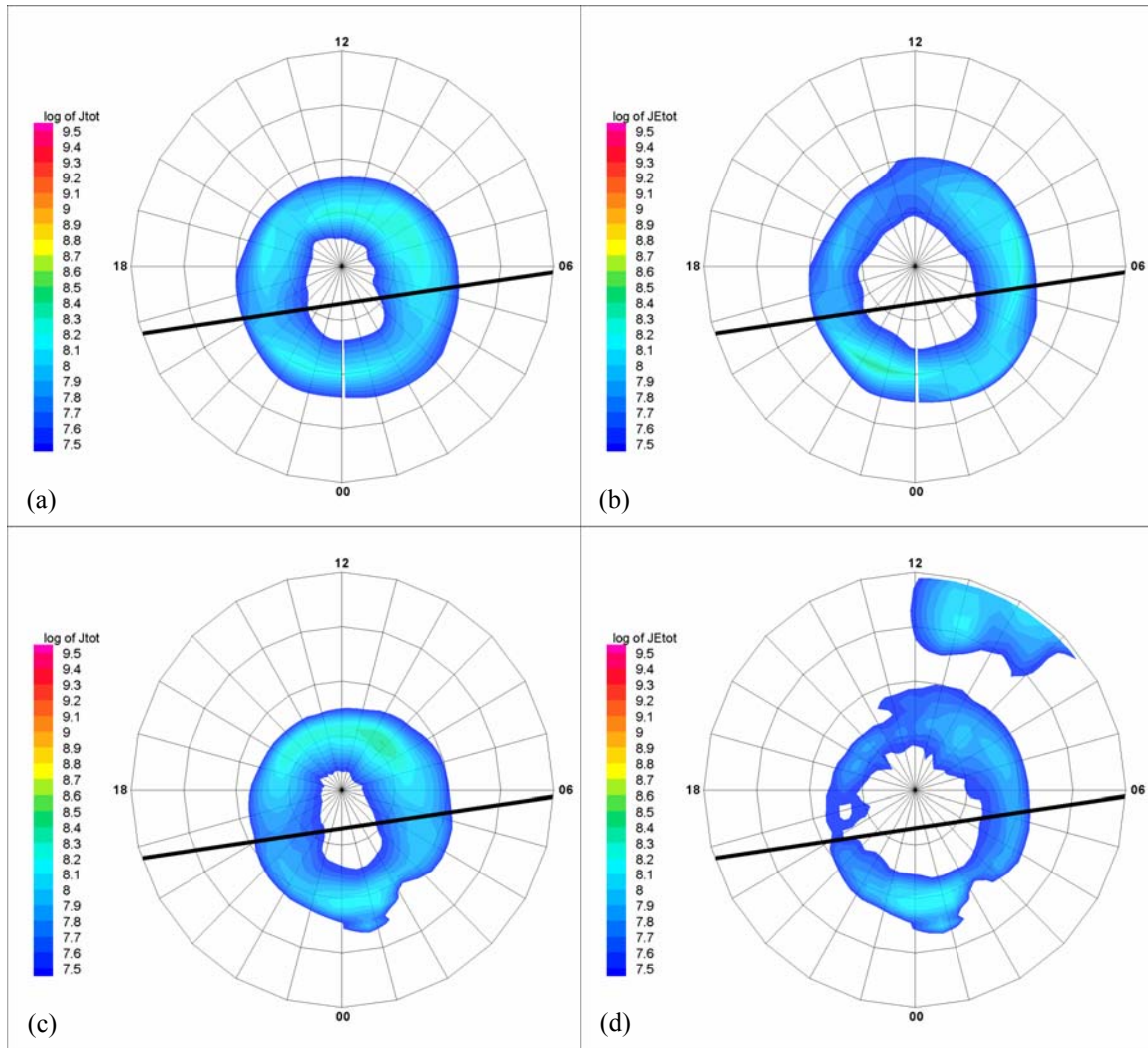


Figure 4.12. April 12, 1992 DMSP F8 pass overlaid on (a) Hardy auroral model,  $Kp = 1$ , number flux (b) Hardy auroral model,  $Kp = 1$ , energy flux (c) ABI auroral model, zone 65-65.9, number flux (d) ABI auroral model, zone 65-65.9, energy flux

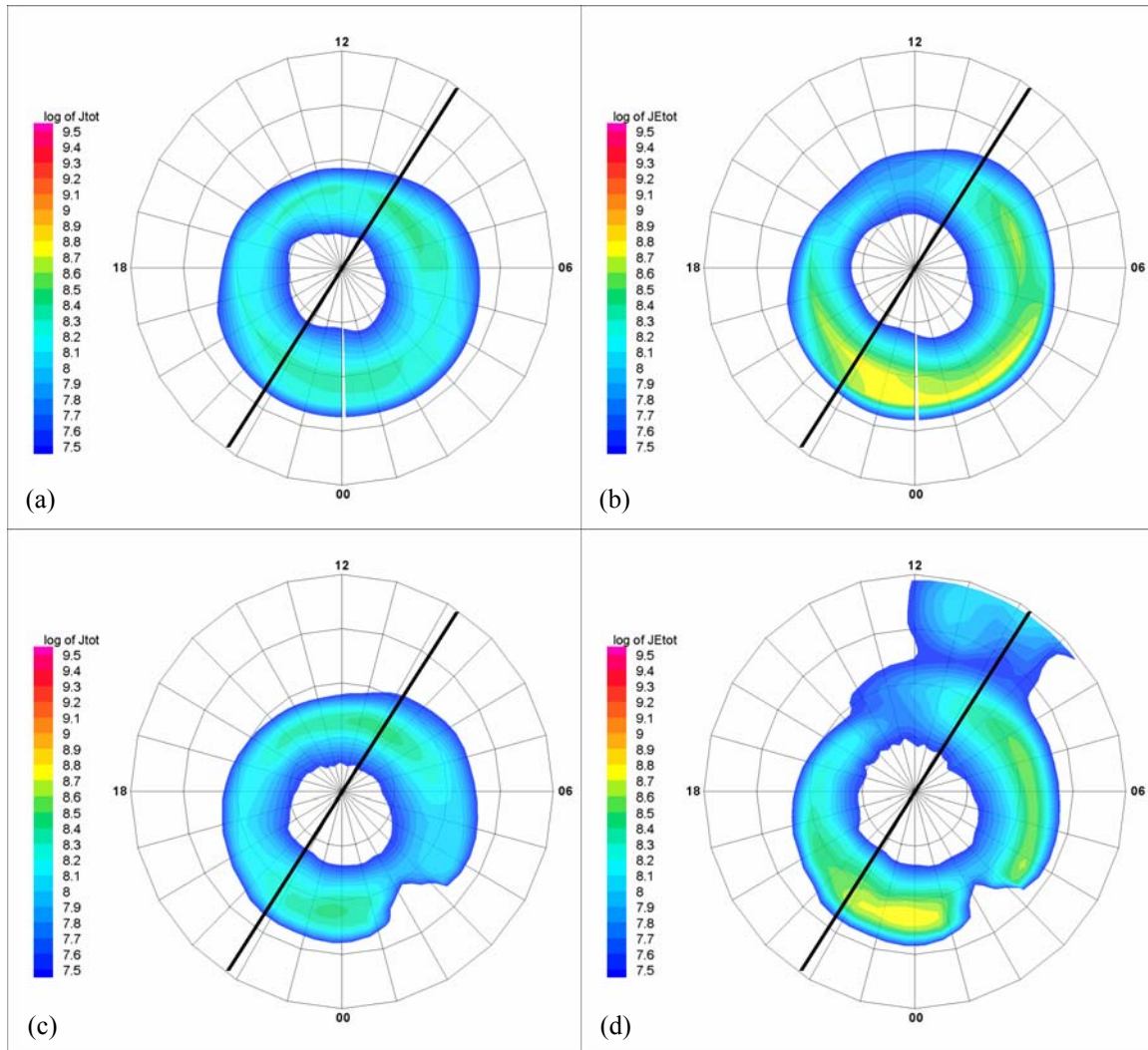


Figure 4.13. July 12, 1988 DMSP F9 pass overlaid on (a) Hardy auroral model,  $K_p = 3$ , number flux (b) Hardy auroral model,  $K_p = 3$ , energy flux (c) ABI auroral model, zone 62-62.9, number flux (d) ABI auroral model, zone 62-62.9, energy flux

The DMSP data and ABI values used in these comparisons were acquired from Dr. Rich at AFRL and the  $K_p$  values were obtained from the World Data Center for Magnetism website.



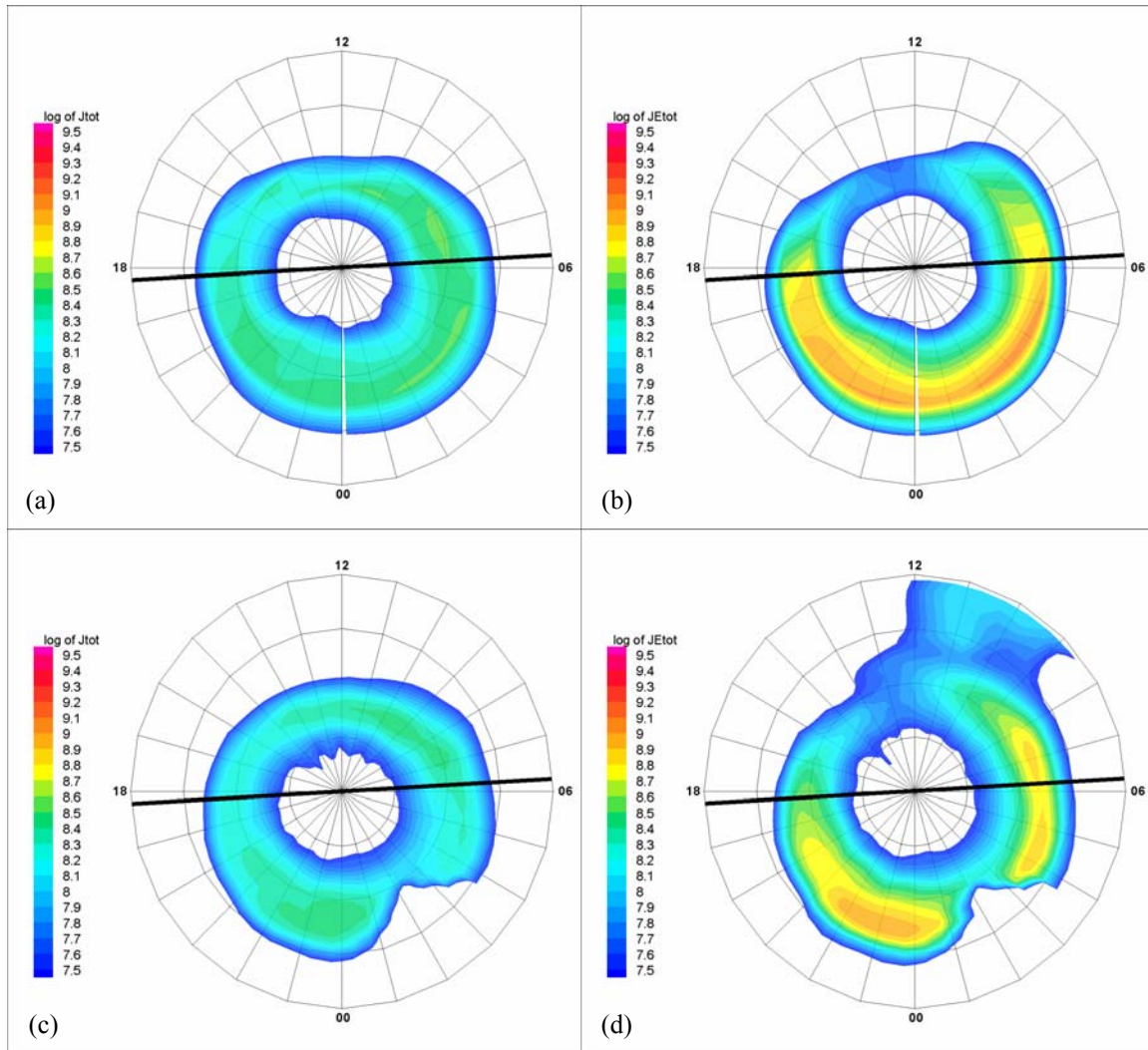


Figure 4.14. April 6, 1994 DMSP F8 pass overlaid on (a) Hardy auroral model,  $K_p = 5$ , number flux (b) Hardy auroral model,  $K_p = 5$ , energy flux (c) ABI auroral model, zone 60-60.9, number flux (d) ABI auroral model, zone 60-60.9, energy flux

#### ***April 12, 1992 DMSP Pass.***

The time of this F8 pass occurred between 1055 UT and 1120 UT in the meridian from 1915 MLT to 0545 MLT. The  $K_p$  averaged to 1 for the entire day with the individual values shown in Table 4.1. The  $K_p$  was reported as 1 during the time of the actual pass, so the  $K_p = 1$  plot is the one used in this comparison. The actual ABI was between 65 degrees and 64.5 (this second value computed for a time seven minutes

before the end of the pass). Therefore, the ABI zone of 65 – 65.9 was used in this comparison since the majority of the pass was at 65 and also this ABI matches better with the statistical  $Kp^*$  of 1 as shown in Table 2.4.

*Table 4.1.  $Kp$  values for April 12, 1992*

UT	$Kp$	UT	$Kp$
0000 – 0300	0+	1200 – 1500	1+
0300 – 0600	2-	1500 – 1800	1+
0600 – 0900	1	1800 – 2100	1-
0900 – 1200	1	2100 - 2400	1-

Figures 4.15 and 4.16 show the raw DMSP F8 data for April 12, 1992 compared with the Hardy auroral model and the smoothed and unsmoothed ABI auroral model. In both of the figures, the equatorward boundaries of the ABI auroral model were consistently higher in latitude than the Hardy auroral model, but correlated better to the DMSP boundaries. Also, the ABI auroral model levels off to background flux magnitudes at similar latitudes as DMSP, but always at a higher flux value. DMSP measured larger gradients than the two models at the equatorward edges of both the integral number flux and integral energy flux. For the peak oval energy fluxes, the Hardy auroral model was a closer match to actual DMSP peak flux levels.

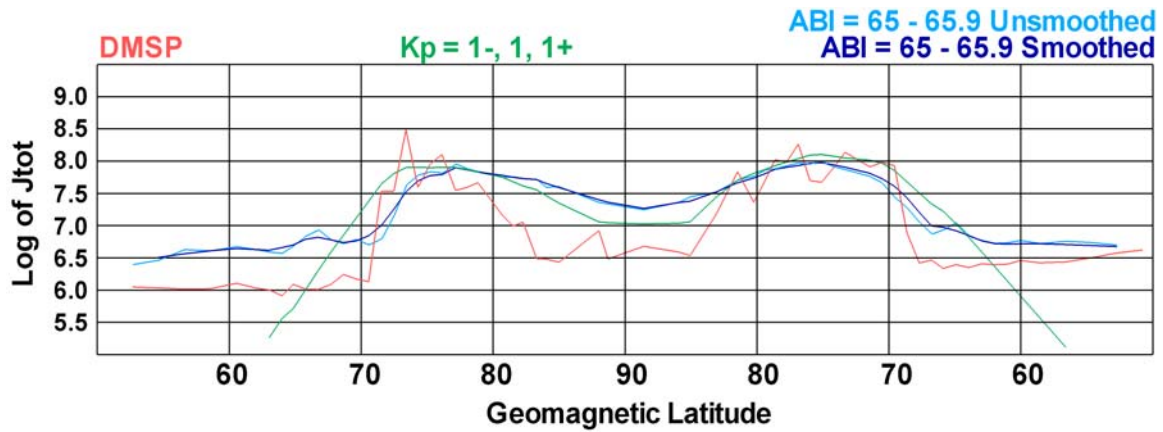


Figure 4.15. April 12, 1992 actual DMSP F8 data compared to ABI auroral model and Hardy auroral model, magnetic latitude vs. number flux

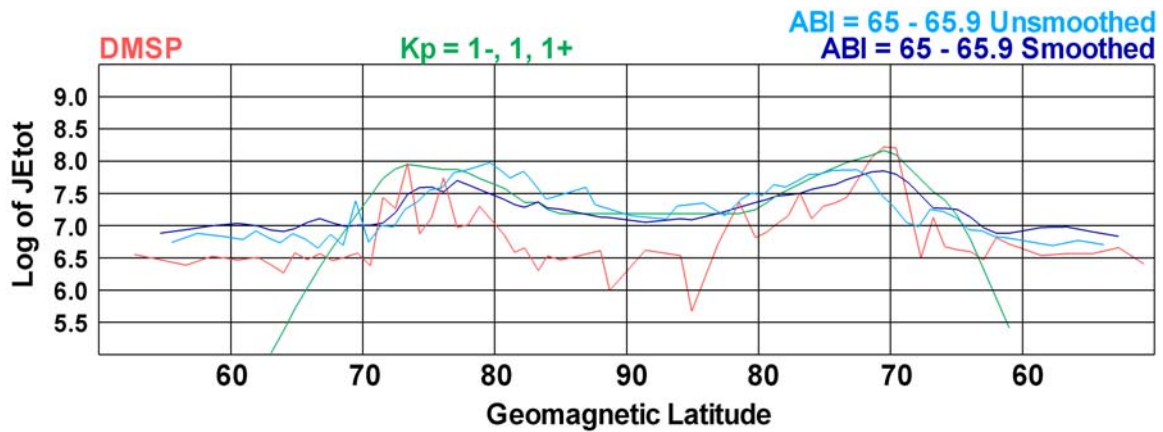


Figure 4.16. April 12, 1992 actual DMSP F8 data compared to ABI auroral model and Hardy auroral model, magnetic latitude vs. energy flux

As noted before, the April 12, 1992 DMSP F8 fluxes were next smoothed slightly to achieve a better consistency with the smoothed statistical models. Figure 4.17 of the integral number flux shows both models actually match up much better with DMSP, especially the peak fluxes. The energy flux in Figure 4.18 indicates a much better match of the ABI auroral model to DMSP. Naturally this smoothing process also has the

negative effect of “blurring” the actual DMSP pass equatorward boundaries (which is exactly the shortcoming of the Hardy model!).

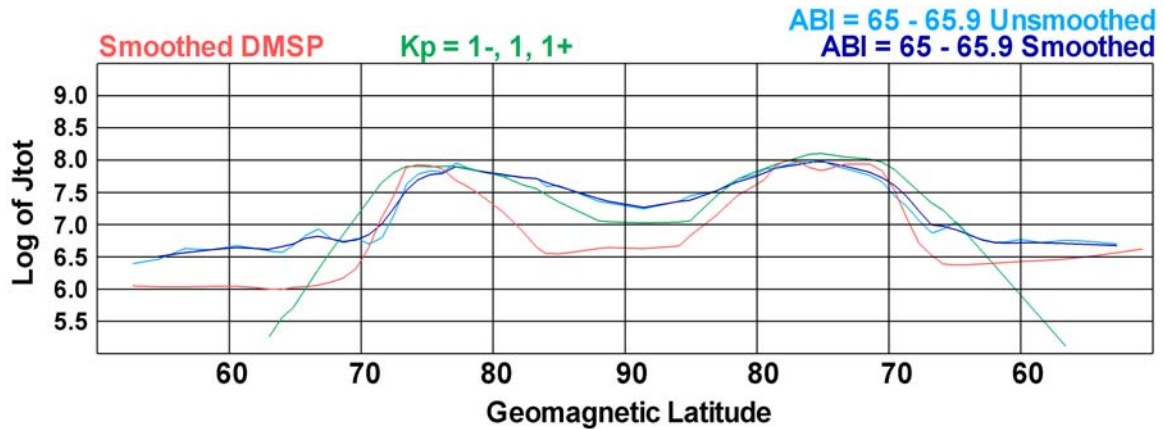


Figure 4.17. April 12, 1992 smoothed DMSP F8 data compared to ABI auroral model and Hardy auroral model, magnetic latitude vs. number flux

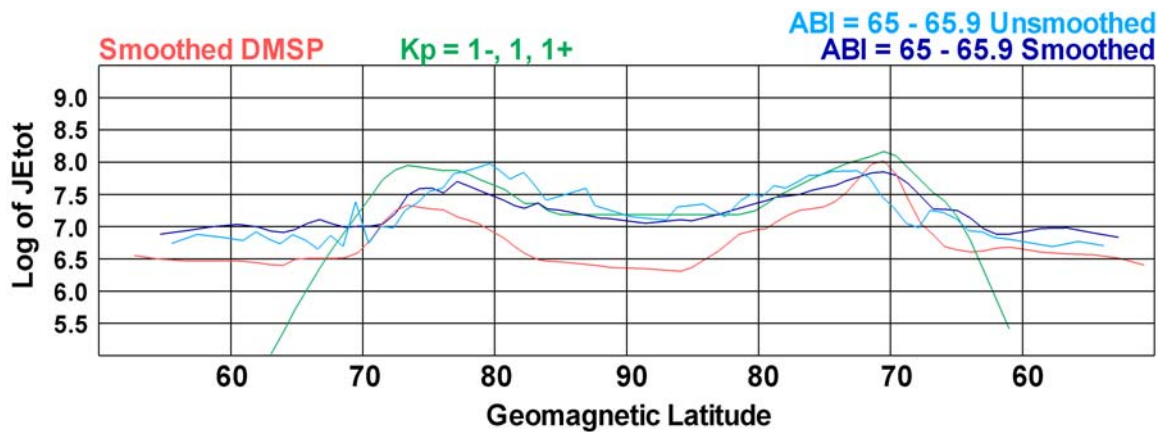


Figure 4.18. April 12, 1992 smoothed DMSP F8 data compared to ABI auroral model and Hardy auroral model, magnetic latitude vs. energy flux

#### July 12, 1988 DMSP Pass.

The time of this F9 pass occurred between 0306 UT and 0329 UT in the meridian from 2145 MLT to 1045 MLT. The  $K_p$  averaged to 3 for the entire day with the

individual values shown in Table 4.2. The  $Kp$  was reported as 3 during the time of the actual pass, so the  $Kp = 3$  plot is the one used in this comparison. The actual ABI was between 63.5 degrees and 62.5 degrees (this second value computed for a time eighteen minutes before the end of the pass). Therefore, the ABI zone of 62 – 62.9 was used in this comparison since the majority of the pass was at 62.5 and also this ABI matches well with a statistical  $Kp^*$  of 3 as shown in Table 2.4.

*Table 4.2.  $Kp$  values for July 12, 1988*

UT	$Kp$	UT	$Kp$
0000 – 0300	3-	1200 – 1500	3+
0300 – 0600	3	1500 – 1800	2+
0600 – 0900	3+	1800 – 2100	3+
0900 – 1200	3	2100 - 2400	3

Figures 4.19 and 4.20 show the raw DMSP F9 data for July 12, 1988 compared with the Hardy auroral model and the smoothed and unsmoothed ABI auroral model. In both of the figures, the gradients of both models at the equatorward edge of the oval on the night side were similar to DMSP but consistently occurred at lower latitudes than DMSP. Both models were a close match to the peak flux of the DMSP data. In Figure 4.19, the equatorward boundaries of the ABI auroral model almost match exactly with the Hardy auroral model. On the poleward boundaries, both models are a good match to the average DMSP flux. Both models were too low in peak flux on the integral number flux chart. For the integral energy flux in Figure 4.20, there was a larger variation in flux between DMSP and the two models, especially on the day side equatorward boundary (right side of the plot).

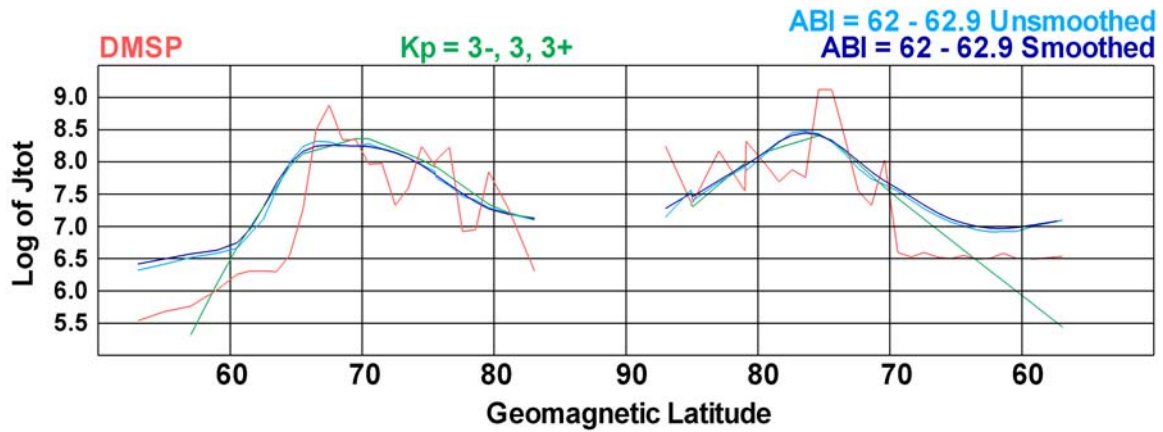


Figure 4.19. July 12, 1988 actual DMSP F9 data compared to ABI auroral model and Hardy auroral model, magnetic latitude vs. number flux

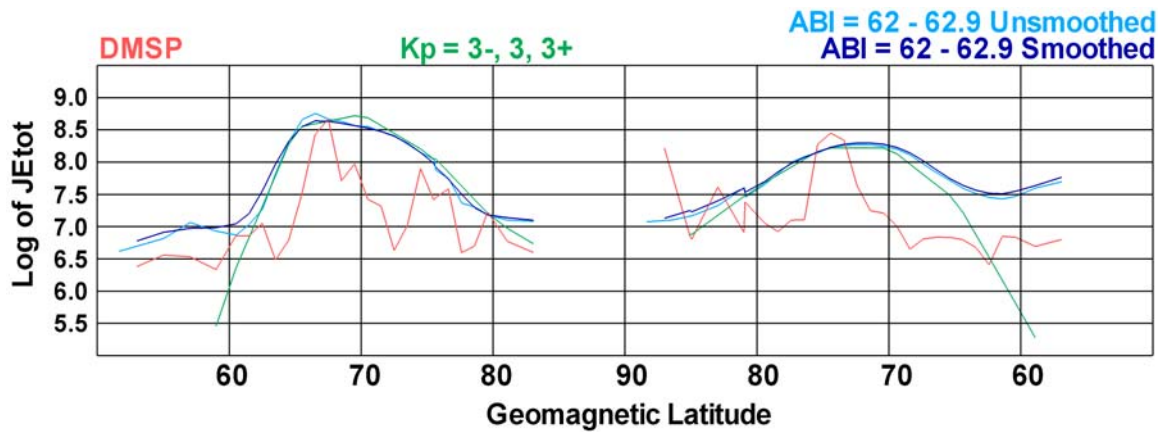


Figure 4.20. July 12, 1988 actual DMSP F9 data compared to ABI auroral model and Hardy auroral model, magnetic latitude vs. energy flux

Figures 4.21 and 4.22 are the smoothed DMSP F9 data for July 12, 1988 compared with both models. Again, the models match up better with DMSP in number flux than energy flux. The poleward boundaries on the number flux plot, Figure 4.21, indicate very good correlation of the models with DMSP. The DMSP integral flux data in Figure 4.22, smoothed out to values well below both models.

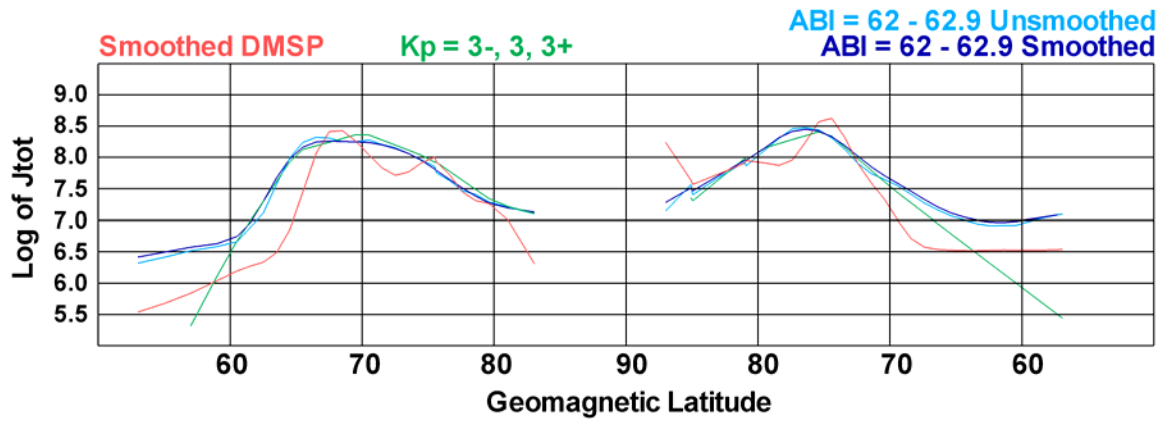


Figure 4.21. July 12, 1988 smoothed DMSP F9 data compared to ABI auroral model and Hardy auroral model, magnetic latitude vs. number flux

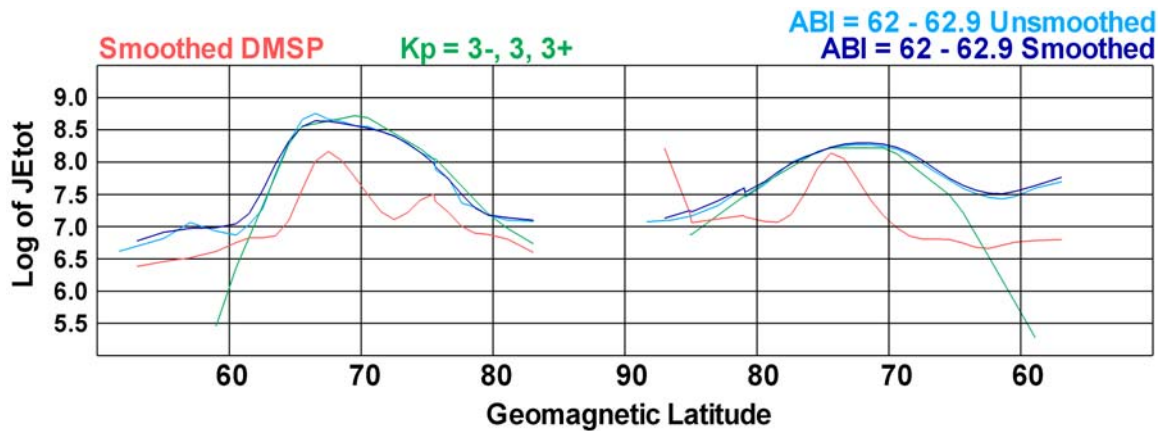


Figure 4.22. July 12, 1988 smoothed DMSP F9 data compared to ABI auroral model and Hardy auroral model, magnetic latitude vs. energy flux

#### April 6, 1994 DMSP Pass.

The time of this F8 pass occurred between 0625 UT and 0646 UT in the dawn to dusk meridian. The  $K_p$  averaged to 5 for the entire day with the individual values shown in Table 4.3. The  $K_p$  was reported 5+ during the time of the actual pass, so the  $K_p = 5$  plot is the one used in this comparison. The ABI was 60.7 for the entire time interval of



the pass. Therefore, the ABI zone 60 – 60.9 was used in this comparison which also matches well with a statistical  $Kp^*$  of 5 as shown in Table 2.4.

*Table 4.3.  $Kp$  values for April 6, 1994*

UT	$Kp$	UT	$Kp$
0000 – 0300	5-	1200 – 1500	5
0300 – 0600	4+	1500 – 1800	5+
0600 – 0900	5+	1800 – 2100	5
0900 – 1200	5+	2100 – 2400	5

Figures 4.23 and 4.24 show the raw DMSP F8 data for April 6, 1994 compared with the Hardy auroral model and the smoothed and unsmoothed ABI auroral model. In the two figures, both models tend to follow the DMSP curve very closely on the poleward boundaries. Both models were also a very good match to the data on the day side equatorward boundaries (right side of the plot), but the ABI auroral model did slightly better on the night side equatorward boundaries (left side of the plot). For the energy flux, Figure 4.24, both models were very similar to DMSP on both the day side equatorward and poleward boundaries.

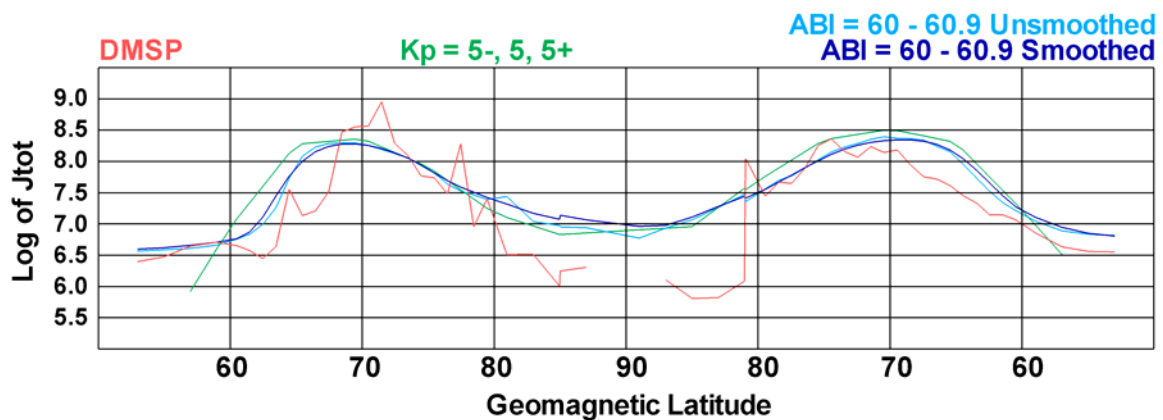


*Figure 4.23. April 6, 1994 actual DMSP F8 data compared to ABI auroral model and Hardy auroral model, magnetic latitude vs. number flux*



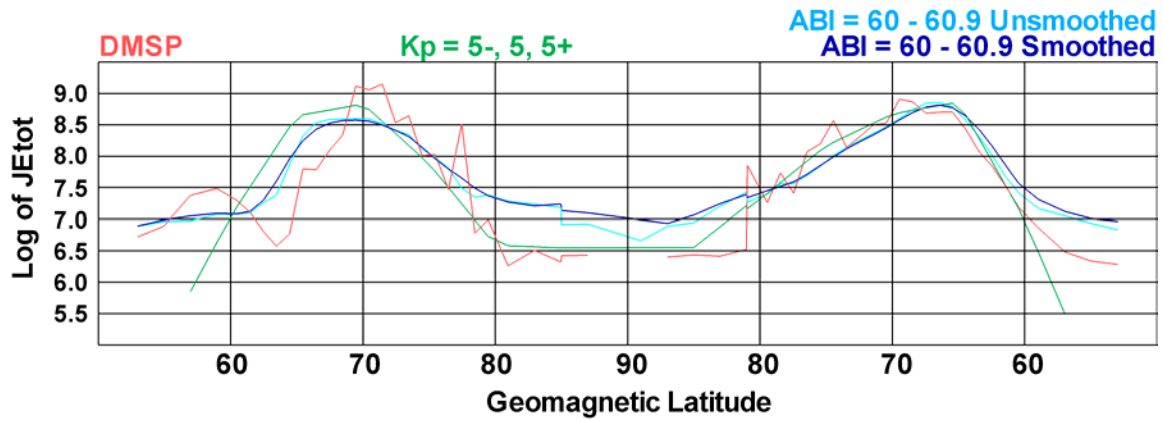


Figure 4.24. April 6, 1994 actual DMSP F8 data compared to ABI auroral model and Hardy auroral model, magnetic latitude vs. energy flux

Figures 4.25 and 4.26 are the smoothed DMSP F8 data for April 6, 1994. Again, both models correspond very well to the poleward boundaries on both plots. The equatorward boundary on the day side in energy flux is the only one that was very similar. The other model equatorward boundaries are still too low in latitude relative to the DMSP pass; however, as in the other April F8 comparison, the ABI model is a better match to the latitude of the actual equatorward boundary than is the Hardy model.

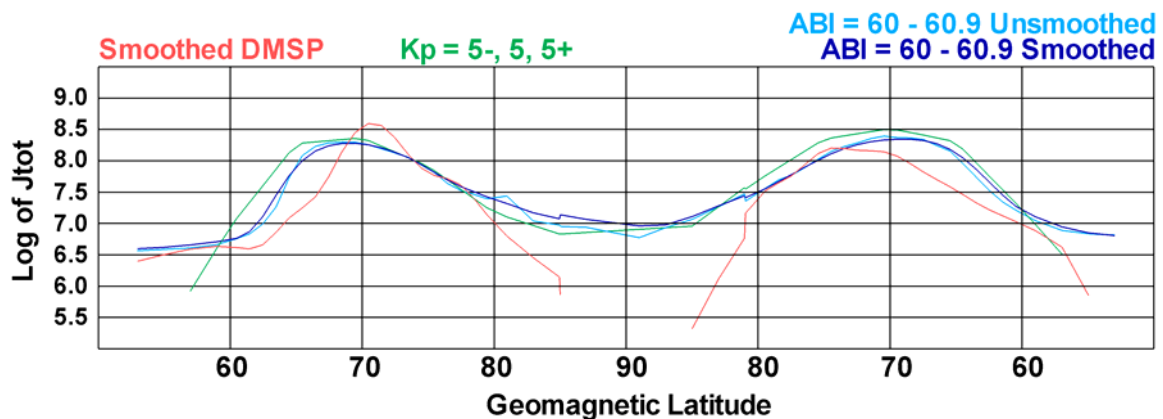


Figure 4.25. April 6, 1994 smoothed DMSP F8 data compared to ABI auroral model and Hardy auroral model, magnetic latitude vs. number flux

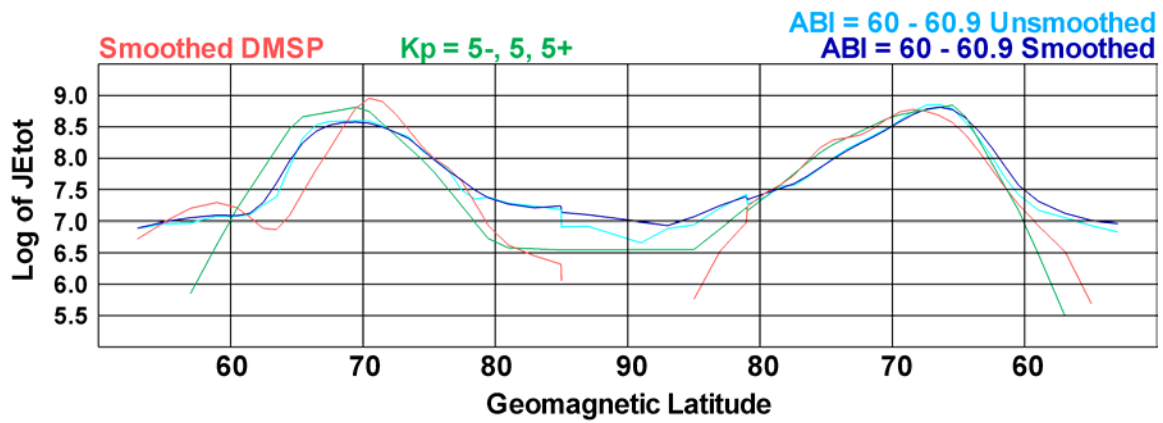


Figure 4.26. April 6, 1994 smoothed DMSP F8 data compared to ABI auroral model and Hardy auroral model, magnetic latitude vs. energy flux

Overall, both models are surprisingly similar in all the comparison cases, especially noting that completely different data sets and parameters were used in their creation.

## 5. Conclusions and Further Study

The position and intensity of the auroral oval has many implications for the Air Force from determining the effects of incoming electron flux on DoD systems to modeling the ionosphere to exploit current HF communications capabilities.

This study used the ABI index to parameterize the statistics of the auroral oval location. This is in contrast to the Hardy *et al.* (1985) work which used  $Kp$  as the “binning” parameter. Thus, the current work represents a move toward a more self-consistent—and presumably more accurate—climatological representation of the auroral oval boundaries. Refinements of our initial results will be necessary; however, preliminary findings suggest that the new ABI auroral oval model is, at worst, comparable to the results achieved by Hardy *et al.* Further refinement of this new model based on the ABI should increase its effectiveness and offer a more reliable alternative as an auroral oval model.

DMSP spacecraft have been flown since the mid 1970s and all of the different satellites have carried precipitating particle spectrometer sensors from the SSJ/2 to the SSJ/5. All future DMSP spacecraft or their replacements will most likely continue to carry similar sensors. Since the ABI is derived directly from observed fluxes measured by DMSP, availability of the index should not be a problem.

Creating a model to predict the location and magnitude of the auroral oval is a very challenging topic. Even though we used a different “binning” parameter than the Hardy *et al.* (1985) study, our study still utilized the Hardy methodology (where possible) in an effort to achieve some measure of consistency between the two models.

Additionally, a special emphasis was placed on using a larger database to make the results as statistically significant as possible. Consequently, a large portion of this research effort was devoted to generating and troubleshooting the code to ingest the gigabytes of data to produce graphical representations of the auroral ovals based on geomagnetic activity levels.

The analysis of the results involved polar projection plots to give visual interpretations of the ovals and line plots to directly compare the results to the Hardy auroral model and actual DMSP observations. Surprisingly, the ovals based on the ABI were very similar to those obtained by Hardy based on  $Kp$ .

### **Recommendations for Further Research**

Several refinements are possible and/or warranted before the new ABI auroral model would enter service as a driver of space weather computer models. First and foremost, the poor statistics of the incomplete ABI ranges (49 through 56.9 and 67 through 68.9) must be “filled in.” Several possibilities are immediately apparent. First, it is likely that some of the one-degree ABI ranges may represent comparable geophysical conditions, and therefore lend themselves to being combined into a single (larger) ABI zone. Such a procedure could also help bolster the statistics on the high end of the ABI scale (i.e., very quiet activity levels). However, it would not be wise to apply this at the low end of the scale (very disturbed conditions), since relatively small changes in ABI may reflect very different geophysical conditions. Second, we could employ an “aliasing” scheme to combine data from different bins whose magnetic latitude difference and ABI difference are equal [Rich, pers. comm., 2003]. For example, for a given MLT, one could combine the differential fluxes from a bin at 60 degrees MLAT (55 – 55.9 ABI

range) together with those data from the bin at 62 degrees MLAT (57 – 57.9 ABI range). Naturally, one would have to set judicious limits on the number of bins to combine. Finally, the “gaps” in the F-8 and F-9 DMSP coverage between 00-04 MLT and 50°-70° MLAT, and 12-16 MLT and 50°-63° MLAT, must also be remedied. The Hardy auroral model must have compensated for this same problem, but the present research did not address this issue.

For the ABI ovals that are already statistically complete, the results of this study and those produced by Hardy *et al.* (1985) are qualitatively very similar. Further, the DMSP pass comparisons provide a first method of quantitative comparison; however, more can be done in this area. One method would be to form difference fields between an ABI auroral oval and a Hardy auroral oval of comparable activity levels. This subtraction of the fluxes would reveal the exact locations and magnitudes of the differences between the two models.

Another approach to test our ABI auroral results would be a comparison against the self-consistent auroral model of Sotirelis & Newell (2000). Their model used the degree of magnetotail stretching as the “binning” parameter, and averaged together only those fluxes similarly located relative to auroral boundaries. Even though my research effort averaged all regions of electron precipitation strictly by MLAT and MLT, the comparison should nonetheless be informative.

In order to more fully test the accuracy of this model, though, more comparisons should be performed against actual DMSP auroral measurements. Due to limited time constraints in completing this study, only three DMSP passes could be extracted and compared. Increasing the number of these comparisons should prove this model’s ability

to consistently provide an auroral oval pattern that is a close approximation to the actual oval boundaries.

Once the complete ABI auroral oval model is achieved, the final step toward operational use is to convert the model into a computational format that can be accessed by space physics computer codes.

## Appendix A: ABI Auroral Model Polar Projection Plots

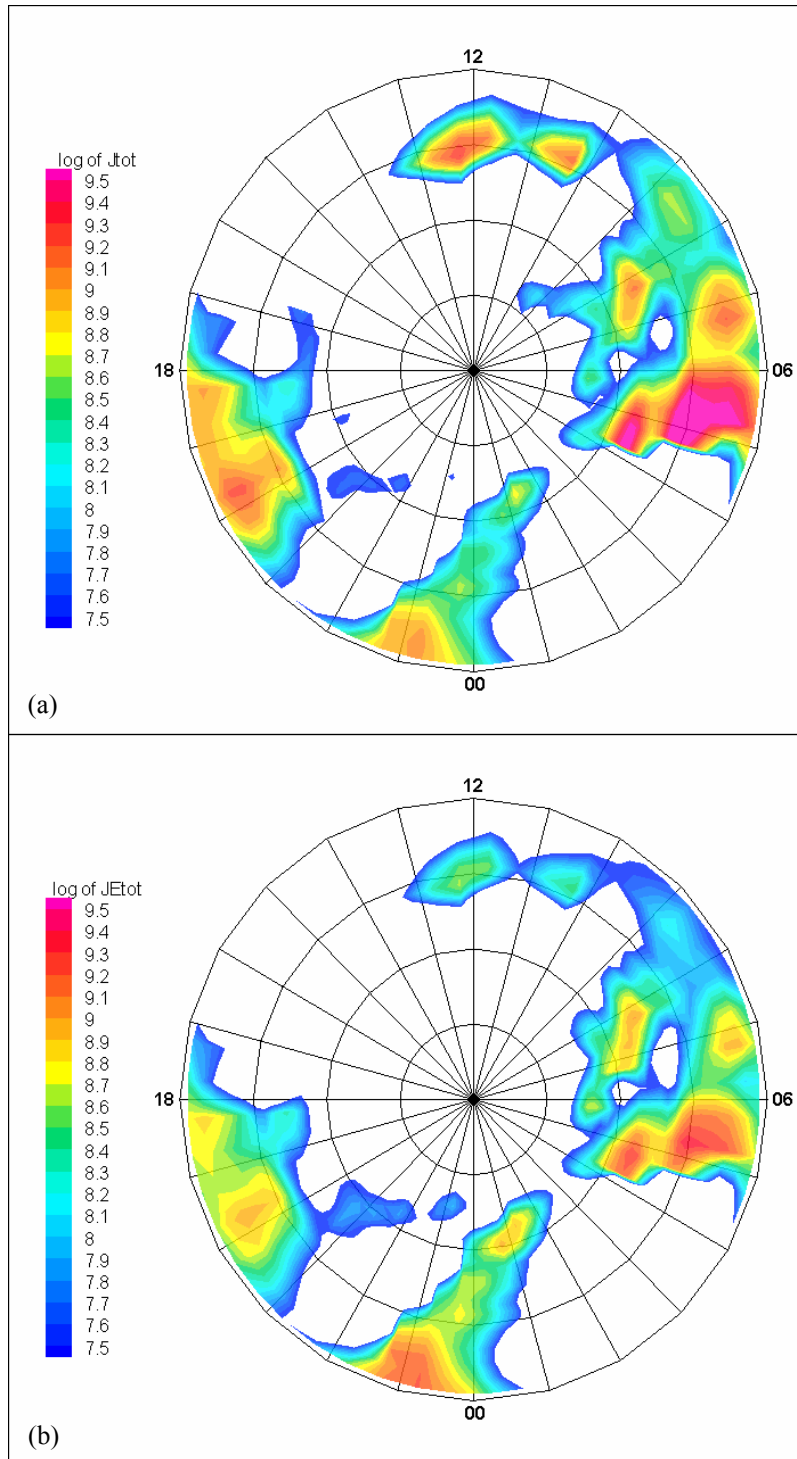


Figure A.1. ABI auroral model zone 49-49.9 for (a) number flux and (b) energy flux

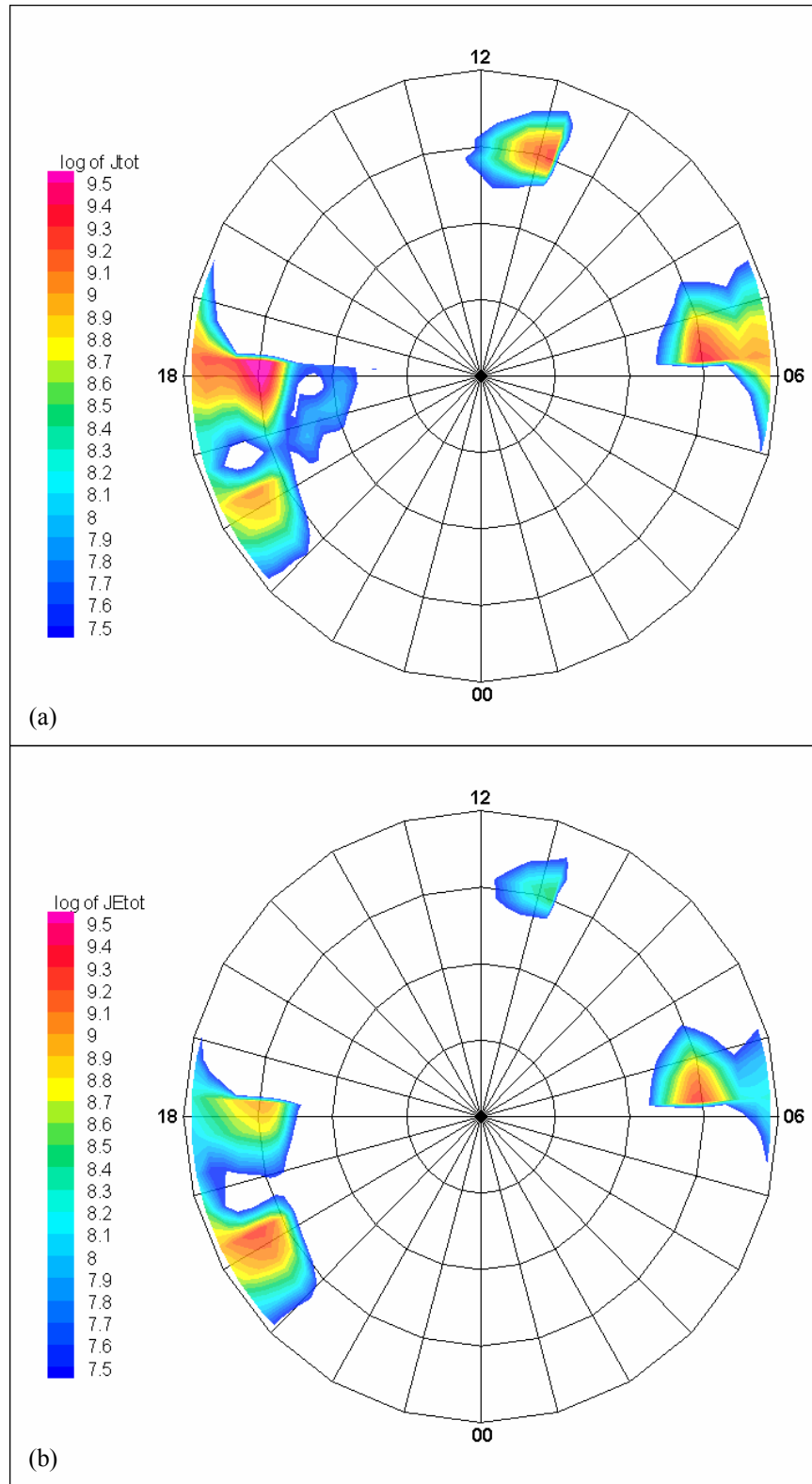


Figure A.2. ABI auroral model zone 50-50.9 for (a) number flux and (b) energy flux



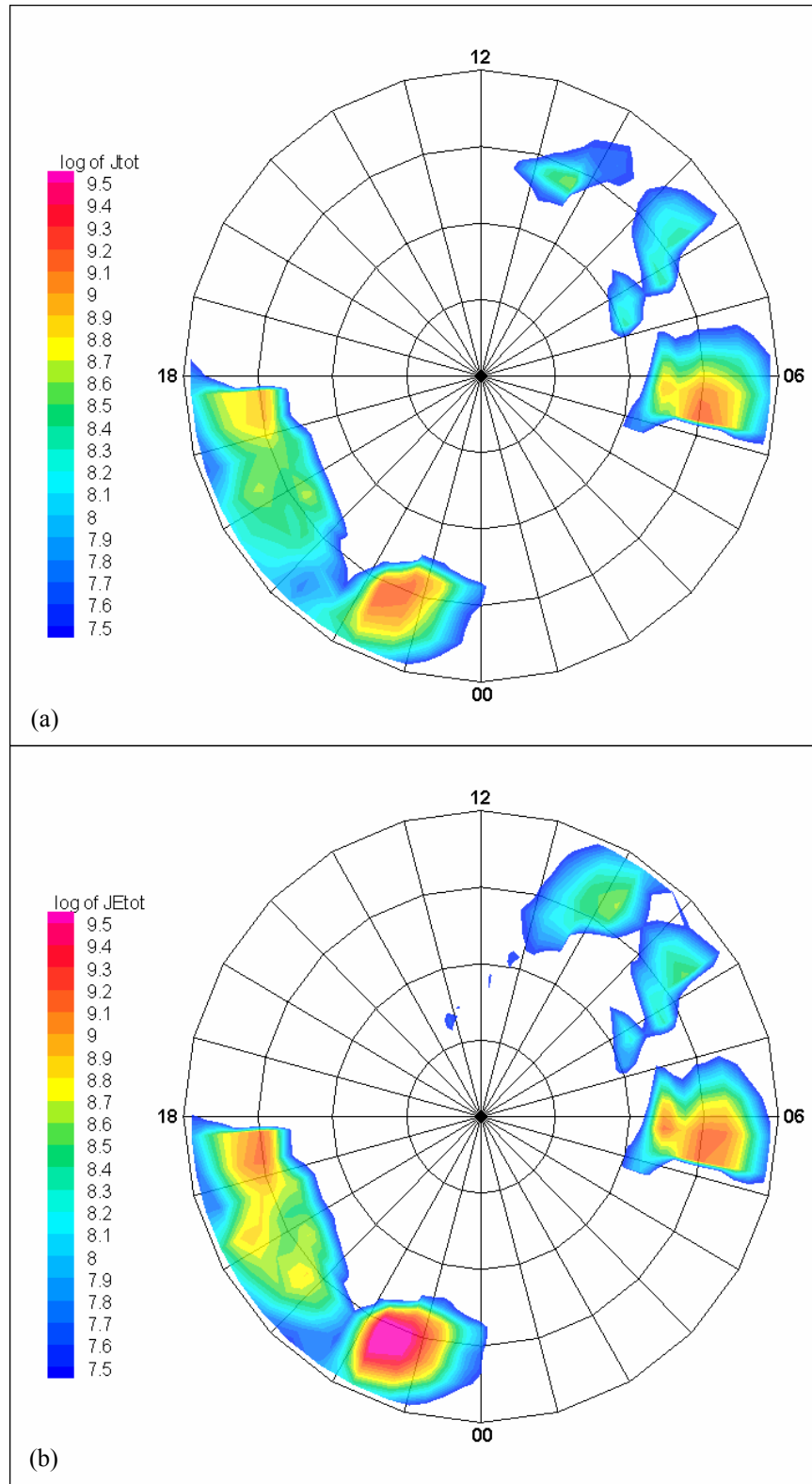


Figure A.3. ABI auroral model zone 51-51.9 for (a) number flux and (b) energy flux

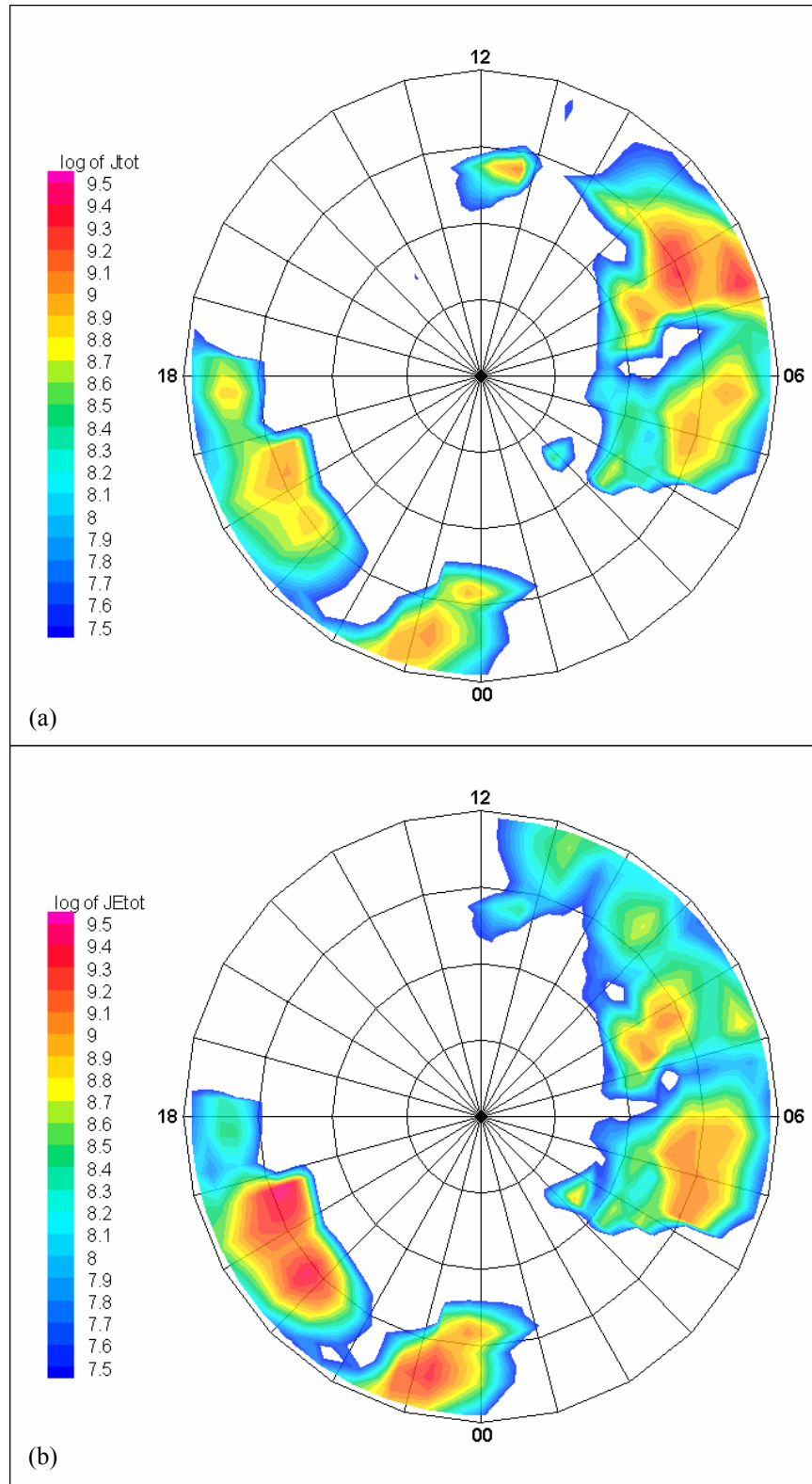


Figure A.4. ABI auroral model zone 52-52.9 for (a) number flux and (b) energy flux

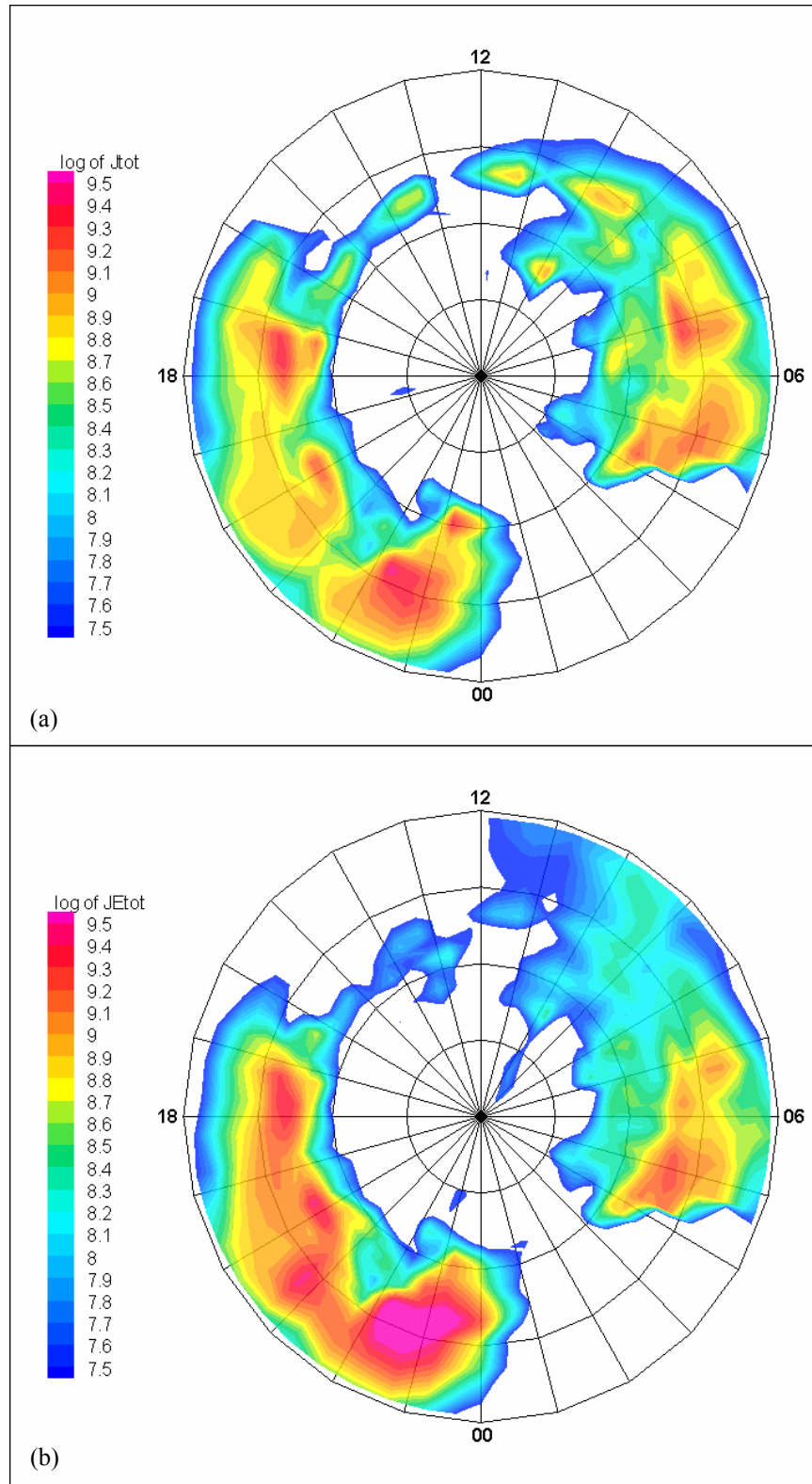


Figure A.5. ABI auroral model zone 53-53.9 for (a) number flux and (b) energy flux

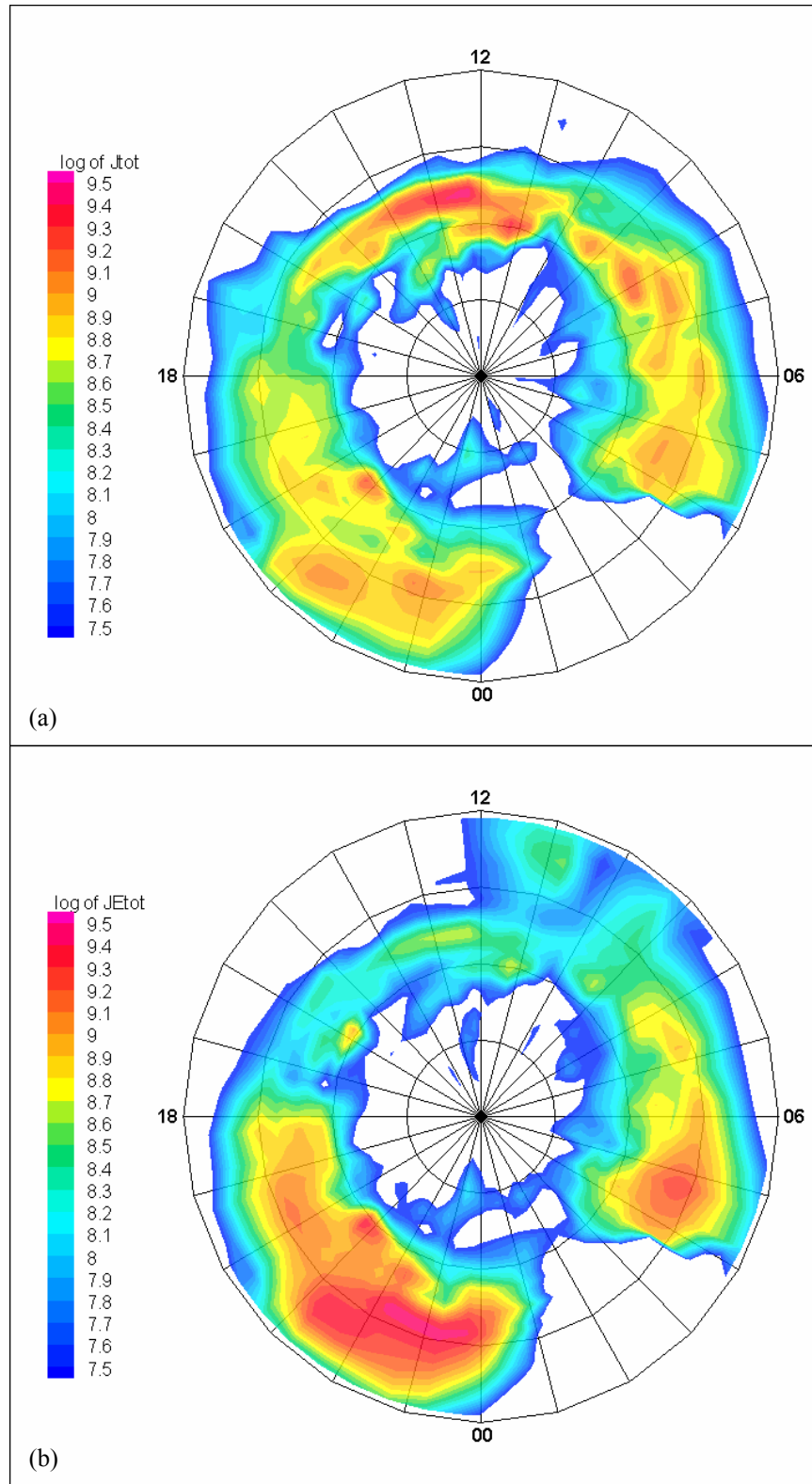


Figure A.6. ABI auroral model zone 54-54.9 for (a) number flux and (b) energy flux

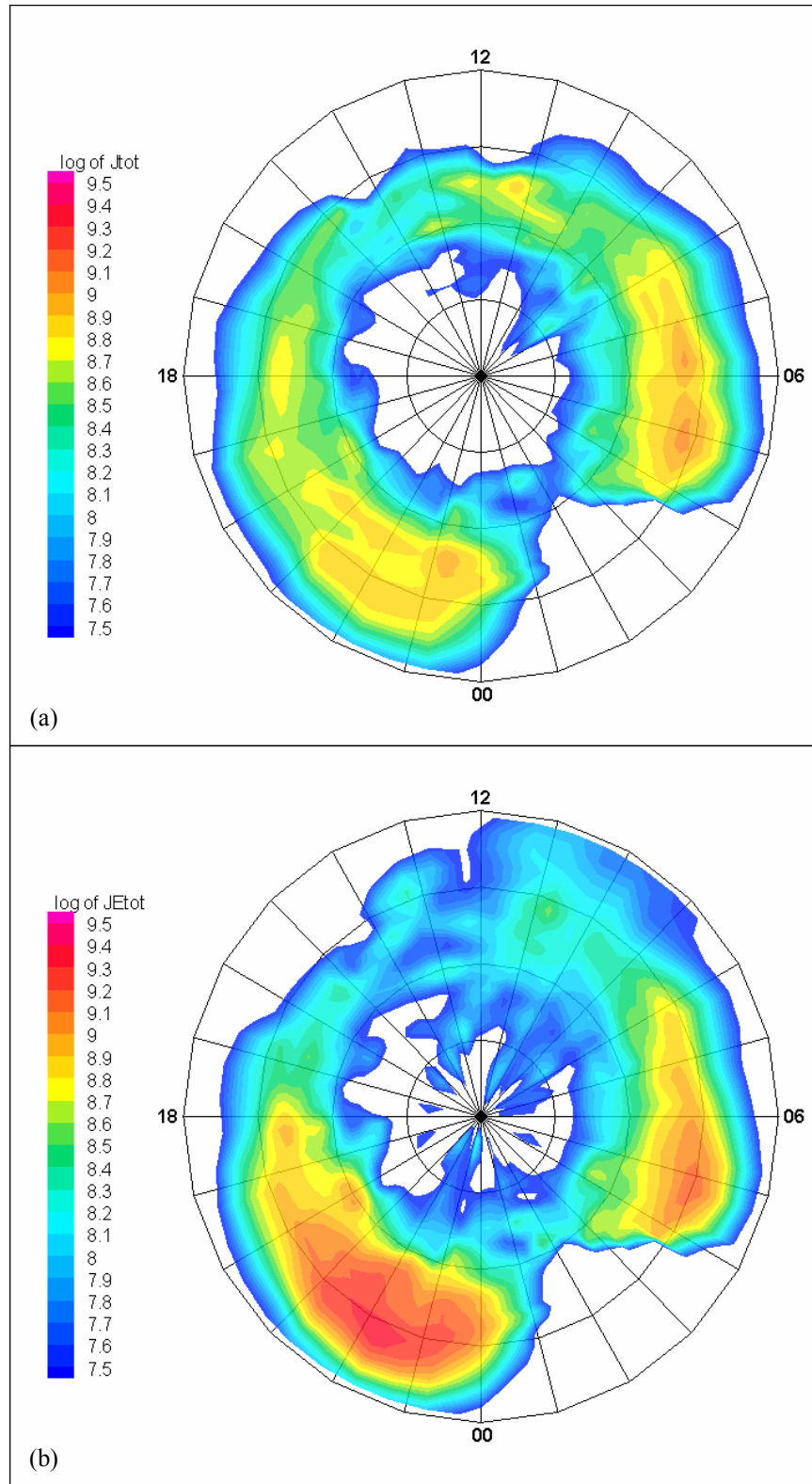


Figure A.7. ABI auroral model zone 55-55.9 for (a) number flux and (b) energy flux

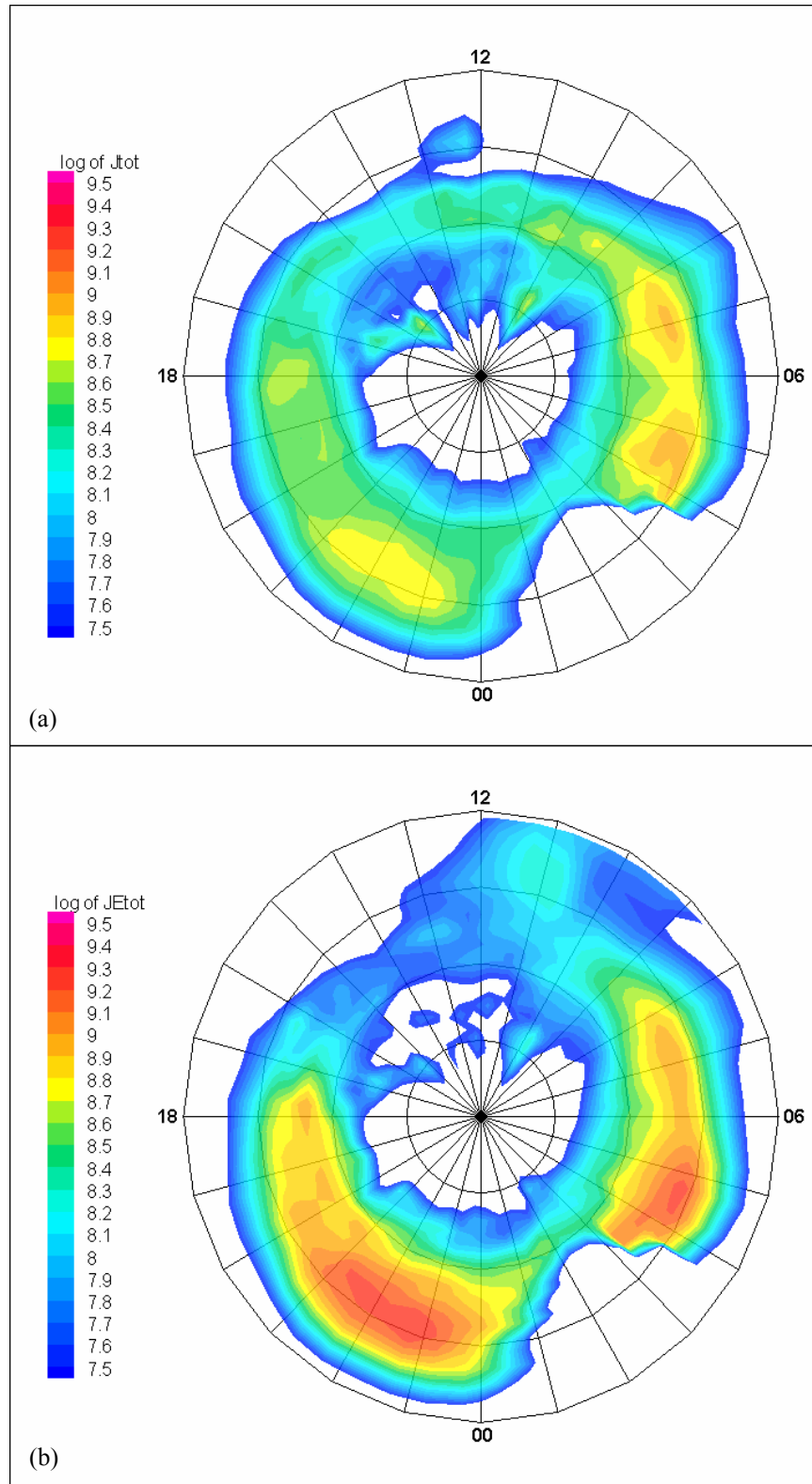


Figure A.8. ABI auroral model zone 56-56.9 for (a) number flux and (b) energy flux

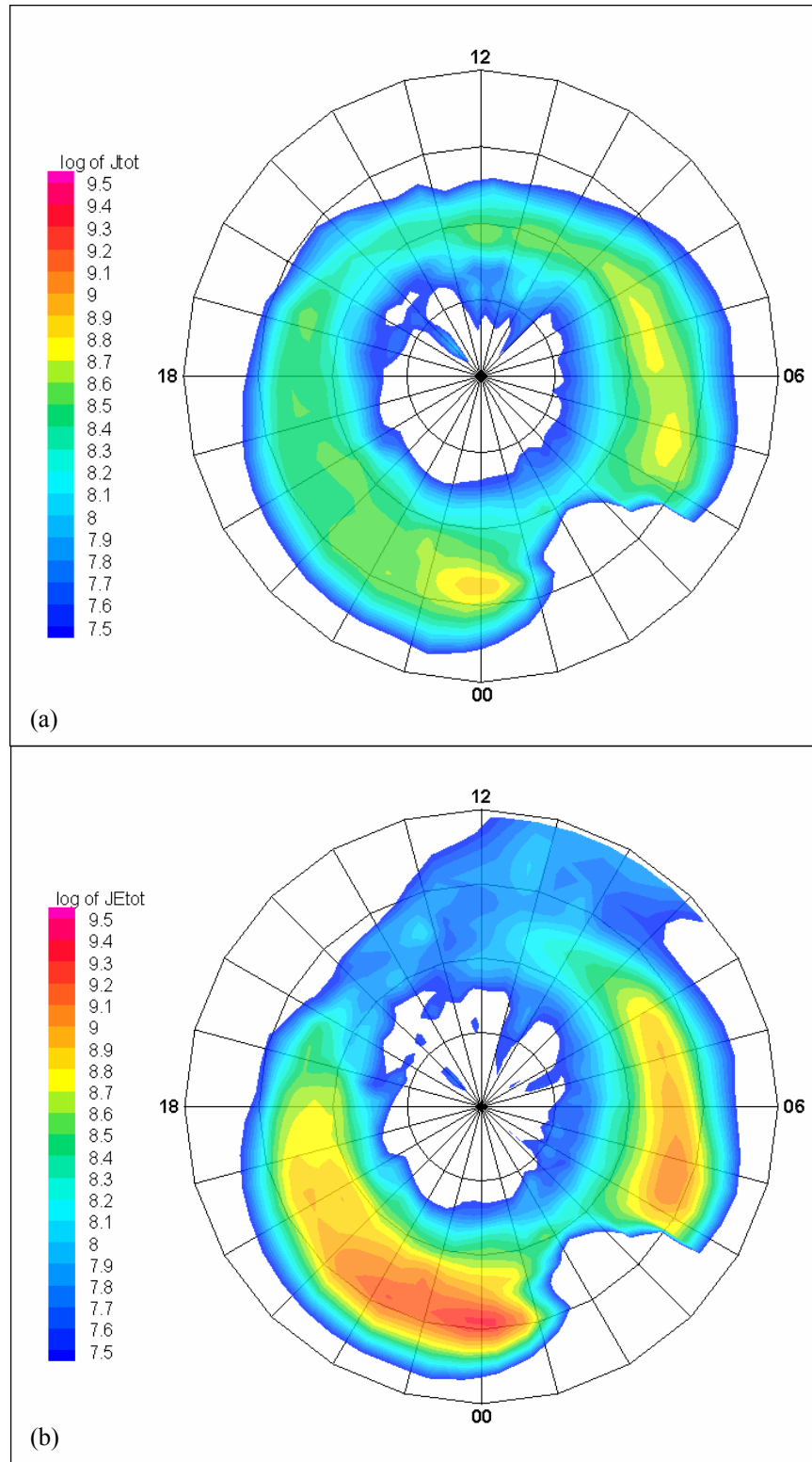


Figure A.9. ABI auroral model zone 57-57.9 for (a) number flux and (b) energy flux

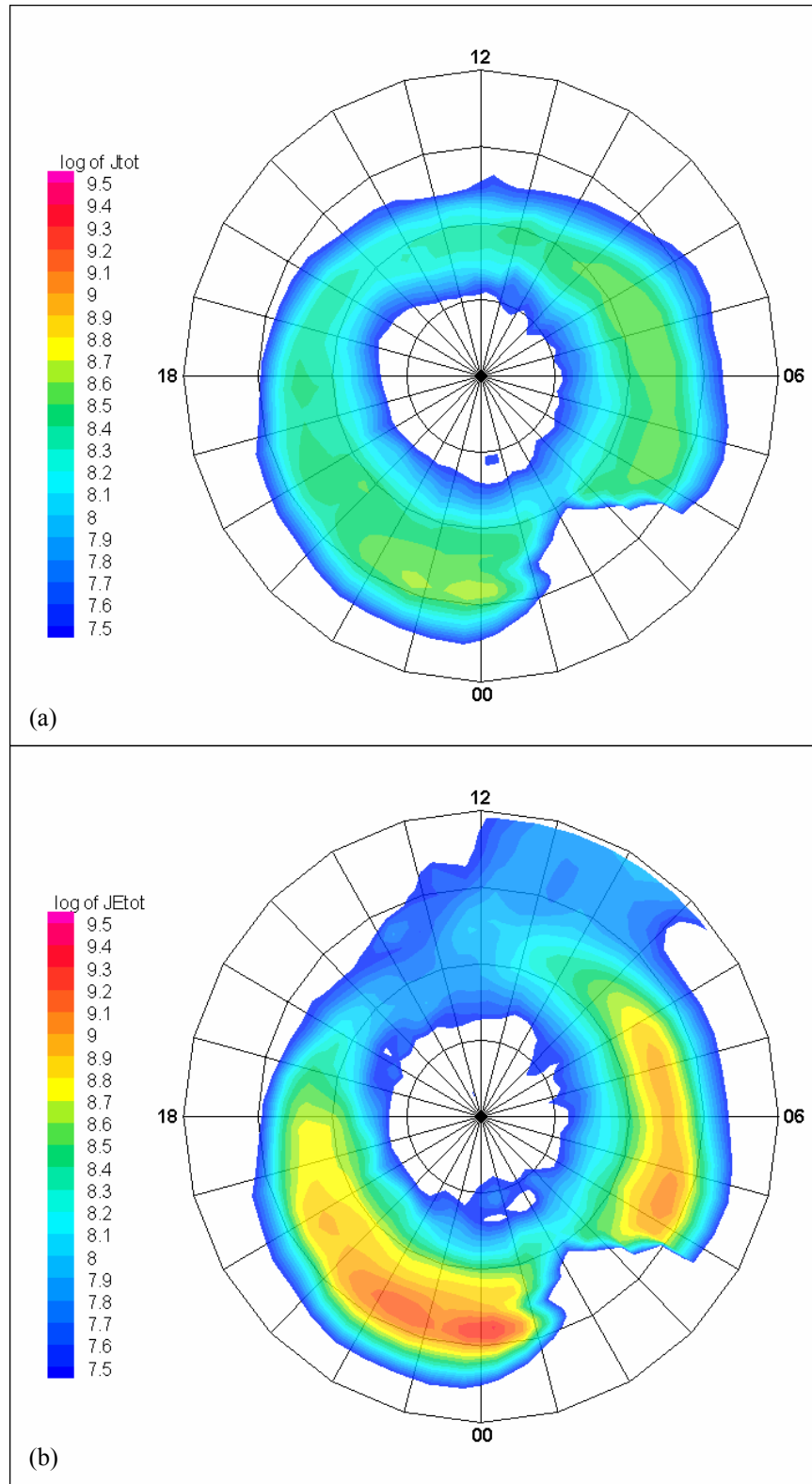


Figure A.10. ABI auroral model zone 58-58.9 for (a) number flux and (b) energy flux



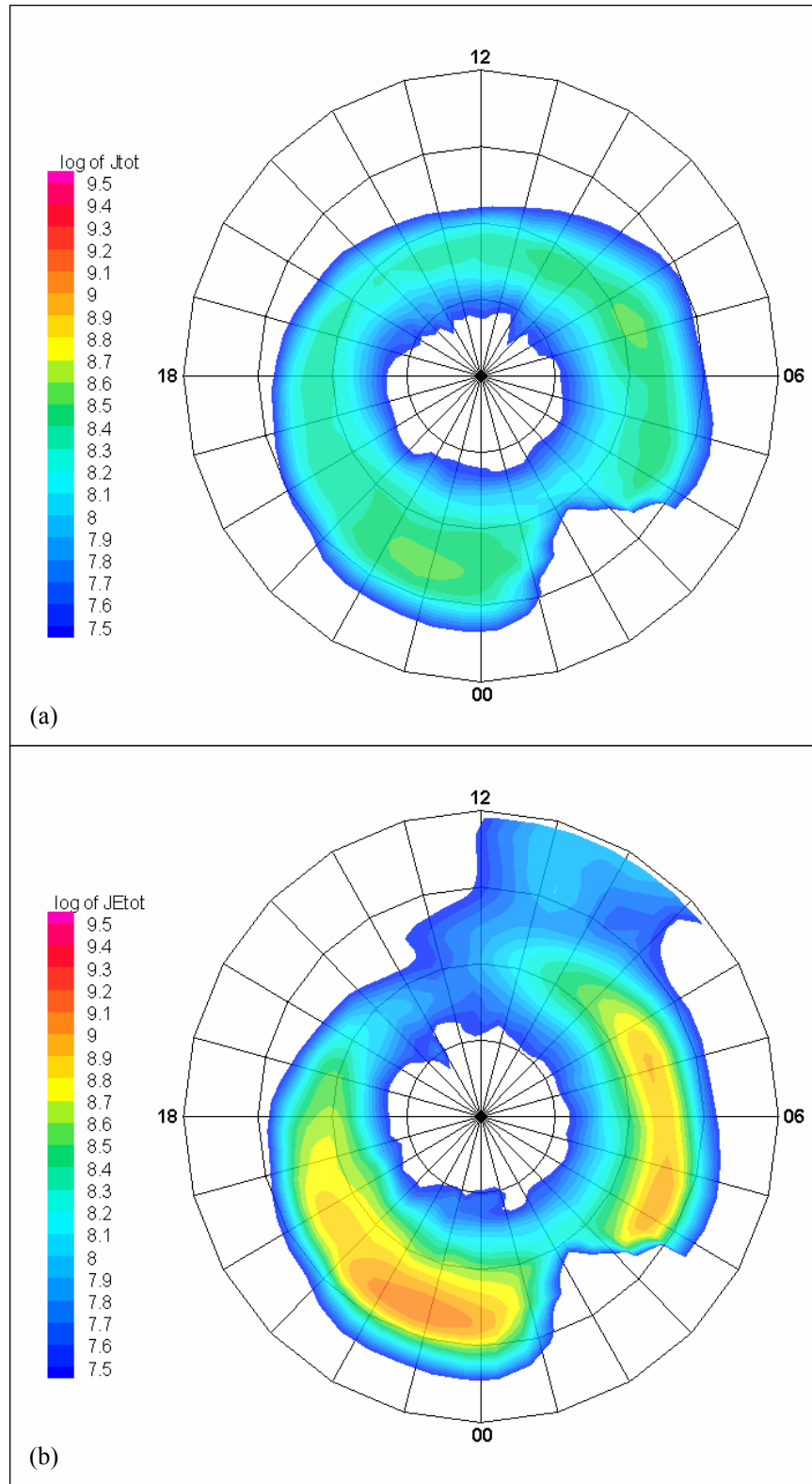


Figure A.11. ABI auroral model zone 59-59.9 for (a) number flux and (b) energy flux

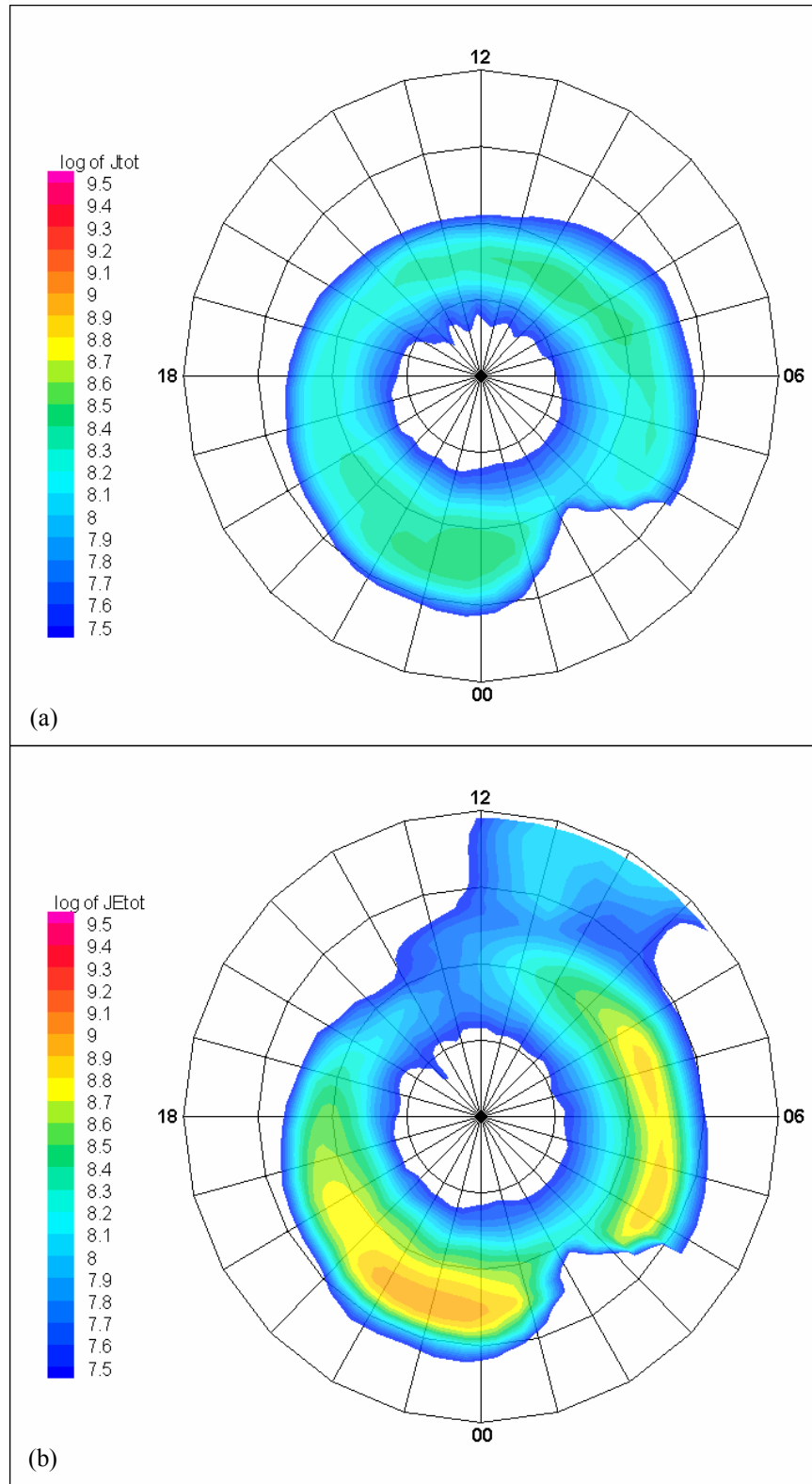


Figure A.12. ABI auroral model zone 60-60.9 for (a) number flux and (b) energy flux

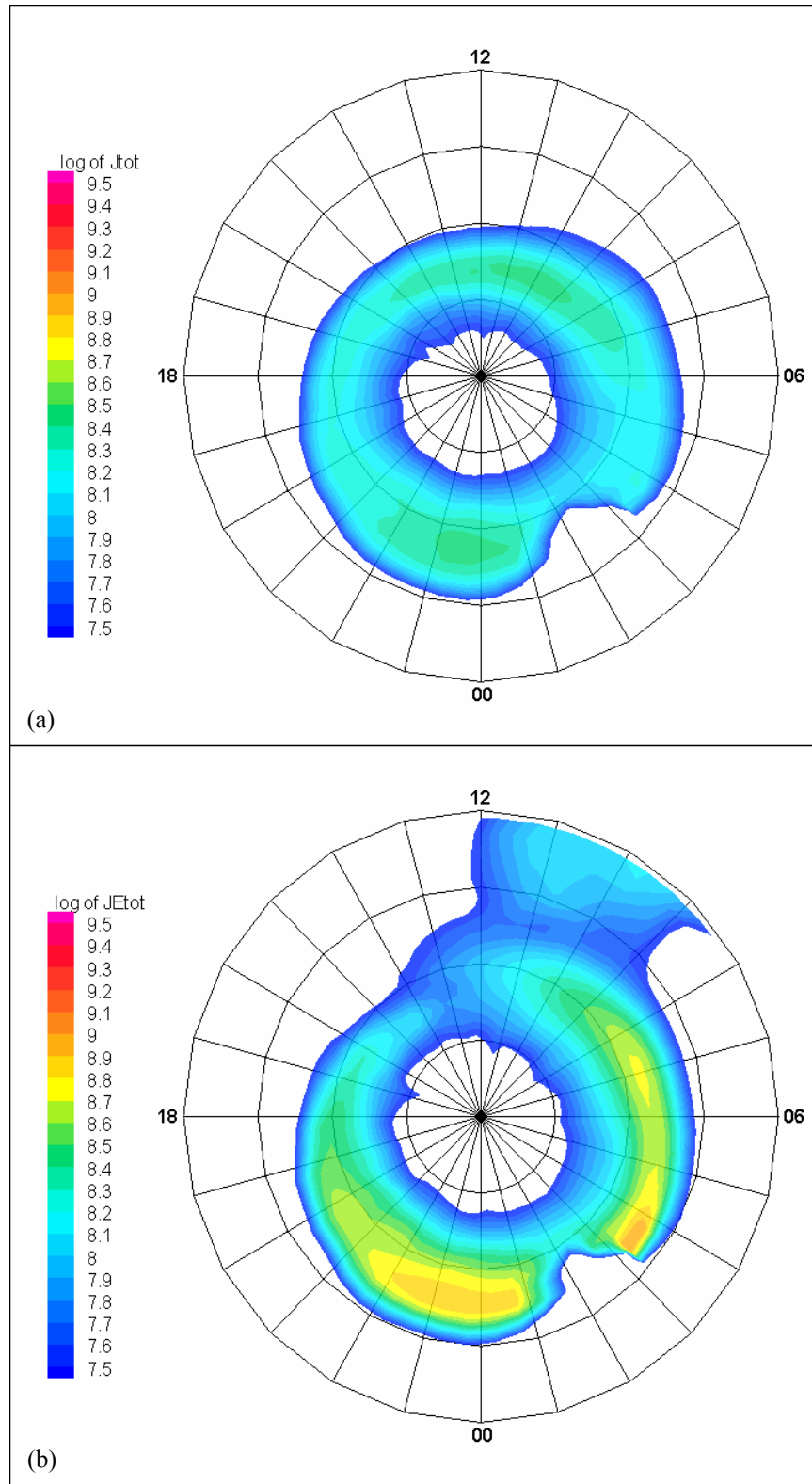


Figure A.13. ABI auroral model zone 61-61.9 for (a) number flux and (b) energy flux

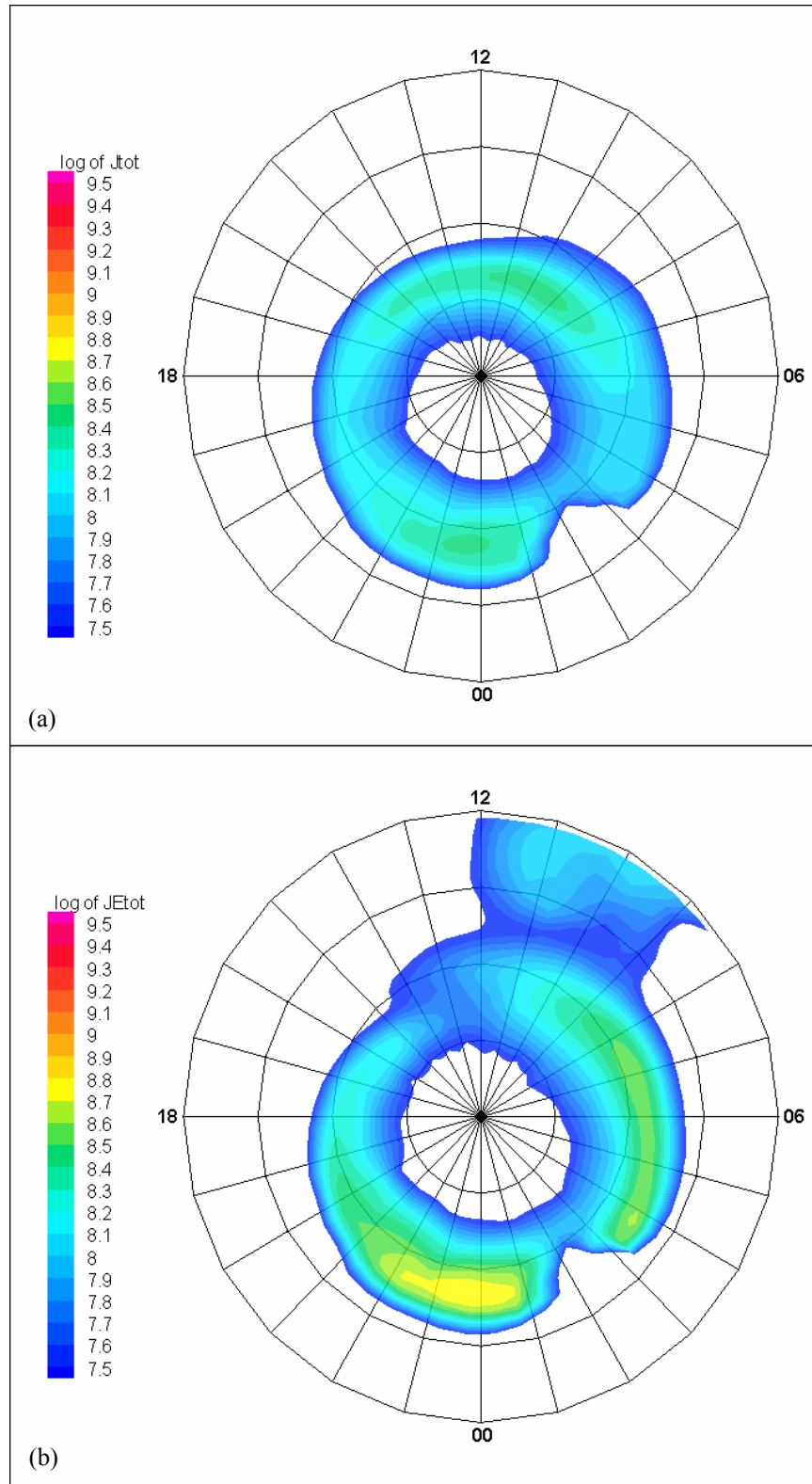


Figure A.14. ABI auroral model zone 62-62.9 for (a) number flux and (b) energy flux

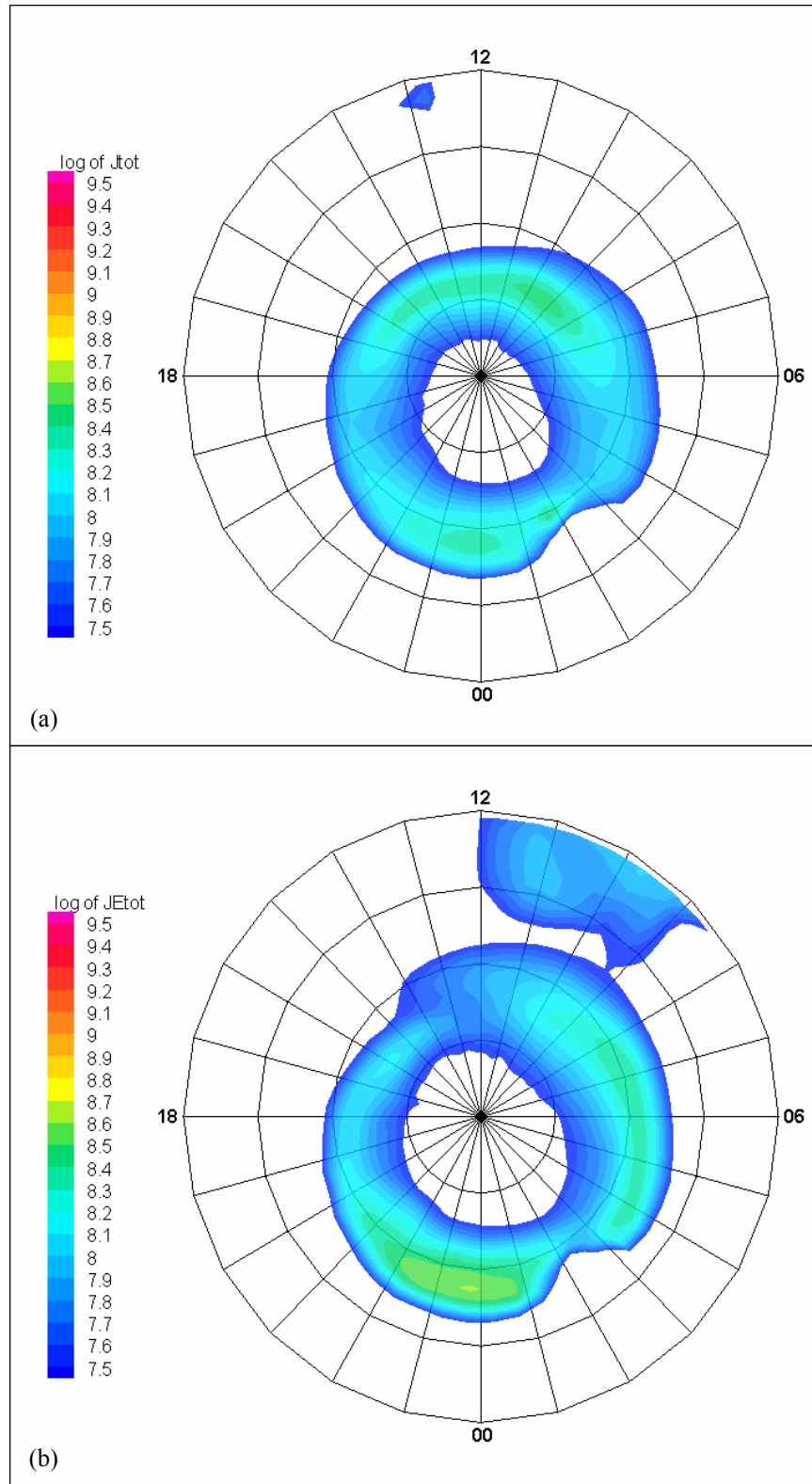


Figure A.15. ABI auroral model zone 63-63.9 for (a) number flux and (b) energy flux

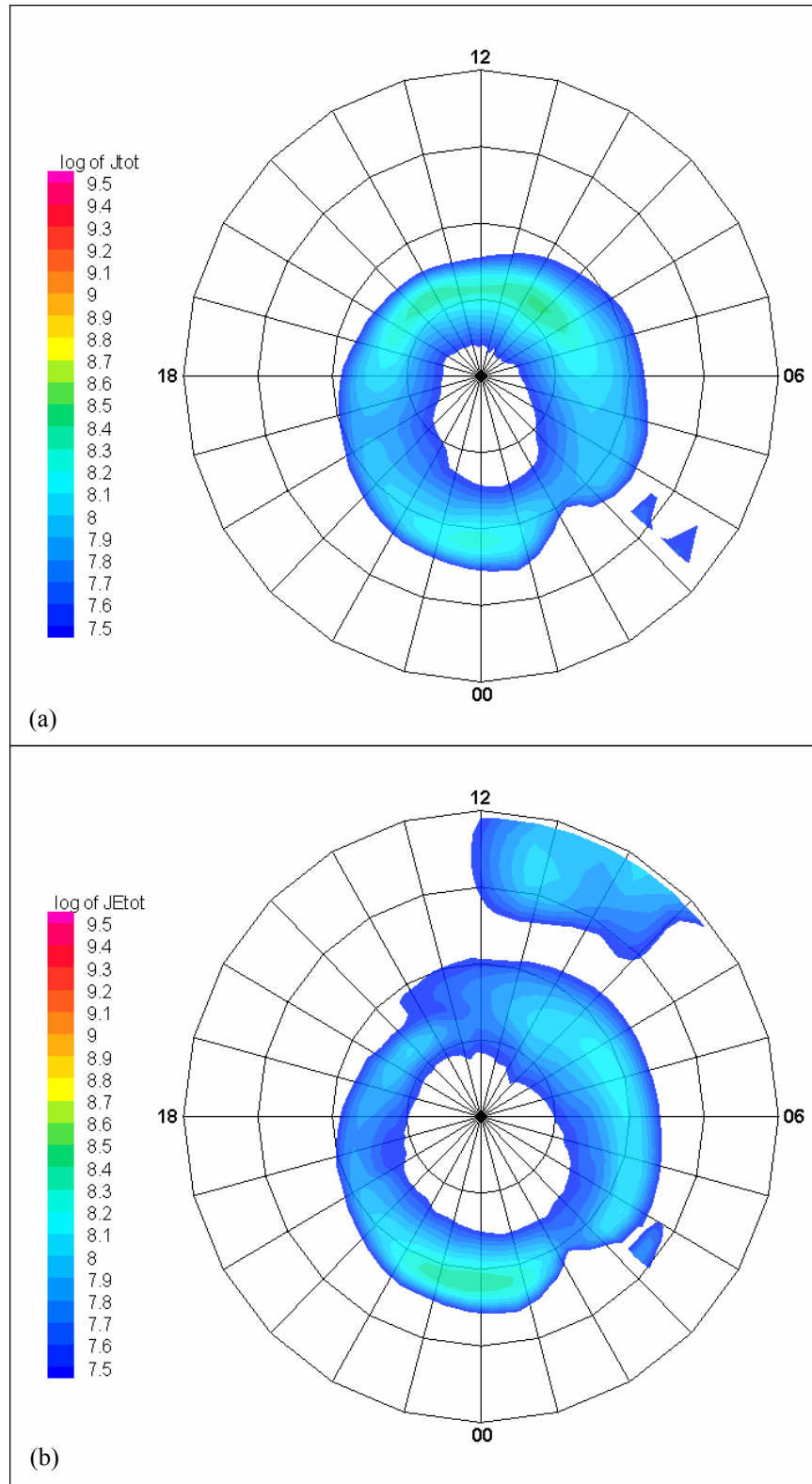


Figure A.16. ABI auroral model zone 64-64.9 for (a) number flux and (b) energy flux

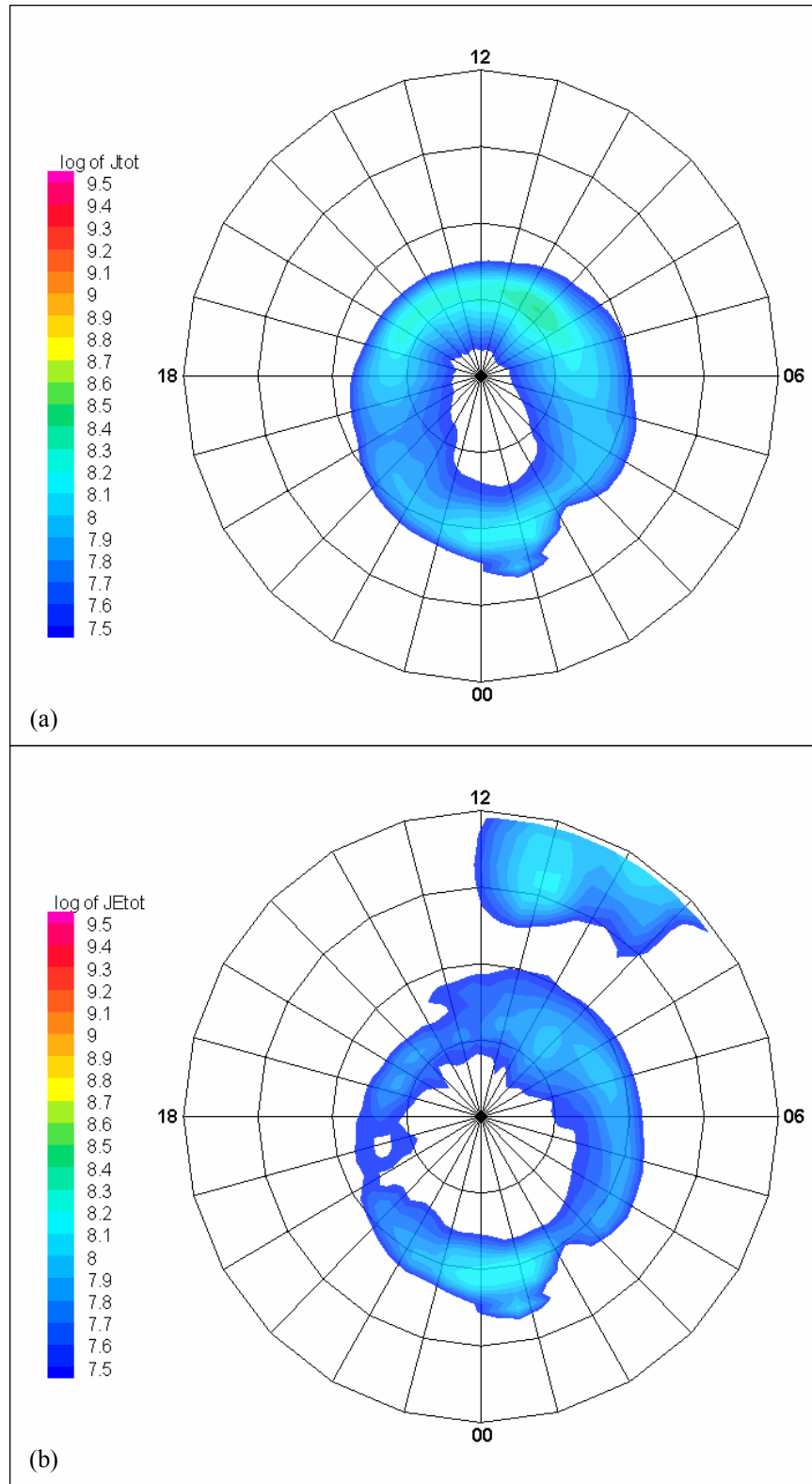


Figure A.17. ABI auroral model zone 65-65.9 for (a) number flux and (b) energy flux

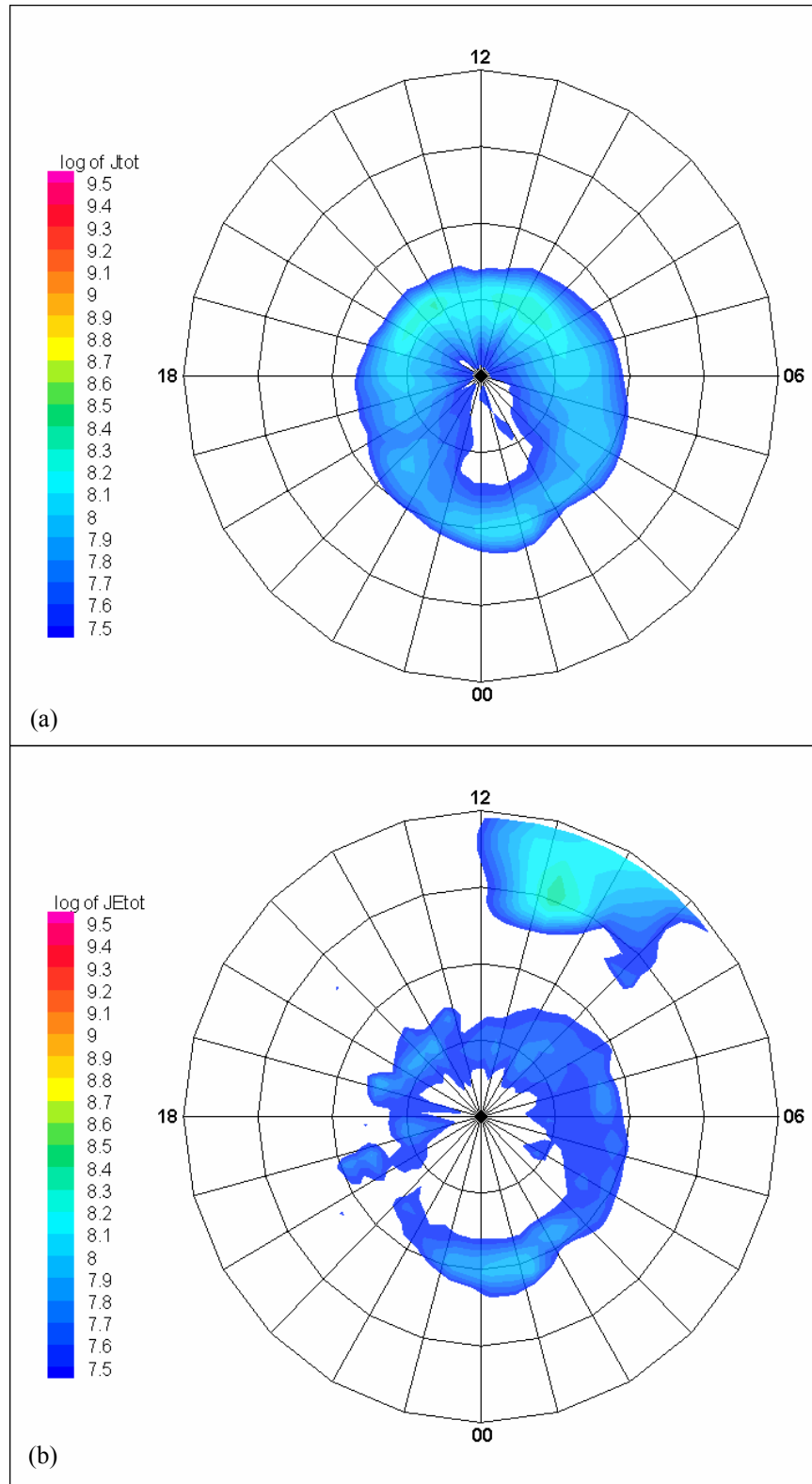


Figure A.18. ABI auroral model zone 66-66.9 for (a) number flux and (b) energy flux



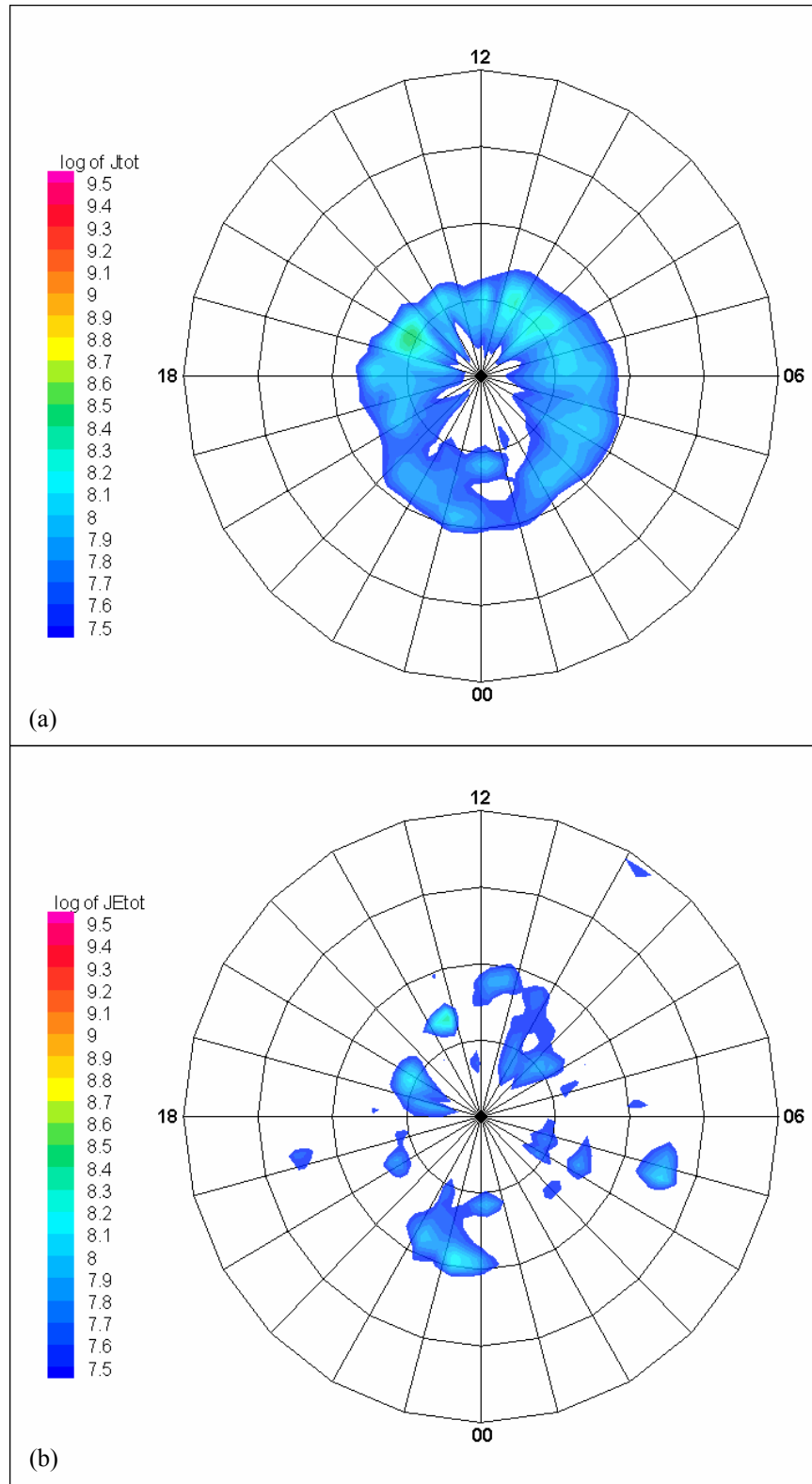


Figure A.19. ABI auroral model zone 67-67.9 for (a) number flux and (b) energy flux

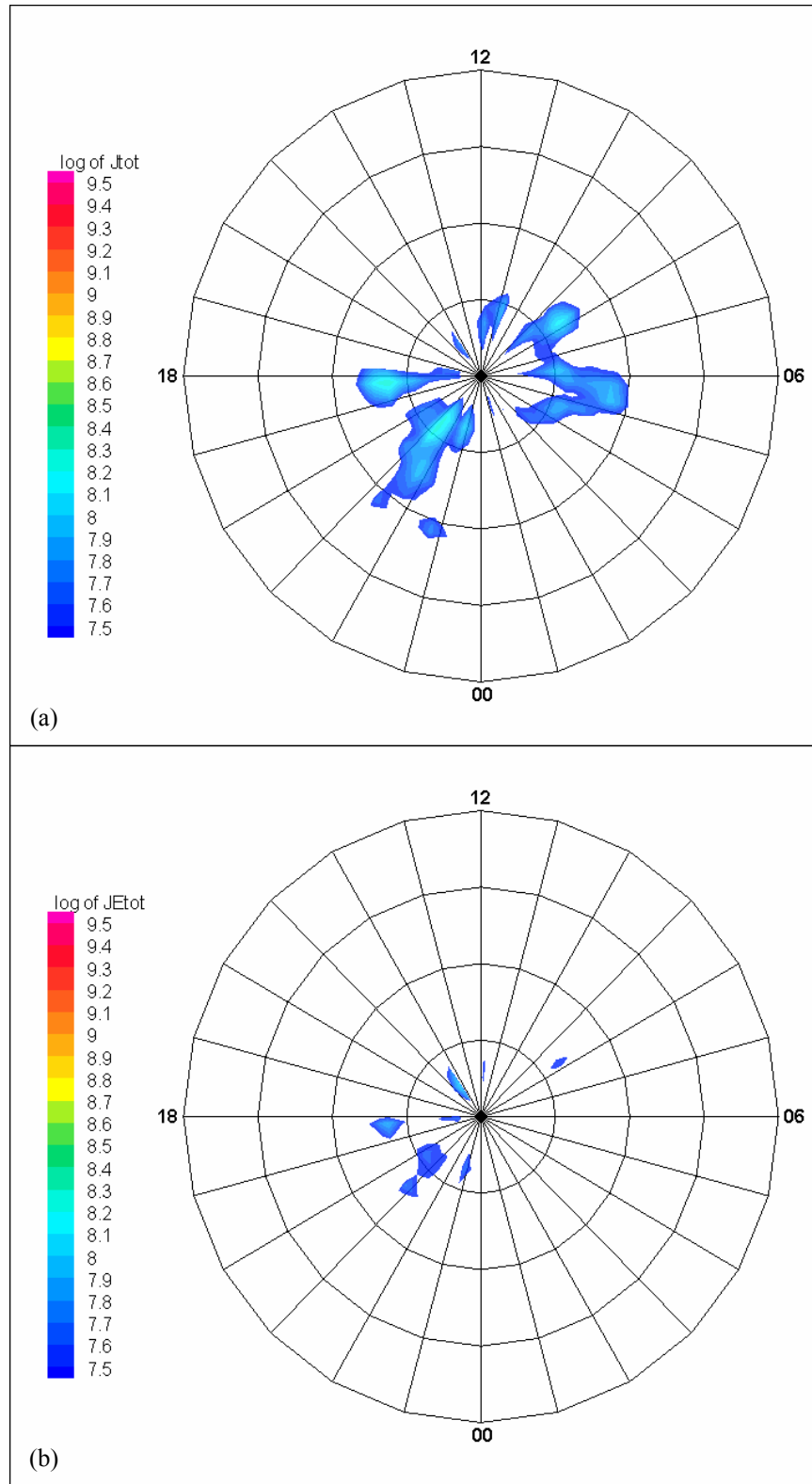


Figure A.20. ABI auroral model zone 68-68.9 for (a) number flux and (b) energy flux

## Appendix B: Hardy Auroral Model Polar Projection Plots

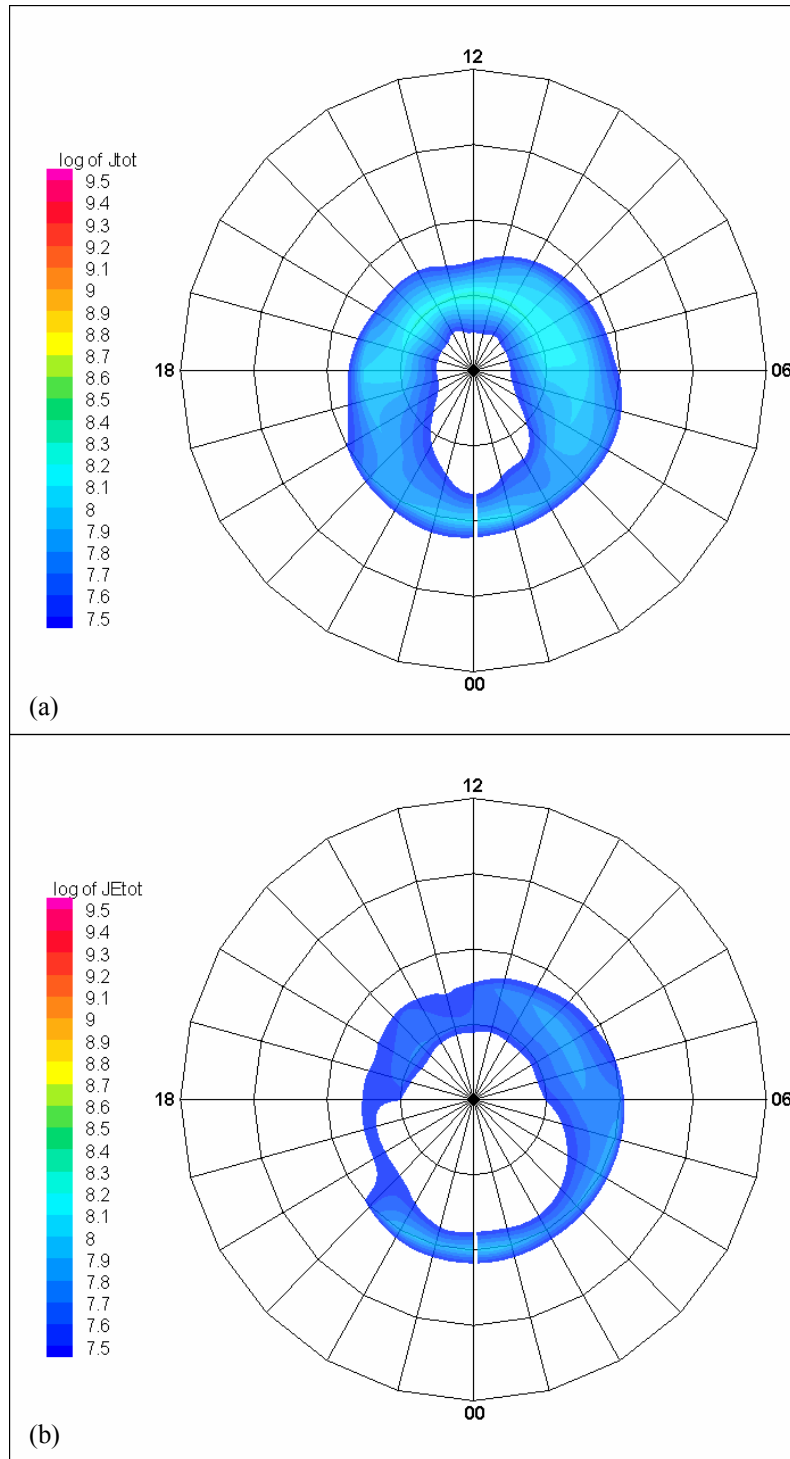


Figure B.1. Hardy auroral model Kp zone 0 for (a) number flux and (b) energy flux

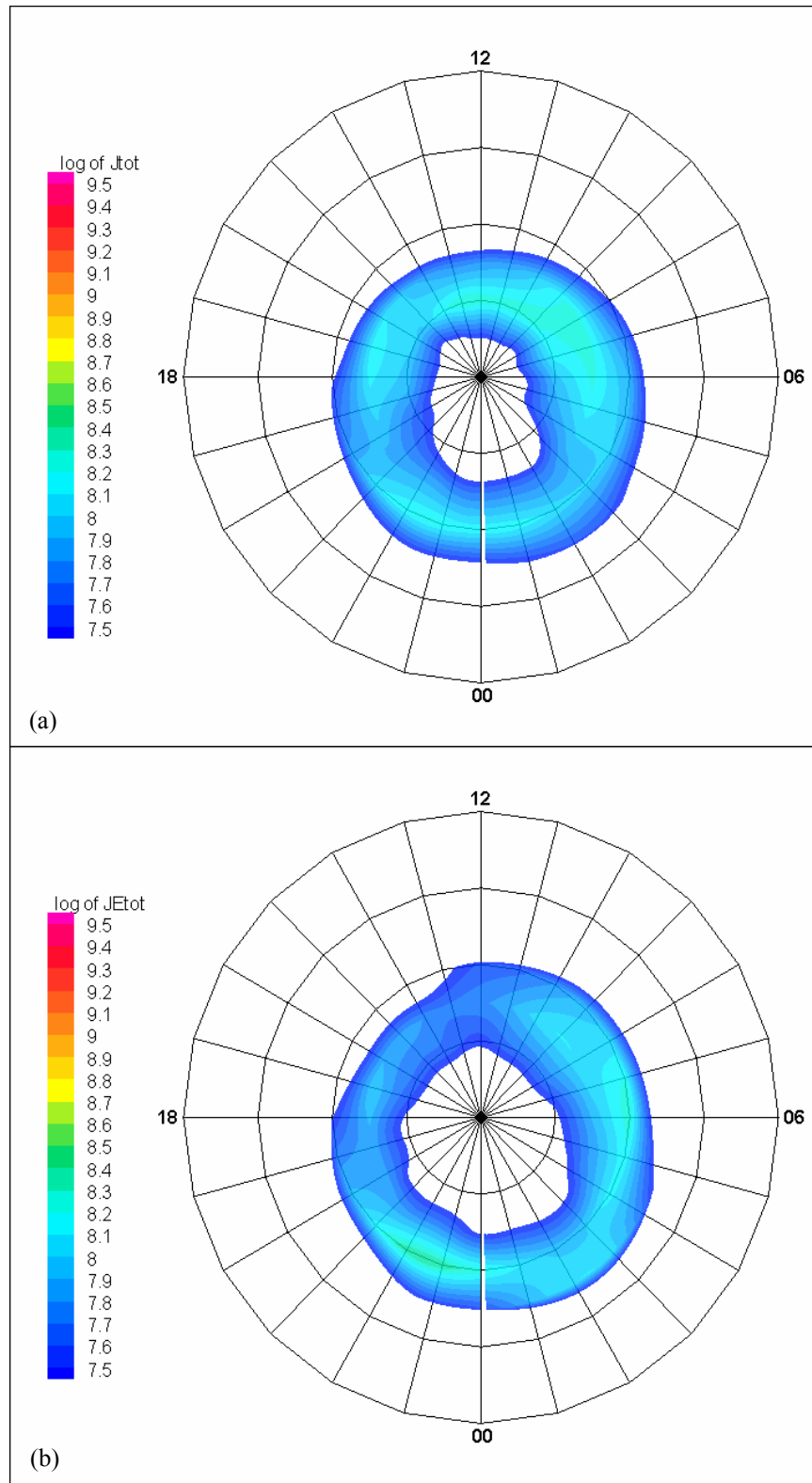


Figure B.2. Hardy auroral model Kp zone 1 for (a) number flux and (b) energy flux

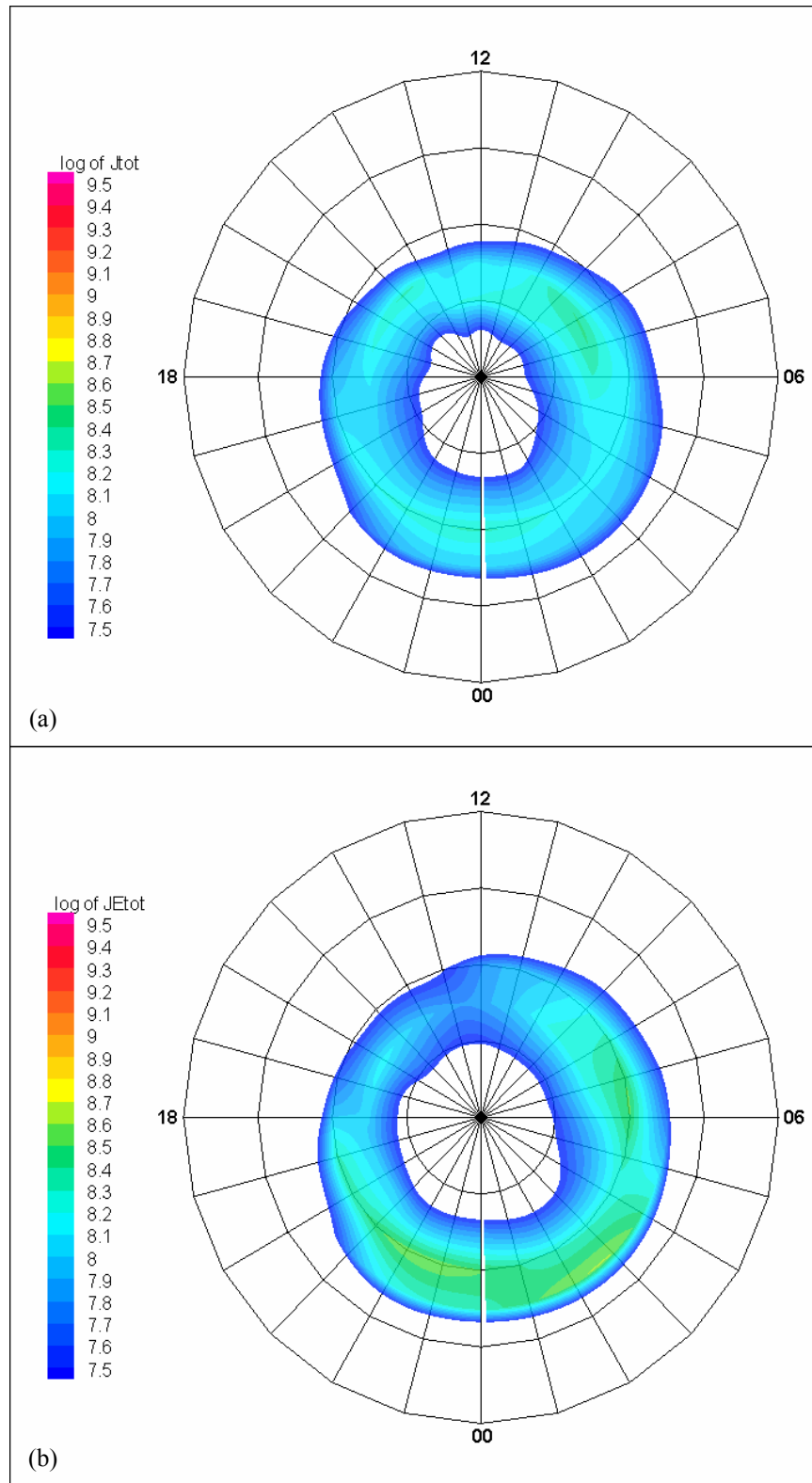


Figure B.3. Hardy auroral model Kp zone 2 for (a) number flux and (b) energy flux

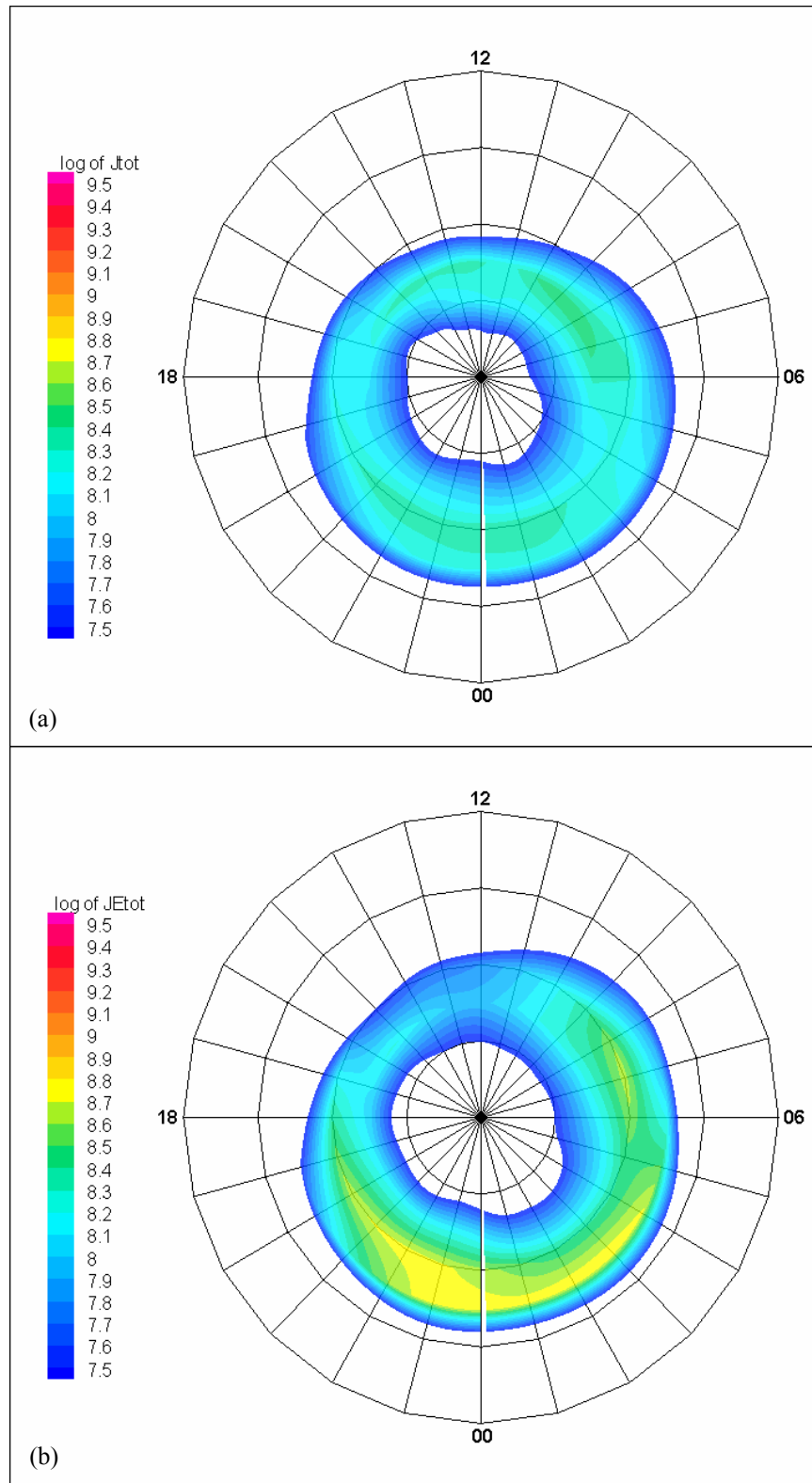


Figure B.4. Hardy auroral model Kp zone 3 for (a) number flux and (b) energy flux

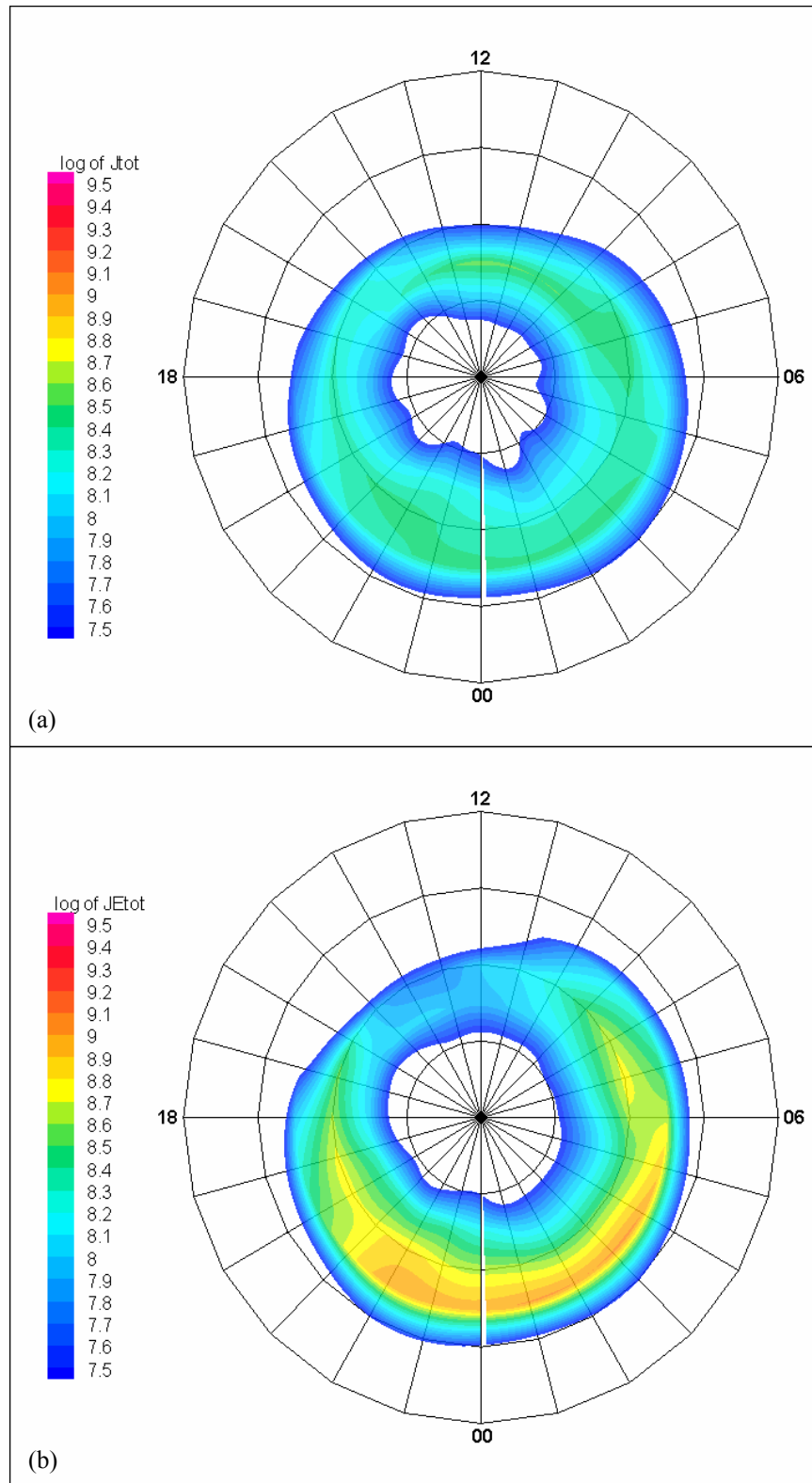


Figure B.5. Hardy auroral model Kp zone 4 for (a) number flux and (b) energy flux

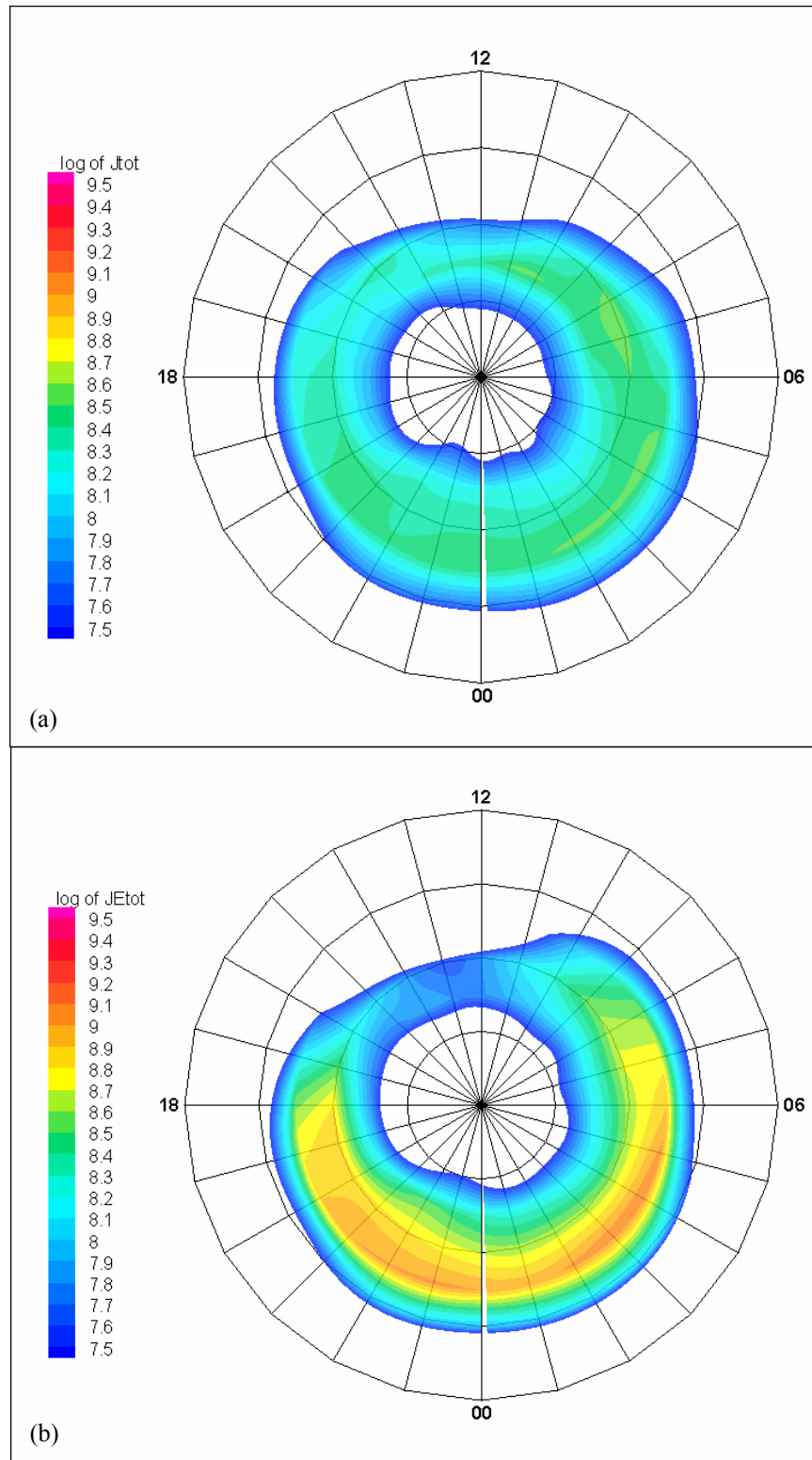


Figure B.6. Hardy auroral model Kp zone 5 for (a) number flux and (b) energy flux



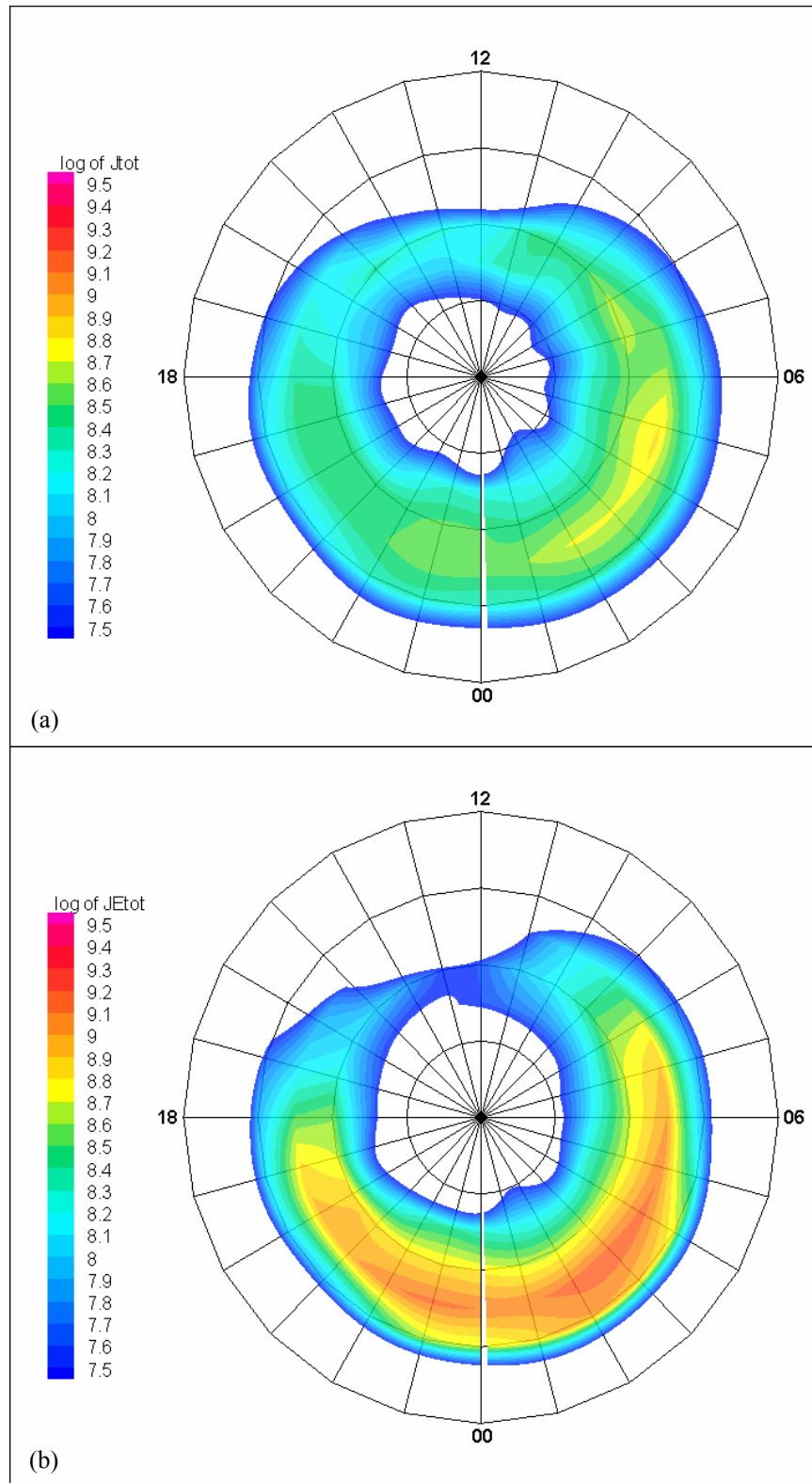


Figure B.7. Hardy auroral model Kp zone 6 for (a) number flux and (b) energy flux

## Bibliography

- Akasofu, S-I. "Auroral Phenomena," in *Auroral Physics*. Eds. Ching -I. Meng, Michael J. Rycroft, and Louis A. Frank. Cambridge: Cambridge University Press, 1991.
- Akasofu, S-I. "The aurora: an electrical discharge phenomenon surrounding the Earth," *Rep. Prog. Phys.*, 44, No. 10: 1123-1149 (October 1981).
- Carlson, H. C. Jr., and A. Egeland. "The Aurora and the Auroral Ionosphere," in *Introduction to Space Physics*. Eds. Margaret G. Kivelson and Christopher T. Russell. Cambridge: Cambridge University Press, 1995.
- Della-Rose, Devin J. Associate Professor, Air Force Institute of Technology, Wright-Patterson AFB OH. Personal Communication. April 2004.
- Deuel, Greg. "Defense Meteorological Satellite Program (DMSP) Satellite F8 Source/Platform." Technical description of satellite. n. pag. [http://ghrc.msfc.nasa.gov:5721/source\\_documents/dmsp\\_f8.html](http://ghrc.msfc.nasa.gov:5721/source_documents/dmsp_f8.html). April 2004.
- Hardy, D. A., M. S. Gussenhoven, and E. Holeman. "A Statistical Model of Auroral Electron Precipitation," *J. Geophys. Res.*, 90, No. A5: 4229-4248 (1 May 1985).
- Hardy, D. A., L. K. Schmitt, M. S. Gussenhoven, F. J. Marshall, H. C. Yeh, T. L. Schumaker, A. Huber, and J. Pantazis. *Precipitating Electron and Ion Detectors (SSJ/4) for the Block 5D/Flights 6-10 DMSP Satellites: Calibration and Data Presentation*. Air Force Geophysics Laboratory, Space Physics Division. Technical Report No. GL-TR-84-0317, 1984.
- Linthe, H. -J. "Kp Sites List," Current list of Kp station names. n. pag. [http://www.gfz-potsdam.de/pb2/pb23/GeoMag/niemegk/kp\\_index/kp\\_sites.html](http://www.gfz-potsdam.de/pb2/pb23/GeoMag/niemegk/kp_index/kp_sites.html). May 2004.
- Madden, D., and M. S. Gussenhoven. *Auroral Boundary Index from 1983 to 1990*. Air Force Geophysics Laboratory, Space Physics Division. Technical Report No. GL-TR-90-0358, 1990.
- Menvielle, M., and A. Berthelier. "The K-Derived Planetary Indices: Description and Availability," *Review of Geophysics*, 29, 3: 415-432 (August 1991).
- Rich, Frederick J. Air Force Research Laboratory, Hanscom AFB MA. Personal Communication. February 2003.
- Schunk, Robert W., and Andrew F. Nagy. *Ionospheres – Physics, Plasma Physics, and Chemistry*. Cambridge: Cambridge University Press, 2000.

Sotirelis, Thomas, and Patrick T. Newell. "Boundary-oriented electron precipitation model," *J. Geophys. Res.*, 105, No. A8: 18,655-18,673 (1 August 2000).

Tascione, Thomas F. *Introduction to the Space Environment* (2<sup>nd</sup> Edition). Malabar FL: Krieger Publishing Company, 1994.

## **Vita**

Captain Keith A. Anderson was born in McPherson, Kansas. He graduated from Saguaro High School in Scottsdale, Arizona and enlisted in the Air Force in the same year where he served as a Contract Specialist. During his enlistment, he was stationed at the 56<sup>th</sup> Contracting Squadron at Luke AFB, Arizona and the 64<sup>th</sup> Contracting Squadron at Reese AFB, Texas where he applied for and was accepted into the Airman Education and Commissioning Program (AECPP). For this program, he was transferred to the AFROTC Detachment 925 at the University of Wisconsin in Madison, Wisconsin to complete his undergraduate studies. He graduated with a B.S. in Atmospheric and Oceanic Sciences and soon after attended Officer Training School at Maxwell AFB, Alabama where he received his commission. His first assignment as a Weather Officer was at the 11<sup>th</sup> Operational Weather Squadron at Elmendorf AFB, Alaska where he served as OIC of one of three forecasting flights. From there, he entered the Graduate School of Engineering and Management, Air Force Institute of Technology at Wright-Patterson AFB, Ohio. He will graduate with a M.S. in space physics and will be stationed at the Space Weather Branch, Air Force Weather Agency at Offutt AFB, Nebraska.

REPORT DOCUMENTATION PAGE				Form Approved OMB No. 0704-0188	
Public reporting burden for this collection of information is estimated to average 1 hour per response, including the time for reviewing instructions, searching existing data sources, gathering and maintaining the data needed, and completing and reviewing this collection of information. Send comments regarding this burden estimate or any other aspect of this collection of information, including suggestions for reducing this burden to Department of Defense, Washington Headquarters Services, Directorate for Information Operations and Reports (0704-0188), 1215 Jefferson Davis Highway, Suite 1204, Arlington, VA 22202-4302. Respondents should be aware that notwithstanding any other provision of law, no person shall be subject to any penalty for failing to comply with a collection of information if it does not display a currently valid OMB control number. <b>PLEASE DO NOT RETURN YOUR FORM TO THE ABOVE ADDRESS.</b>					
1. REPORT DATE (DD-MM-YYYY) June 2004		2. REPORT TYPE Master's Thesis		3. DATES COVERED (From - To) June 2003 – May 2004	
4. TITLE AND SUBTITLE  DERIVATION OF A SELF-CONSISTENT AURORAL OVAL MODEL USING THE AURORAL BOUNDARY INDEX				5a. CONTRACT NUMBER	
				5b. GRANT NUMBER	
				5c. PROGRAM ELEMENT NUMBER	
6. AUTHOR(S)  Anderson, Keith A., Capt, USAF				5d. PROJECT NUMBER	
				5e. TASK NUMBER	
				5f. WORK UNIT NUMBER	
7. PERFORMING ORGANIZATION NAME(S) AND ADDRESS(ES)  Air Force Institute of Technology Graduate School of Engineering and Management (AFIT/EN) 2950 Hobson Way, Building 640 WPAFB OH 45433-7765				8. PERFORMING ORGANIZATION REPORT NUMBER  AFIT/GAP/ENP/04-01	
9. SPONSORING / MONITORING AGENCY NAME(S) AND ADDRESS(ES)  Lt Col William B. Cade HQ AFWA/DNX Offutt AFB, NE 68113				10. SPONSOR/MONITOR'S ACRONYM(S)	
				11. SPONSOR/MONITOR'S REPORT NUMBER(S)	
12. DISTRIBUTION / AVAILABILITY STATEMENT  APPROVED FOR PUBLIC RELEASE; DISTRIBUTION UNLIMITED					
13. SUPPLEMENTARY NOTES					
14. ABSTRACT <p>The position and intensity of the auroral oval has many implications for the Air Force from determining the effects of incoming electron flux on DoD systems to modeling the ionosphere to exploit current HF communications capabilities. The auroral morphology is a good indicator of the level at which space weather and its near-Earth consequences are occurring, and thus it is important to develop an auroral prediction model. However, since no purely physics-based models exist to describe the temporal and spatial evolution of the auroral zone, space weather practitioners and researchers are forced to produce statistical representations, “organized” by some relevant geophysical parameter. Currently, the most widely used model is the Hardy et al. (1985) auroral oval model, which is binned according to the Kp index. The Kp index is a mid-latitude measure of planetary geomagnetic activity, and was presumed to be well-correlated to the size and shape of the auroral region. However, subsequent research has shown that Kp is probably not the best binning parameter. This study used the Auroral Boundary Index (ABI) to parameterize the statistics of the auroral oval location since it is a measurement of the electron fluxes computed directly from sensors aboard the DMSP satellites. Thus, the current work represents a move toward a more self-consistent—and presumably more accurate—climatological representation of the auroral oval boundaries. This was accomplished by recreating the process performed by Hardy et al., substituting the ABI for the Kp index and deriving an entirely new set of auroral ovals based on almost 11 years of DMSP data from the F8 and F9 satellites. To quantitatively assess the differences between the two models, electron flux values were compared to actual DMSP data of individual satellite passes. Preliminary findings suggest that the new ABI auroral oval model is, at worst, comparable to the results achieved by Hardy et al. Further refinement of this new model based on the ABI should increase its effectiveness and offer a more reliable alternative to previous auroral models.</p>					
15. SUBJECT TERMS  Aurora, Auroral Oval Model, Electron Precipitation, DMSP, SSI/4, Auroral Boundary Index					
16. SECURITY CLASSIFICATION OF:			17. LIMITATION OF ABSTRACT	18. NUMBER OF PAGES	19a. NAME OF RESPONSIBLE PERSON
a. REPORT	b. ABSTRACT	c. THIS PAGE			Devin J. Della-Rose, Maj, USAF (ENP)
U	U	U	UU	108	19b. TELEPHONE NUMBER (include area code) (937) 255-3636, ext 4514 e-mail: Devin.Della-Rose@afit.edu

## INSTRUCTIONS FOR COMPLETING SF 298

**1. REPORT DATE.** Full publication date, including day, month, if available. Must cite at least the year and be Year 2000 compliant, e.g. 30-06-1998; xx-06-1998-, xx-xx-1998.

**2. REPORT TYPE.** State the type of report, such as final, technical, interim, memorandum, master's thesis, progress, quarterly, research, special, group study, etc.

**3. DATES COVERED.** Indicate the time during which the work was performed and the report was written, e.g., Jun 1997 - Jun 1998; 1-10 Jun 1996; May - Nov 1998; Nov 1998.

**4. TITLE.** Enter title and subtitle with volume number and part number, if applicable. On classified documents, enter the title classification in parentheses.

**Ba. CONTRACT NUMBER.** Enter all contract numbers as they appear in the report, e.g. F33615-86-C-5169.

**5b. GRANT NUMBER.** Enter all grant numbers as they appear in the report, e.g. AFOSR-82-1234.

**5c. PROGRAM ELEMENT NUMBER.** Enter all program element numbers as they appear in the report, e.g. 61101A.

**5d. PROJECT NUMBER.** Enter all project numbers as they appear in the report, e.g. 1F665702D1257; ILIR.

**5e. TASK NUMBER.** Enter all task numbers as they appear in the report, e.g. 05; RF0330201; T4112.

**5f. WORK UNIT NUMBER.** Enter all work unit numbers as they appear in the report, e.g. 001; AFAPL30480105.

**6. AUTHOR(S).** Enter name(s) of person(s) responsible for writing the report, performing the research, or credited with the content of the report. The form of entry is the last name, first name, middle initial, and additional qualifiers separated by commas, e.g. Smith, Richard, J, Jr.

**7. PERFORMING ORGANIZATION NAME(S) AND ADDRESS(ES).** Self-explanatory.

**8. PERFORMING ORGANIZATION REPORT NUMBER.**

Enter all unique alphanumeric report numbers assigned by the performing organization, e.g. BRL-1234; AFWL-TR-85-4017-Vol-21-PT-2.

**9. SPONSORING/MONITORING AGENCY NAME(S)**

**AND ADDRESS(ES).** Enter the name and address of the organization(s) financially responsible for and monitoring the work.

**10. SPONSOR/MONITOR'S ACRONYM(S).** Enter, if available, e.g. BRL, ARDEC, NADC.

**11. SPONSOR/MONITOR'S REPORT NUMBER(S).**

Enter report number as assigned by the sponsoring/monitoring agency, if available, e.g. BRL-TR-829; -21 5.

**12. DISTRIBUTION/AVAILABILITY STATEMENT.** Use agency-mandated availability statements to indicate the public availability or distribution limitations of the report. If additional limitations/ restrictions or special markings are indicated, follow agency authorization procedures, e.g. RD/FRD, PROPIN, ITAR, etc. Include copyright information.

**13. SUPPLEMENTARY NOTES.** Enter information not included elsewhere such as: prepared in cooperation with; translation of; report supersedes; old edition number, etc.

**14. ABSTRACT.** A brief (approximately 200 words) factual summary of the most significant information.

**15. SUBJECT TERMS.** Key words or phrases identifying major concepts in the report.

**16. SECURITY CLASSIFICATION.** Enter security classification in accordance with security classification regulations, e.g. U, C, S, etc. If this form contains classified information, stamp classification level on the top and bottom of this page.

**17. LIMITATION OF ABSTRACT.** This block must be completed to assign a distribution limitation to the abstract. Enter UU (Unclassified Unlimited) or SAR (Same as Report). An entry in this block is necessary if the abstract is to be limited.